AFFDL-TR-72-37

AN ANALYSIS OF THE STABILITY AND CONTROL CHARACTERISTICS OF AN EJECTOR WING V/STOL DURING TRANSITION

GEORGE KURYLOWICH
JAMES M. MARTIN

FOREWORD

This report was prepared to provide the Aeronautical Systems Division with a preliminary evaluation of the stability and control characteristics of an ejector wing configuration V/STOL in transition. The work included determination of the thrust levels necessary to meet the control requirements specified in MIL-F-83300 for a Level 1 category vehicle. A parallel effort was conducted for a stowable rotor configuration and comparisons were made between the stability and control characteristics of this vehicle and the handling characteristics of the ejector wing configuration. In addition, the downwash characteristics of the ejector wing configuration were evaluated.

This analysis was conducted over a six-month time period beginning in August 1971 under Project No. D095 entitled "Application Studies of Cold Thrust Augmentation (V/STOL)." The authors gratefully acknowledge the members of the Computer Science Center at WPAFB for their cooperation during this evaluation.

This report was submitted by the authors in April 1972.

This technical report has been reviewed and is approved.

C. B. WESTBROOK
Chief, Control Criteria Branch
Flight Control Division
Air Force Flight Dynamics
Laboratory

ABSTRACT

An analysis was performed to investigate the longitudinal stability and control characteristics of an ejector wing configuration V/STOL in transition. A derivative approach was used to obtain dynamic responses about specified trim speeds, and analysis of these responses provided an insight into the significant characteristics that might affect the pilot's control over the aircraft. The thrust levels necessary to meet the control requirements specified in MIL-F-83300 for a Level 1 category vehicle were determined as well. A similar study was made for a stowable rotor configuration, and results for the stowable rotor V/STOL and the ejector wing configuration were compared. Finally, the downwash characteristics of the ejector wing configuration were evaluated in terms of their effect on ground equipment and personnel. Spray generation during hover over water is also discussed.

TABLE OF CONTENTS

ILLUSTRATIONS

ILLUSTRATIONS CONTINUED

TABLES

LIST OF SYMBOLS

A, B, C, D, E	Coefficients of characteristic equation
A_u, B_u, C_u, D_u	Coefficients of numerator in forward velocity transfer function
A_w, B_w, C_w, D_w	Coefficients of numerator in vertical velocity transfer function
$A_\theta, B_\theta, C_\theta$	Coefficients of numerator in pitch angle transfer function
A_{e_λ}	Wing ejector exit area (ft^2)
A_{e_N}	Nose ejector exit area (ft^2)
A_{e_p}	Exit area of propulsive (core) jet engines (ft^2)
$\bar{c}$	Mean aerodynamic chord of wing (ft)
c.g.	Center of gravity (% $\bar{c}$)
$\hat{C}_D$	Ejector wing drag coefficient ($\hat{C}_b = D1_{\alpha=0} / \rho A_{e_\lambda} V_J^2$)
$\hat{C}_{D_\alpha}$	Ejector wing drag curve slope with α ($\hat{C}_{D_\alpha} = \frac{1}{\rho A_{e_\lambda} V_J^2} \frac{\partial D1}{\partial \alpha}$)
$\hat{C}_L$	Ejector wing lift coefficient ($\hat{C}_L = L1_{\alpha=0} / \rho A_{e_\lambda} V_J^2$)
$\hat{C}_{L_\alpha}$	Ejector wing lift curve slope with α ($\hat{C}_{L_\alpha} = \frac{1}{\rho A_{e_\lambda} V_J^2} \frac{\partial L1}{\partial \alpha}$)
$\hat{C}_m$	Ejector wing pitching moment coefficient ($\hat{C}_m = M1_{\alpha=0} / \bar{c} \rho A_{e_\lambda} V_J^2$)
$\hat{C}_{m_\alpha}$	Ejector wing pitching moment slope with α ($\hat{C}_{m_\alpha} = \frac{1}{\rho A_{e_\lambda} V_J^2} \frac{\partial M1}{\partial \alpha}$)
$\Delta C_D(i_t)$	Horizontal tail contribution to drag ($\Delta C_D = D3 / \frac{1}{2} \rho V^2 S_w$)

LIST OF SYMBOLS CONTINUED

$\Delta C_L(i_t)$	Horizontal tail contribution to lift ($\Delta C_L = L_3/\frac{1}{2}\rho V^2 S_w$)
$\Delta C_m(i_t)$	Horizontal tail contribution to pitching moment ($\Delta C_m = M_3/\frac{1}{2}\rho V^2 \bar{c} S_w$)
g	Acceleration due to gravity (32.2 ft/sec^2)
H_E	Altitude of ejector system above ground level (ft)
h	Altitude of vehicle c.g. (ft)
HP_{excess}	Excess horsepower available for acceleration
I_{xx}	Moment of inertia about X body axis (slug ft^2)
I_{yy}	Moment of inertia about Y body axis (slug ft^2)
I_{zz}	Moment of inertia about Z body axis (slug ft^2)
i_p	Propulsive (core) engine tilt angle (rad or deg)
i_t	Horizontal tail incidence angle (rad or deg)
IFR	Instrument flight rules
l_t	Distance from c.g. to $\bar{c}/4$ of horizontal tail (ft)
l_N	Nose ejector moment arm (ft)
l_p	Length of propulsive (core) engines (ft)
L_1, D_1, M_1	Wing ejector lift, drag, and pitching moment (lb and ft-lbs)
L_2, D_2, M_2	Nose ejector lift, drag, and pitching moment (lb and ft-lbs)
L_3, D_3, M_3	Lift, drag, and pitching moment due horizontal tail (lb and ft-lbs)
M	Pitching moment (ft-lb)
m	Vehicle mass (lb-sec^2/ft)
M_4	Pitching moment due to c.g. shift (ft-lb)
M_{i_p}	Pitching moment derivative due to engine tilt angle i_p $(\frac{1}{I_{yy}} \frac{\partial M}{\partial i_p})$

LIST OF SYMBOLS CONTINUED

M_{i_t}	Pitching moment derivative due to tail incidence angle i_t $(\frac{1}{I_{yy}} \frac{\partial M}{\partial i_t})$
M_q	Pitching moment derivative due to pitch rate q $(\frac{1}{I_{yy}} \frac{\partial M}{\partial q})$
$M_{q_{SAS}}$	SAS pitching moment derivative due to q $(\frac{1}{I_{yy}} \frac{\partial M_{SAS}}{\partial q})$
$M_{q_{TOT}}$	Total pitching moment derivative due to q $(M_q + M_{q_{SAS}})$
M_u	Pitching moment derivative due to u speed perturbation $(\frac{1}{I_{yy}} \frac{\partial M}{\partial u})$
M_{V_J}	Pitching moment derivative due to wing ejector velocity V_J $(\frac{1}{I_{yy}} \frac{\partial M}{\partial V_J})$
$M_{V_{J_P}}$	Pitching moment derivative due to engine exit velocity V_{J_P} $(\frac{1}{I_{yy}} \frac{\partial M}{\partial V_{J_P}})$
M_w	Pitching moment derivative due to vertical velocity w $(\frac{1}{I_{yy}} \frac{\partial M}{\partial w})$
$M_{w_{SAS}}$	SAS pitching moment derivative due to w $(\frac{1}{I_{yy}} \frac{\partial M_{SAS}}{\partial w})$
$M_{w_{TOT}}$	Total pitching moment derivative due to w $(M_w + M_{w_{SAS}})$
M_{T_N}	Pitching moment derivative due to nose ejector thrust T_N $(\frac{1}{I_{yy}} \frac{\partial M}{\partial T_N})$
M_λ	Pitching moment derivative due to ejector door angle λ $(\frac{1}{I_{yy}} \frac{\partial M}{\partial \lambda})$
N_P	Normal force exerted on aft jet engines (lbs)

LIST OF SYMBOLS CONTINUED

$\bar{q}$	Forward speed dynamic pressure (psf)
q	Vehicle pitch rate (rad/sec)
$\bar{q}_E$	Dynamic pressure along center line of downwash (psf)
r_p	Spanwise radial station on proprotor blade (ft)
s	Laplace variable
SAS	Stability Augmentation System
S_H	Horizontal tail area (ft^2)
$S_{H_{modified}}$	Modified horizontal tail area (ft^2)
S_w	Wing reference area (ft^2)
t	Time (sec)
T	Thrust (lbs)
$T_{available}$	Thrust available for acceleration (lbs)
T_N	Thrust of nose ejector (lbs)
T_p	Thrust of aft jet engines (lbs)
T_{total}	Total thrust (lbs)
T/W	Thrust-to-weight ratio
u,w	Velocity perturbations about trim where these velocities are directed along the X and Z axes of a body fixed axis system (fps)
U_d	Up flow through proprotor disk plane as shown in Figure 59 (fps)
U_T	Velocity relative to the rotor blade as shown in Figure 59 (fps)
V	Trim velocity (fps or knots)
V_c	Speed at which conversion is complete (fps or knots)
V_J	Wing ejector efflux velocity (fps)

LIST OF SYMBOLS CONTINUED

V_{J_p}	Propulsive engines exit velocity (fps)
V/V_J	Velocity ratio where V and V_J are defined above
W	Weight of aircraft (lbs)
W_{boom}	Width of the wing booms (ft)
W_p	Width of jet engines at end of fuselage (ft)
X,Z	Components of resultant aerodynamic force along the X and Z axis of a body-fixed axis system as shown in Figure 5 (lbs)
ΔX_{cg}	c.g. shift along X axis (ft)
X_e, Z_e, M_e	Forces and pitching moment on propulsive engines (lbs and ft-lbs)
X_{i_p}	X control derivative due to engine tilt angle i_p $(\frac{1}{m}\frac{\partial X}{\partial i_p})$
X_{i_t}	X control derivative due to tail incidence angle i_T $(\frac{1}{m}\frac{\partial X}{\partial i_t}$
X_p	Horizontal moment arm for aft jet engines (ft)
X_q	X derivative due to q $(\frac{1}{m}\frac{\partial X}{\partial q})$
X_{T_N}	X control derivative due to nose ejector thrust $T_N(\frac{1}{m}\frac{\partial X}{\partial T_N})$
X_u	X derivative due to longitudinal velocity u$(\frac{1}{m}\frac{\partial X}{\partial u})$
X_{V_J}	X control derivative due to wing ejector efflux velocity $V_J(\frac{1}{m}\frac{\partial X}{\partial V_J})$
$X_{V_{J_p}}$	X control derivative due to aft jet engine exit velocity V_{J_p} $(\frac{1}{m}\frac{\partial X}{\partial V_{J_p}})$
X_w	X derivative due to vertical velocity perturbation w $(\frac{1}{m}\frac{\partial X}{\partial w})$

LIST OF SYMBOLS CONTINUED

$X_\delta, Z_\delta, M_\delta$	Control derivatives (general)
X_λ	X control derivative due to ejector door angle $\lambda (\frac{1}{m} \frac{\partial X}{\partial \lambda})$
Z_{i_p}	Z control derivative due to engine tilt angle $i_p (\frac{1}{m} \frac{\partial Z}{\partial i_p})$
Z_{i_t}	Z control derivative due to tail incidence angle $i_t (\frac{1}{m} \frac{\partial Z}{\partial i_t})$
Z_p	Vertical moment arm for aft engines (ft)
Z_q	Z derivative due to q $(\frac{1}{m} \frac{\partial Z}{\partial q})$
Z_{T_N}	Z control derivative due to nose ejector thrust $T_N (\frac{1}{m} \frac{\partial Z}{\partial T_N})$
Z_u	Z derivative due to forward speed perturbation $u (\frac{1}{m} \frac{\partial Z}{\partial u})$
Z_{V_J}	Z control derivative due to wing ejector efflux velocity $V_J (\frac{1}{m} \frac{\partial Z}{\partial V_J})$
$Z_{V_{J_p}}$	Z control derivative due to engine exit velocity $V_{J_p} (\frac{1}{m} \frac{\partial Z}{\partial V_{J_p}})$
Z_w	Z derivative due to vertical velocity perturbation $w (\frac{1}{m} \frac{\partial Z}{\partial w})$
Z_λ	Z derivative due to ejector door angle $\lambda (\frac{1}{m} \frac{\partial Z}{\partial \lambda})$
α	Angle of attack (rad or deg)
α_p	Proprotor angle of attack (rad)
Δ	A symbol used in the characteristic equation
δ_e	Elevator deflection angle (deg or rad)

LIST OF SYMBOLS CONTINUED

θ	Vehicle pitch angle (rad or deg)
θ_b	Blade collective angle as shown in Figure 59 (rad)
ϕ	Vehicle roll angle (rad or deg)
ϕ_b	Blade inflow angle as shown in Figure 59 (rad)
ψ	Yaw angle (rad or deg)
ψ_b	Blade azimuth angle as shown in Figure 59 (rad or deg)
$(\Delta\theta/\Delta V)$	Trim change parameter (deg/knot)
λ	Ejector door angle (rad/deg)
ρ	Density ($slugs/ft^3$)
ν	Induced downwash into proprotor disk plane (fps)
ω	Damped natural frequency ($\omega_n\sqrt{1-\xi^2}$)
ω_n	Natural frequency (sec^{-1})
Λ	Proprotor rotational speed (rad/sec)
ζ	Damping ratio
$\zeta_1, \zeta_2, \zeta_3$	Angular regions of pilot visibility (rad)
$\dot{} = \frac{d}{dt}$	Derivative with respect to time

Other symbols are defined at the point of use.

SECTION I

INTRODUCTION

This analysis was performed to investigate the longitudinal stability and control characteristics of an ejector wing configuration during transition (Figures 1 and 2). A linear or derivative approach was used to obtain dynamic responses about specified trim speeds in the transitional flight corridor. Analysis of these responses provided an insight into the significant characteristics in the dynamic response of the vehicle that might affect the pilot's control over the aircraft. By this means, some of the flying qualities of the unaugmented vehicle were evaluated. When the handling qualities of this configuration were found to be deficient according to Reference 1, modifications to the vehicle geometry and two feedback loops of a Stability Augmentation system (SAS) were considered to improve the handling characteristics.

In addition to the above, a longitudinal stability and control evaluation was conducted for the Sikorsky stowable rotor configuration (see Figure 3 and Reference 2). This part of the effort was performed to make comparisons between the thrust requirements and the handling characteristics of an ejector wing configuration and a stowable rotor aircraft in hover and during transition.

Reference 1 contains the flying qualities requirements for V/STOLs from hover through transitional flight.

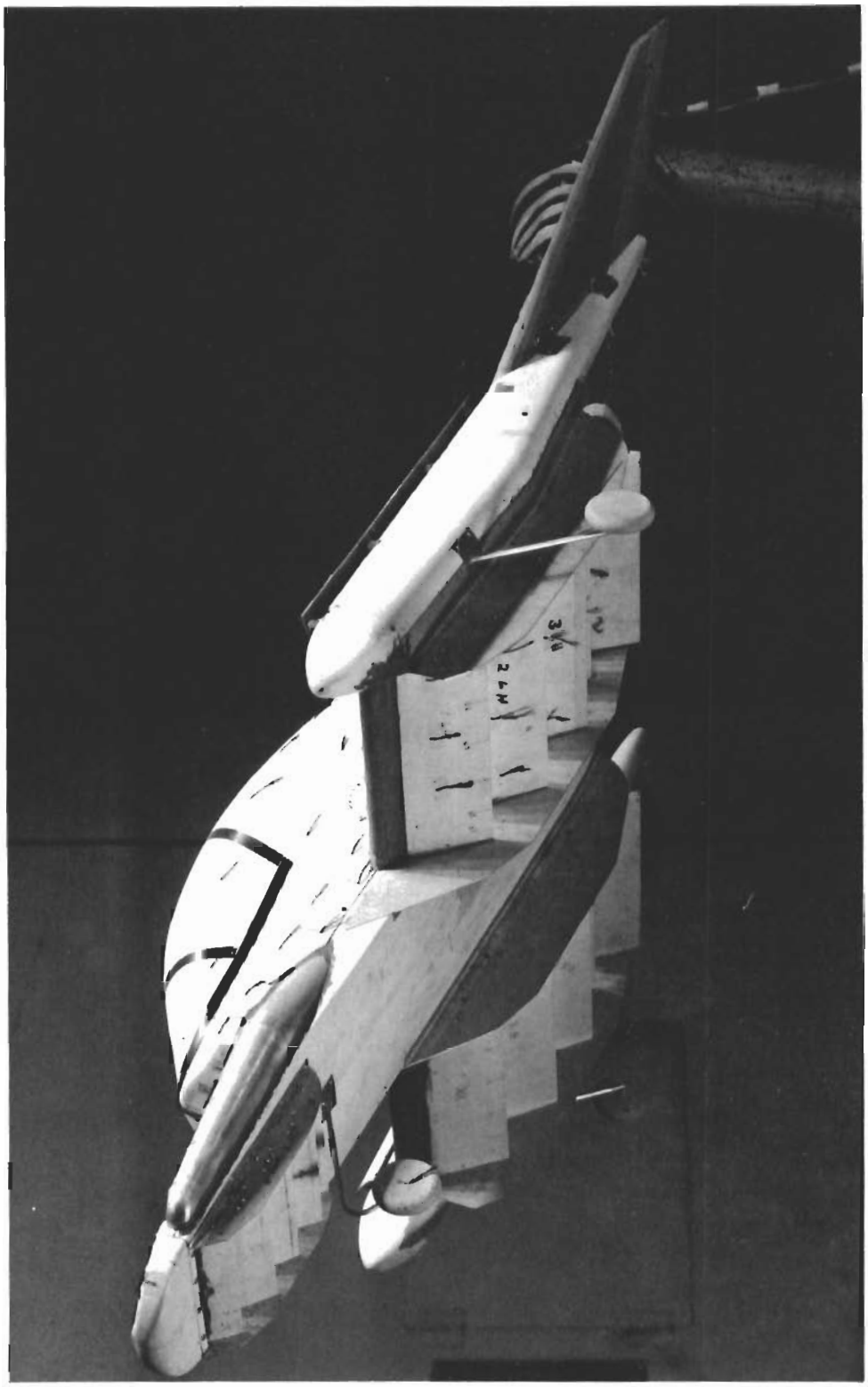

Figure 1. Model of Ejector Wing Configuration

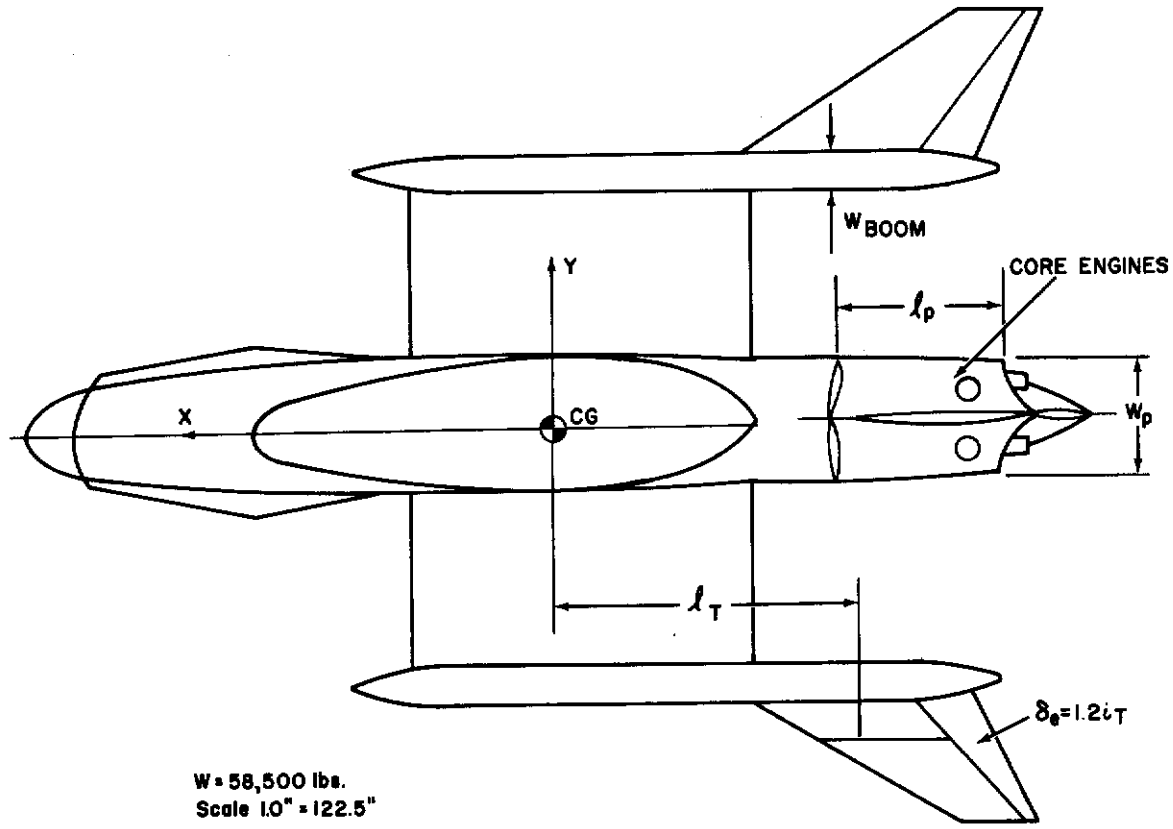

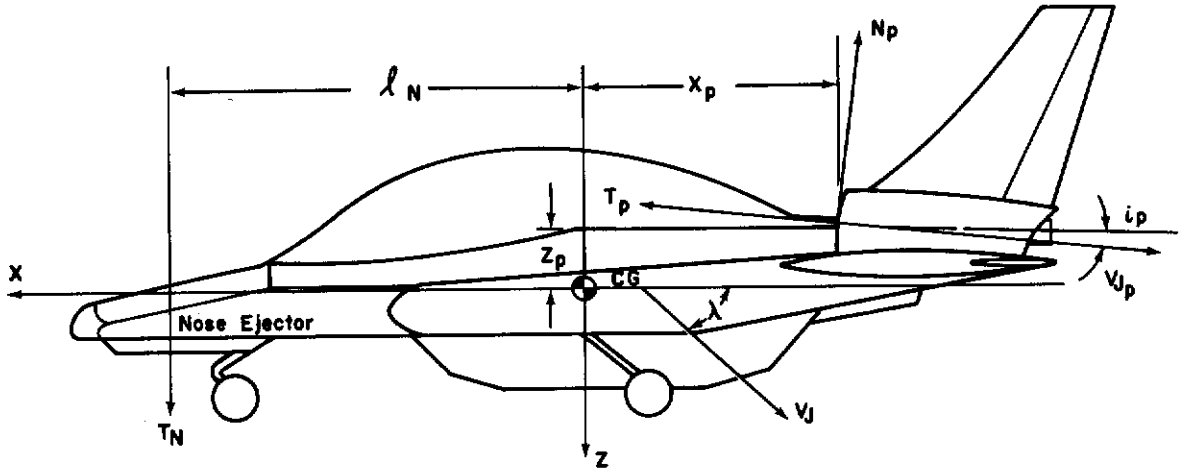

Figure 2. Schematic of Ejector Wing Configuration

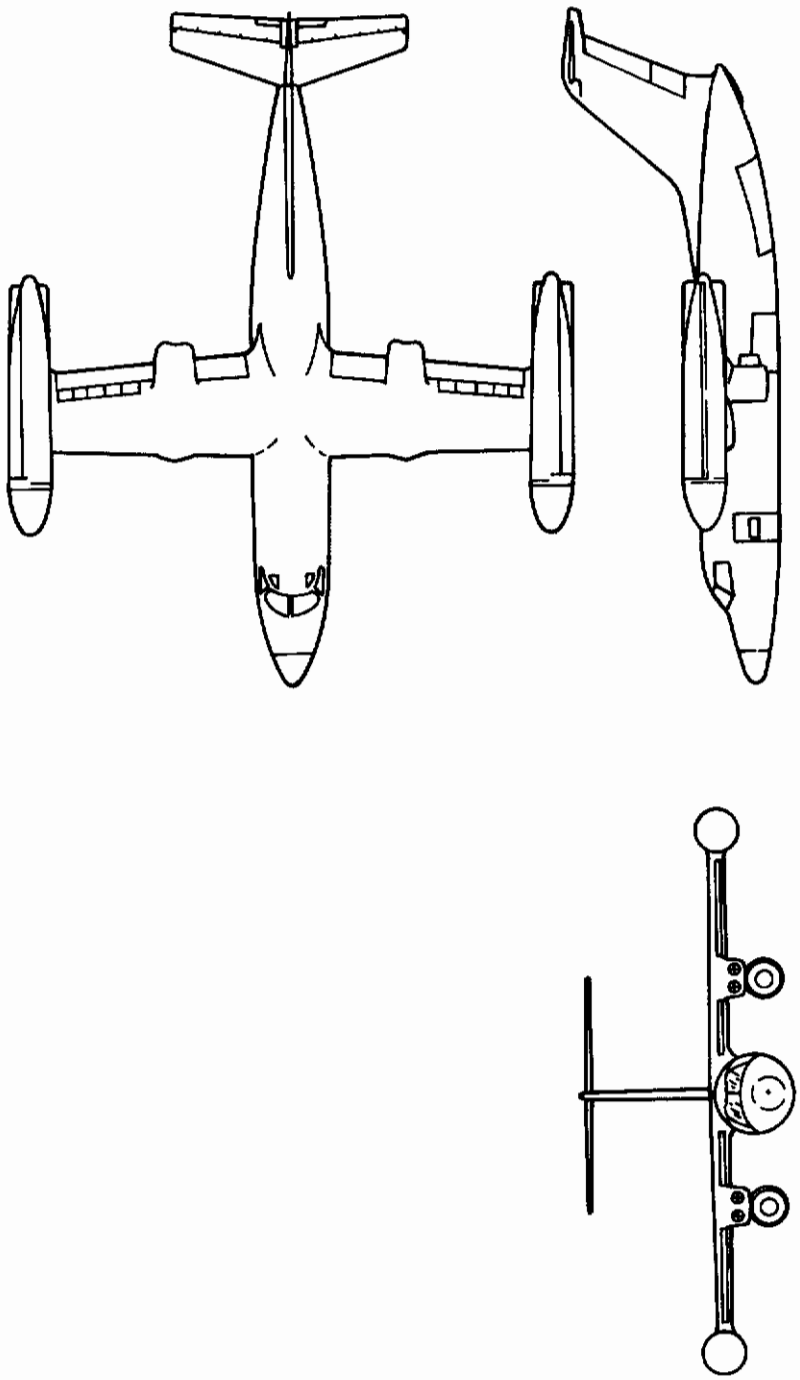

Figure 3. Rescue/Recovery Aircraft

This specification classifies the wing ejector configuration and the Sikorsky stowable rotor vehicle as Class II type aircraft, which means they are medium weight, low-to-medium maneuverability concepts. This classification includes such aircraft as utility, search and rescue, medium transport/cargo/tanker, antisubmarine, assault transport, reconnaissance, heavy attack, and trainers for Class II type vehicles.

Three levels are used to categorize the flying qualities in the specification:

Level 1: The flying qualities of the concept are clearly adequate for the fulfillment of the mission.

Level 2: The flying qualities are such as to increase the work load of the pilot and/or degrade mission effectiveness. The mission, however, can be fulfilled.

Level 3: The flying qualities of the vehicle are such that the workload of the pilot is excessive and/or mission effectiveness is inadequate.

Level 1 is to be met for normal operation, while Levels 2 and 3 allow degradations in infrequently encountered conditions, including failure state.

The specification provides the criteria that vehicles must meet to be categorized in these levels. These tests were applied to the ejector wing and stowable rotor configurations in evaluating their flying qualities. No effort was made to include the effects of component

failure, cg shift due to component failure, fuel sequencing, intolerable buffet, structural vibrations and flexibility, perturbations due to gusts, internal mechanics of the controls (i.e., servo valves and actuators), and internal system design due to the addition of a SAS since these considerations were felt to be beyond the scope of this study. Matters concerning takeoff, landing, and ground handling, power run-up, cold and wet-weather operation, and related topics have not been included in this evaluation.

The report summarizes the analysis for determining the longitudinal aerodynamic representation for the ejector wing configuration and discusses the aerodynamic representation of the Sikorsky stowable rotor vehicle. The results of the flying qualities evaluation are presented as well as the effects of downwash on ground personnel and on the safety of the vehicle during hover. The concluding remarks and recommendations are based on results of these analyses. Appendices I, II, and III provide backup information.

SECTION II

ANALYSIS DETERMINING VEHICLE FLIGHT CHARACTERISTICS

1. PRELIMINARY ANALYSIS

The usual practice in a stability and control analysis is to assume that the aerodynamic loads can be expanded in a Taylor series about an equilibrium trimmed flight condition and that only the first term in this expansion is important. This leads to a linear model for the aerodynamic representation, commonly known as a set of "stability derivatives," which lend themselves quite well to classical linear analyses, although rigorous application is limited to small departures from the equilibrium trimmed flight point. The equations of motion simplify to differential equations with constant coefficients and the question of whether the system is stable or not can be determined by the use of Routh's method (Reference 3). The characteristic equation of the equations of motion can be used to obtain the flight modes and root loci, while the transfer functions yield the response to any prescribed input. Further simplification, obtained by assuming that the longitudinal and lateral equations of motion are decoupled, leads to two sets of three equations each. These sets can be dealt with separately. The important thing here is that simple closed-form analytical solutions can be obtained without solving the equations of motion by means of some numerical integration scheme.

The validity of using the above approach here is subject to question. The aerodynamic forces and moments exerted on a V/STOL in transition can be highly nonlinear with large excursions from the

equilibrium flight condition. For example, angle of attack and sideslip excursions of $\pm 90°$ are possible even for modest perturbations in plunge and sideslip velocities near hover. In addition, the aerodynamic coefficients in the equations of motion are varying with time as the ejector doors are closed or opened in the case of the ejector wing configuration, so that the use of constant coefficients in these equations is not valid. Also, large accelerations can be experienced by the V/STOL in transition, and the vehicle is rarely in a state of equilibrium during this mode of flight. Finally, V/STOL's such as helicopters and tilt rotor configurations are highly coupled between the longitudinal and lateral modes so that the full six degrees of freedom equations of motion should be used to obtain the flight characteristics of this type of vehicle.

To be rigorous then, an analysis of a V/STOL's flight characteristics during transition should be performed by using a nonlinear set of aerodynamics with nonlinear equations of motion in 6-degree-of-freedom. This course means that an analytical solution to the equations is unlikely and that the equations would have to be solved by using a numerical integration scheme on a digital computer. An example of such an analysis is given in Reference 4.

Nevertheless, the linear or derivative approach discussed above was used for a preliminary evaluation. We felt that sufficient information could be obtained to at least indicate or suggest that the ejector wing and stowable rotor concepts may have good flying capabilities. If the handling characteristics of these vehicles were

found to be deficient, fixes such as modifications to the vehicle geometry or the inclusion of a SAS in the system could be readily investigated by this type of analysis.

2. AERODYNAMIC REPRESENTATION OF THE WING EJECTOR CONFIGURATION

Wind tunnel data exist for the aerodynamic forces and moments exerted on a model of a V/STOL with a cold thrust ejector in the wing. The model used in the wind tunnel test program and shown in Figure 1 is a 1/5 scale version of the 13,000 lb Research Test Vehicle or RTV (References 5 and 6). The wind tunnel data obtained with this model was scaled up to a configuration weighing 58,500 lbs. We felt that such a representation would be sufficiently accurate for a preliminary analysis of the handling characteristics of an ejector wing air rescue aircraft of the Class II type (Reference 1). No corrections were made for Reynolds number effects in scaling the data since adequate data is not available at this time to make this correction for a wing ejector type system.

The results of the aerodynamic data analysis for the ejector wing configuration is discussed in full in Appendix I. The vehicle is shown in Figure 2. The wing cross section is indicated in Figure 4 and the stability and body axes for this configuration are given in Figure 5. In addition, relevant dimensions, areas, weights and inertias for this configuration are presented in Table I.

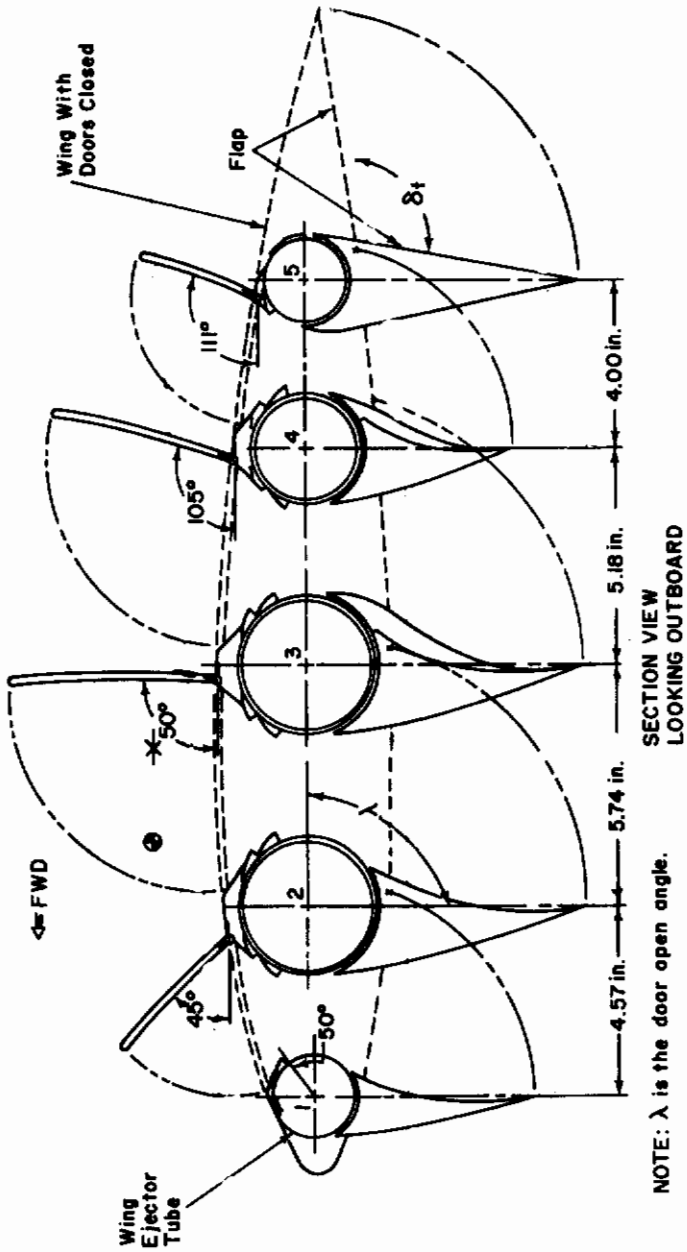

Figure 4. Wing Model Cross Section

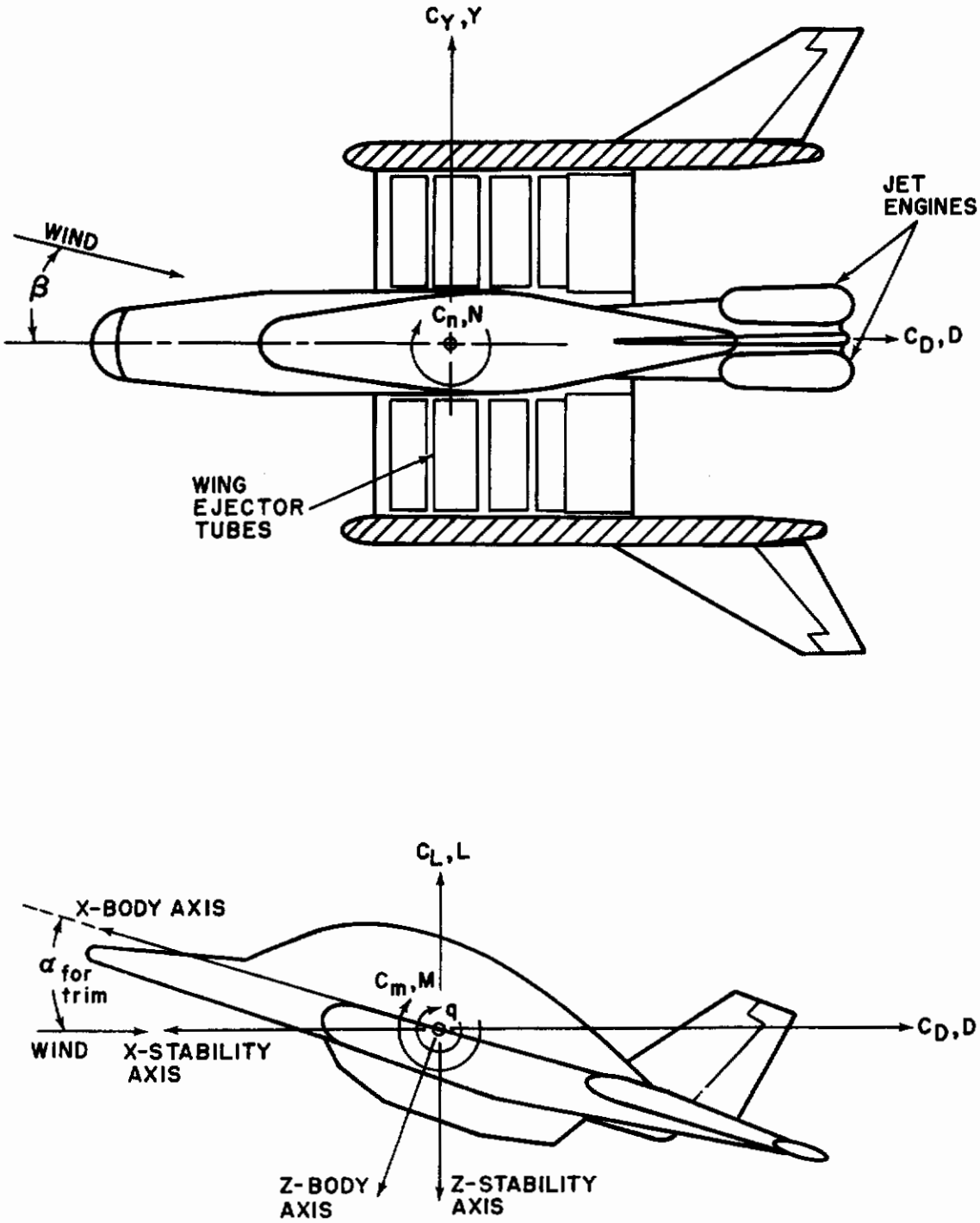

Figure 5. Stability and Body Axis Systems

TABLE I. EJECTOR WING CONFIGURATION

DESIGN PARAMETERS

Design Gross Weight, lb.	58,500
Wing	
Area, ft^2	835.7
Span, in	420.
Root Chord, in	286.
Tip Chord, in	286.
M.A.C., in	286.
Taper Ratio	1.0
Sweep @ $0.25\bar{c}$, deg	0
Airfoil Section	64_2A215(Modified)
Horizontal Tail	
Area, ft^2	111.
Span, in	118.5
Root Chord, in	206.
Tip Chord, in	63.2
M.A.C., in	148.
Taper Ratio	0.307
Airfoil Section	0010
Sweep @ $0.25\bar{c}$, deg	56.35
Vertical Tail:	
Area, ft^2	113.4
Span, in	165.5
Root Chord, in	137.5
Tip Chord, in	58.8

TABLE I (CONTINUED)

Taper Ratio	0.4
M.A.C., in	102.5
Airfoil Section	0010
Fuselage:	
Length of Body, in	650.
Width of Body, in	111.5
Height of Body, in	153.
Length of Boom, in	559.
Width of Boom, in	28.5
Height of Boom, in	68.
ℓ_T(From tail ac to cg), in	283.
ℓ_N(From nose ejector to cg), in	341.
Center of Gravity (% $\bar{c}$)	36.
Moments of Inertia: slugs-ft^2	
I_{xx}	251,000.
I_{yy}	286,000.
I_{zz} where the cg is located at the 36%$\bar{c}$	515,000.
Engines:	
X_p (Horizontally from cg to N_p), in	336.5
Z_p (Vertically from cg to N_p), in	47.7
Core Engine Exit Area, ft^2	19.95
Nose Ejector Exit Area, ft^2	50.3

NOTE: Moment of inertia variation with cg shift or change in vehicle weight have not been computed.

The aerodynamic data for the Sikorsky stowable rotor configuration is discussed in Reference 2. The vehicle is shown in Figure 3, and relevant design parameters are given in Tables II, III, and IV.

3. TRIM ANALYSIS, GENERAL

The linearized set of longitudinal equations of motion used in this evaluation describes transient behavior of the vehicle about a trimmed condition. Therefore, the equilibrium condition of the vehicle at preselected trim speeds V through transition must be determined before the equations of motion are applied. For simplicity, it was assumed that most of the transition would be flown with a zero angle of attack schedule and that altitude would be kept constant at 3000 ft during a 90°F day. This meant that $\dot{h} = \theta = \alpha = 0$ and that the trim equations (Equation 16 of Appendix I) became

$$\begin{aligned} X &= 0 \\ Z + mg &= 0 \\ M &= 0 \end{aligned} \qquad (1)$$

where X, Z, and M are the forces and moments including aerodynamic and thrust effects about the body-fixed axis system, as shown in Figure 5. Appendix I presents details concerning the formulations of X,Z, and M reactions.

4. TRIM ANALYSIS EJECTOR WING CONFIGURATION

Equation 1 was used in solving for trim for the ejector wing configuration shown in Figure 2. Two assumptions were used: (1) the hot core gas from the propulsive engines at the rear of the fuselage

TABLE II. SIKORSKY STOWABLE ROTOR CONFIGURATION

DESIGN PARAMETERS

Design Gross Weight, lbs	65,000
Design Hover Gross Weight, lbs	56,400
Design Hover Disk Loading, psf	15
Vertical Load Factor Limit	3
NRP Cruise Speed, kts	390
Cruise Altitude, ft	10,000
Equivalent Flat Plat Area, ft^2	19.6
Internal Fuel Capacity, lbs	10,601
Rotors	
Radius, ft	25.5
Chord, ft	2.4
No. of Blades/Rotor	5
Blade Twist, deg	-25
Solidity	0.15
Blade Aspect Ratio	10.6
Tip Speed, fps	750
Wing	
Area, ft^2	650
Span, ft	60.8
Aspect Ratio	5.68
Wing Loading, psf	100
Sweep @ 0.25c, deg	0
Airfoil Thickness Ratio	0.18

TABLE II (CONTINUED)

Planform Taper Ratio	0.7
Root Chord, ft	12.58
Tip Chord, ft	8.81
Usable Fuel Capacity, lbs	9,364
Vertical Tail	
Area (effective), ft^2	191
Area (exposed), ft^2	167
Span, ft	16.9
Aspect Ratio	1.5
Sweep @ 0.25c, deg	36
Airfoil Thickness Ratio	12
Taper Ratio	0.5
Root Chord, ft	15.08
Tip Chord, ft	7.54
Moment Arm (Wing ac to Tail ac), ft	33.6
Volume Coefficient	.162
Horizontal Tail	
Area, ft^2	164
Span, ft	27.2
Aspect Ratio	4.5
Sweep @ 0.25c, deg	15
Airfoil Thickness Ratio	0.12
Taper Ratio	0.5
Root Chord, ft	8.04
Tip Chord, ft	4.02
Moment Arm (Wing ac to Tail ac), ft	43.3
Volume Coefficient	1.01

TABLE II (CONTINUED)

Fuselage	
Surface Area, ft^2	2,084
Length, ft	72.3
Depth, ft	10.25
Cabin Length, ft	30
Cabin Height, ft	7
Cabin Width, ft	7.75
Propulsion	
Gas Generators (GE1/10J1)	
Number	4
Design Scale Factor	0.408
Emergency Rating Scale Factor	0.440
Remote Power Turbines	
Number	4
Design Mass Flow, lb/sec	30.8
Remote Cruise Fans	
Number	2
Design Mass Flow, lb/sec	57.1
Drive System	
Power Turbine Output	
Horsepower/Turbine	4,215
Design Speed, rpm	15,000
Cross Shaft	
Horsepower	6,320
Design Speed, rpm	7,000
Rotors	

TABLE II (CONTINUED)

Horsepower/Rotor	6,100
Design Speed, rpm	281

TABLE III

CENTER OF GRAVITY DATA

(Design Gross Weight)

Mode	Fuselage Station, in		% MAC	
	Fwd	Aft	Fwd	Aft
Helicopter	386.0	415.5	12.8	36.9
Proprotor	375.5	405.8	4.0	28.9
Fan	382.2	410.7	9.7	32.9

TABLE IV

MOMENT OF INERTIA SUMMARY

(Design Gross Weight)

Mode	Moment of Inertia, slug-ft^2			
	Ixx	Iyy	Izz	Ixz
Helicopter	564,000	268,700	735,700	32,100
Proprotor	543,700	253,100	740,400	28,800
Fan	546,900	264,000	748,100	30,700

could be diverted at an angle i_p to the body-fixed X-axis to provide pitch moment at low transitional flight speeds; and (2) assumed that the nose ejector (Figures 1 and 2) would not be used during transition for maneuvering. At low transitional speeds near hover, all pitch moment trimming or balancing was performed by the diverted hot core gas at the propulsive engines and not by the horizontal stabilizer; horizontal surface trimming capability is negligible at low forward flight speeds. On the other hand, near the completion of transition all of the pitch moment trimming was performed by the horizontal stabilizer. The transition from propulsive engine tilt to horizontal deflection to supply trim pitching moment occurred in an approximately linear fashion between 40 and 110 knots.

The results of the trim computations for the ejector wing vehicle are shown in Figures 6 through 13, together with the results for a modified version of this aircraft. The modification produced a 10% increase in horizontal tail surface area, which was made to improve the static stability of the vehicle at the mid to high transitional speed range. This modification increased vehicle weight from 58,500 to 58,633 lbs, and increased the inertia I_{yy} by 3620 slugs-ft^2. Otherwise the two configurations were physically identical, with the center of both vehicles located at 36%$\bar{c}$. The additional weight and inertia due to the larger tail and the additional ballasting necessary to maintain the same c.g. was determined from data given in Reference 7.

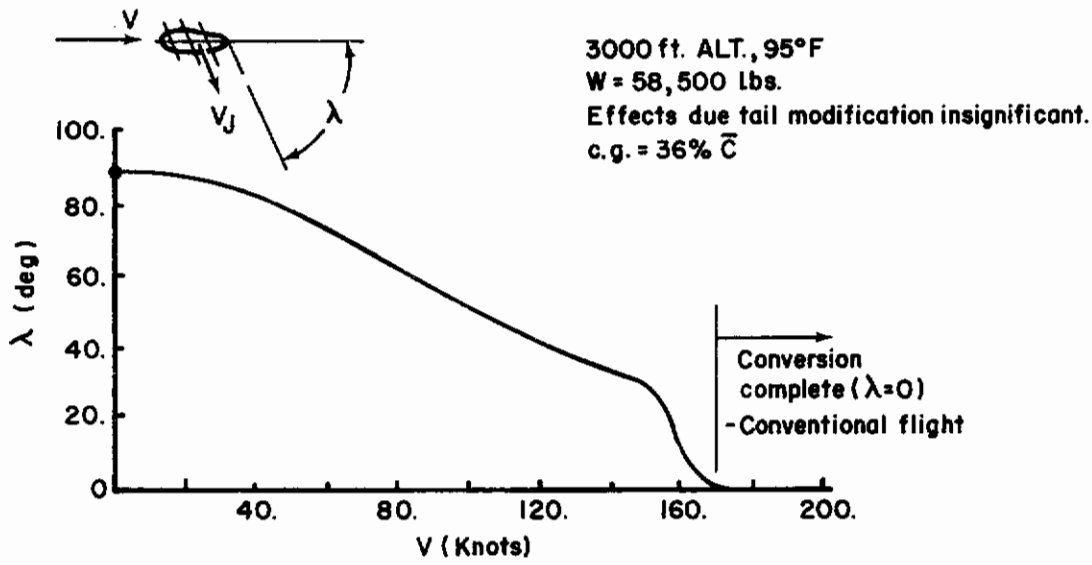

Figure 6. Ejector Door Angle Schedule, Trim

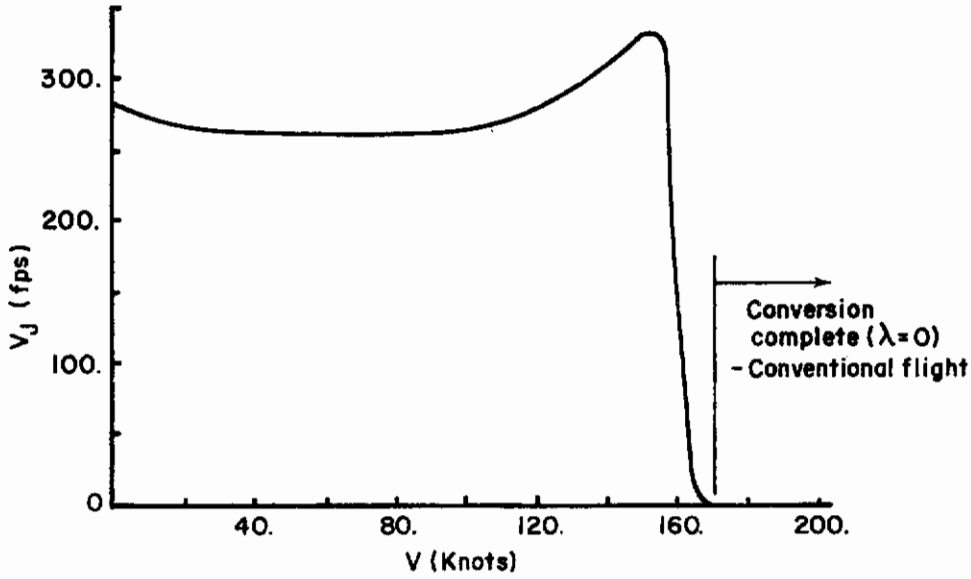

Figure 7. Ejector Efflux Velocity Required for Trim

No consideration was given to the effects of this change on the aeroelastic behavior or upon the structural integrity of the configuration. As mentioned previously, these considerations were beyond the scope of this study.

Figure 6 gives the scheduled variation of wing ejector door angle λ with transitional flight velocity. Starting with $\lambda = 90°$ in hover, these doors are slowly rotated with increase in velocity until they are sealed at V = 170 knots. At this speed, the wing ejector system is not in use and the vehicle has completed transition to the conventional flight regime. Figure 7 gives the wing ejector efflux velocity required to maintain altitude and a constant trim speed as transition progresses. Again, the ejector is turned off when transition is complete at 170 knots.

Figure 8 gives the angle of attack schedule followed during this transition. Zero angle of attack was maintained up to 150 knots into the conversion; the ejector door angle λ was 30° at this point. Between 150 and 170 knots the doors were closed off and the vehicle rotated by the pilot to approximately 14° at completion of conversion. Little or no stall margin remains at this angle of attack, and the results indicate that transition should have been completed at a higher flight speed. This would have permitted entry into the conventional flight mode at a lower and more reasonable trim angle of attack. No attempt was made to determine the optimum transitional flight path. Many paths exist within the permissible flight corridors for transition from hover to forward flight, but this analysis considers only one. Establishing permissible flight corridors

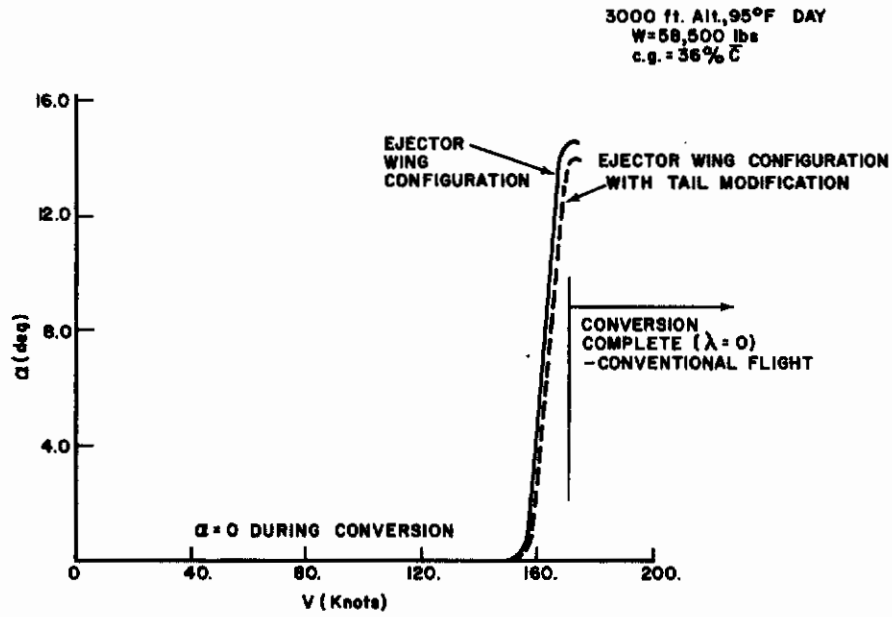

Figure 8. Angle of Attack Schedule, Trim

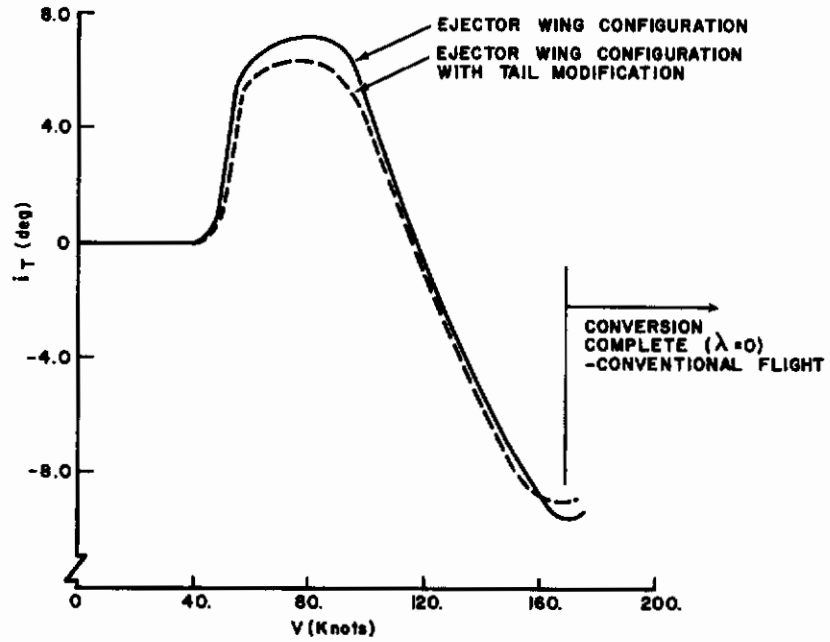

Figure 9. Elevator Angle Schedule, Trim

through transition and determining the optimum flight scheme for performing conversion were beyond the scope of this study.

The results indicate that for the configuration used in this analysis, transition should not be completed before V = 170 knots. This presumes that the flap system is actuated directly with the wing ejector door, so that $\delta_f = \lambda$ (Figure 4). The flaps are assumed to be completely retracted when the wing ejector system is closed, so the vehicle enters the conventional flight mode in the "clean" configuration. (Flap actuation is discussed further in Appendix I.) The conversion flight speed could be lowered by providing an additional ΔC_L margin with a flap system that can be operated independently of the wing ejector system.

Figures 9, 10, and 11 give the horizontal surface deflection angle i_T (the elevator is geared to the horizontal such that $\delta_e = 1.2\ i_T$), the propulsive engine exit velocity V_{J_P}, and the propulsive engine tilt angle i_p as a function of trim speed. As mentioned previously, the horizontal surface is ineffective for providing trim pitching moment at low forward speeds; therefore, i_T was maintained at zero below V = 40 knots (Figure 9). Here the pitching moment required to trim was produced by tilting the propulsive engine thrust relative to the body fixed axis (Figures 10 and 11). Use of the horizontal surface to provide trim moment is phased in between 40 and 110 knots, and the propulsive engine is gradually phased out, until the horizontal surface

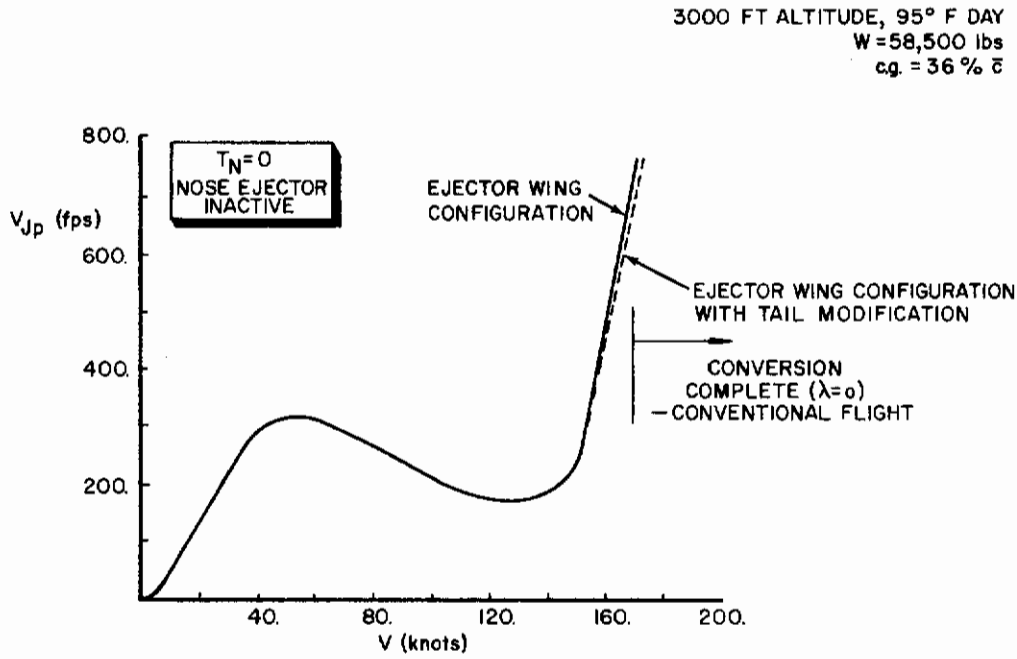

Figure 10. Propulsive Engine Efflux Velocity, Trim

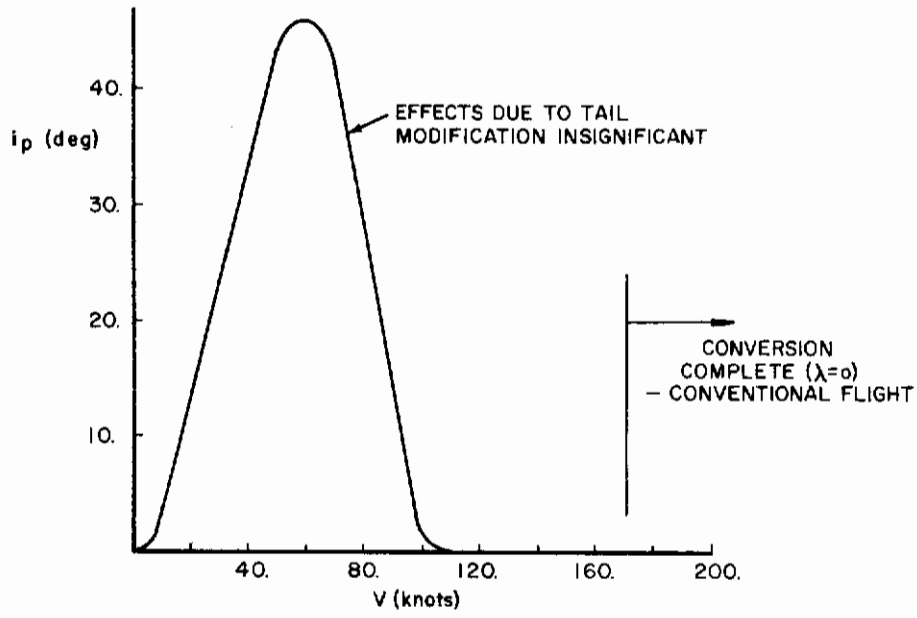

Figure 11. Propulsive Engine Tilt Angle, Trim

carries all of the control load at $V \geq 110$ knots. This is seen in Figure 11, where $i_p = 0$ for $V \geq 110$ knots and the propulsive thrust vector is parallel to the X-axis of the body-fixed axis system.

Figure 12 gives the total trim thrust required throughout this transition. This thrust does not include additional margins necessary for maneuvering the vehicle in pitch and climb and for the operation of a SAS. Nor does it include losses due to inefficiencies in the propulsive engines and the ejector system, and frictional losses in the ducting between the engines and the wing ejector. Figure 13 presents the same total trim thrust as given in Figure 12 but in terms of thrust-to-weight ratio.

5. TRIM ANALYSIS STOWABLE ROTOR CONFIGURATION

The static trim analysis at preselected trim speeds V through a nominal transition was performed for the Sikorsky stowable rotor configuration. Results are given in detail in Reference 2. Trim in the rotor mode of flight was performed with $\dot{h} = \theta = \alpha = 0$. In addition, data given in Reference 8 for this vehicle suggest that the nominal transition may have been performed at an altitude of 2500 ft and for a 93°F day. These values for trim pitch attitude, altitude, and temperature correspond reasonably well to the values selected in trimming the ejector wing configuration during its nominal transition discussed above.

During hover, the proprotors are aligned vertically or at a zero shaft tilt angle (Figure 14). Climb control is obtained by simultaneous application of collective pitch to both proprotors

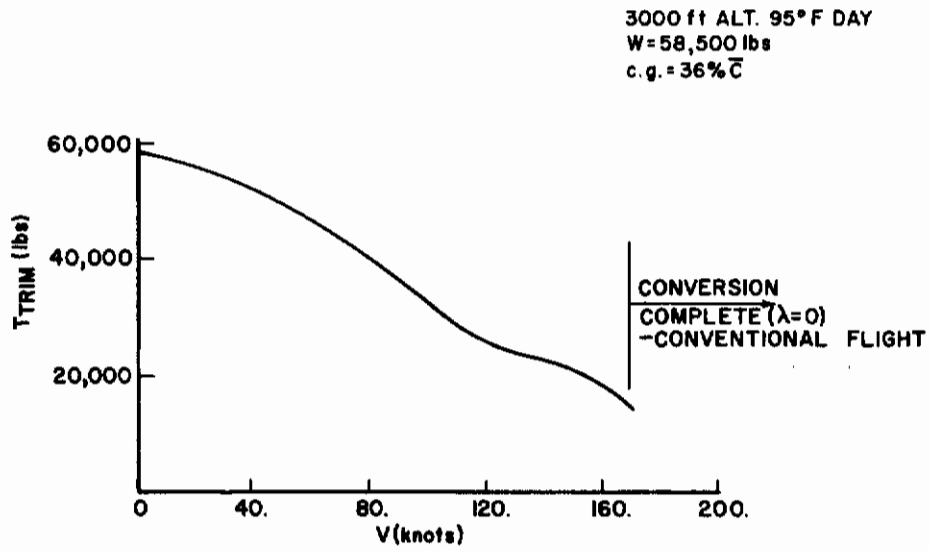

Figure 12. Thrust Required for Trim

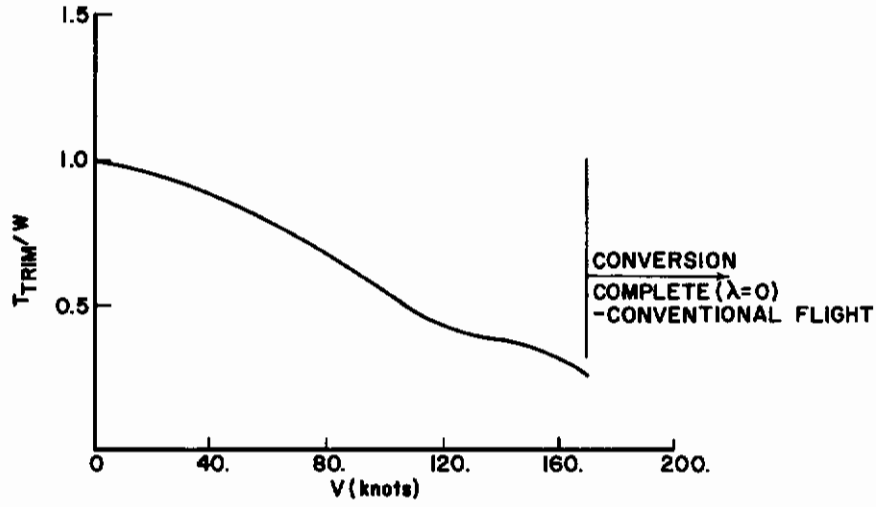

Figure 13. Thrust-to-Weight Ratio for Trim

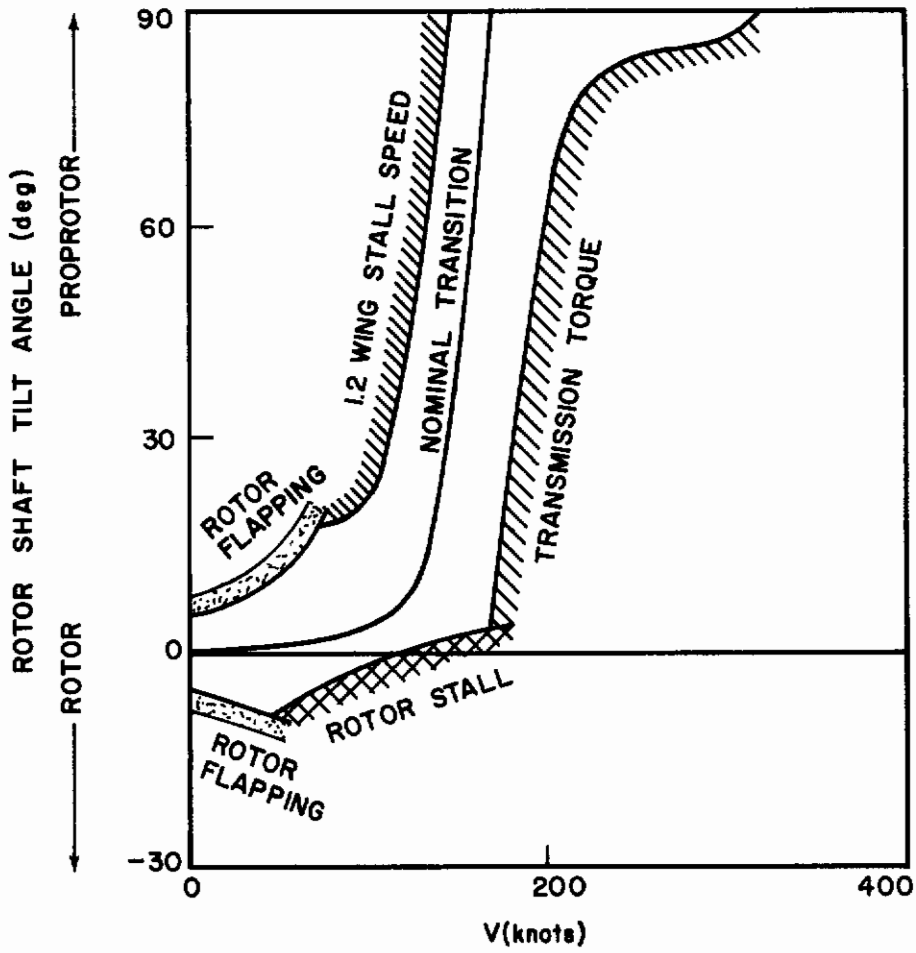

Figure 14. Transition Constraints, Stowable Rotor Configuration

(Figure 15); pitching moments are generated by applying longitudinal cyclic pitch (Figure 16); roll control is obtained by differential pitch between the left and right proprotors; and yaw moments are generated by differential longitudinal cyclic control between the two proprotors. At approximately 160 knots into the nominal transition, the total pitch control load is carried by the elevator (Figure 16). In addition, the proprotors complete conversion to a shaft tilt angle of 90° at this transitional forward flight speed and operate in the propeller state where the velocity vector is aligned with the shaft axes of the proprotors (Figures 14 and 15). Cruise speeds up to 236 knots are possible in this mode of flight according to Reference 2. If higher forward flight speeds are desired, power is transferred from the proprotors to the cruise fans shown in Figure 3. The proprotors are feathered, decelerated to a stop, and folded rearward into slots in the wing tip pylons.

This stowable rotor configuration completes conversion to the propeller mode of flight at approximately 160 knots. The vehicle flies in the conventional flight mode as a propeller driven aircraft for V > 160 knots if blade fold and stow procedures are not initiated. The ejector wing configuration of Figure 1 completes conversion to the conventional flight mode at approximately the same speed in the nominal transition discussed above. Figure 6 was the scheduled variation of wing ejector door angle λ with transitional flight velocity. The doors are rotated with increasing forward velocity until they are sealed at V = 170 knots.

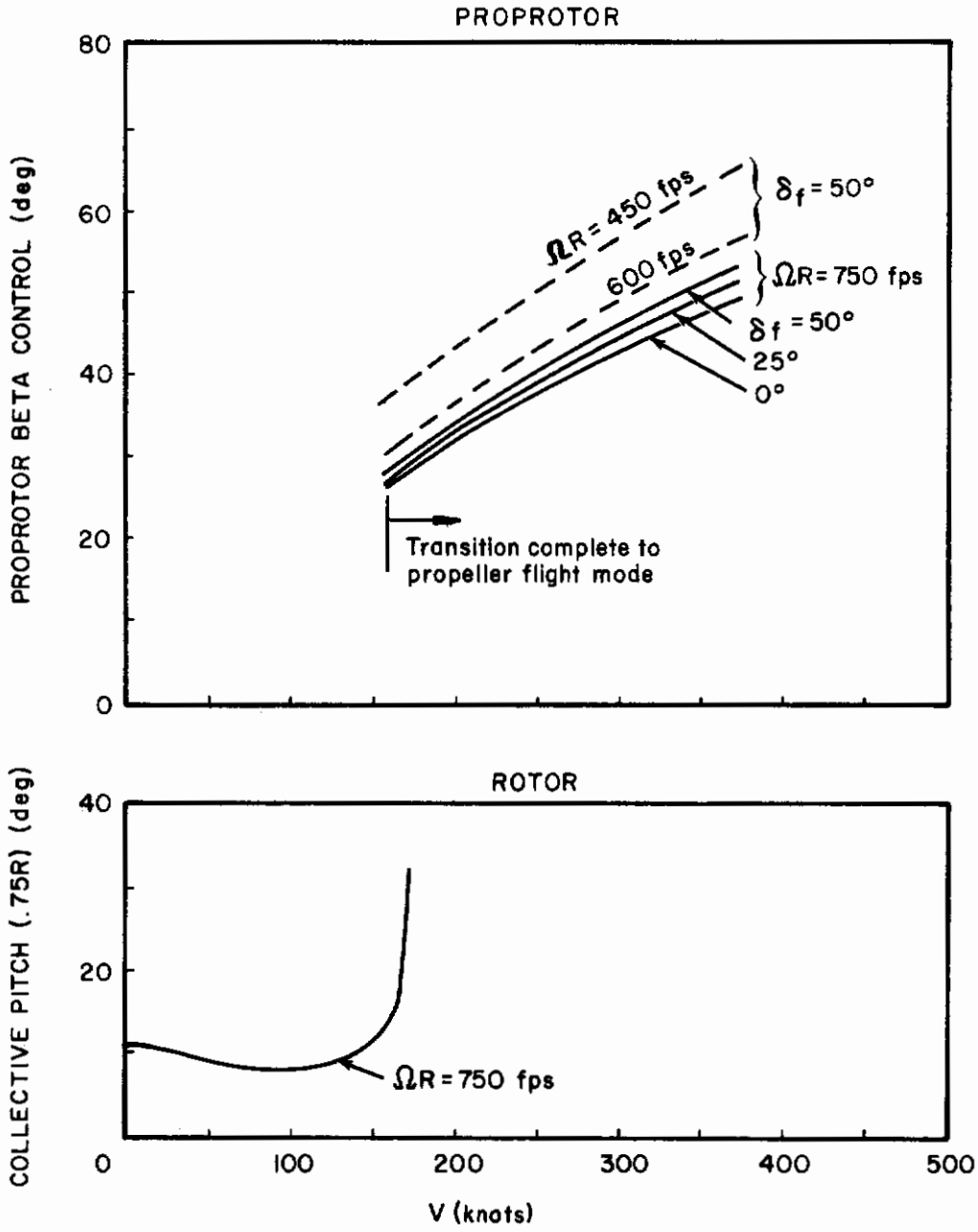

Figure 15. Blade Pitch Control Requirements

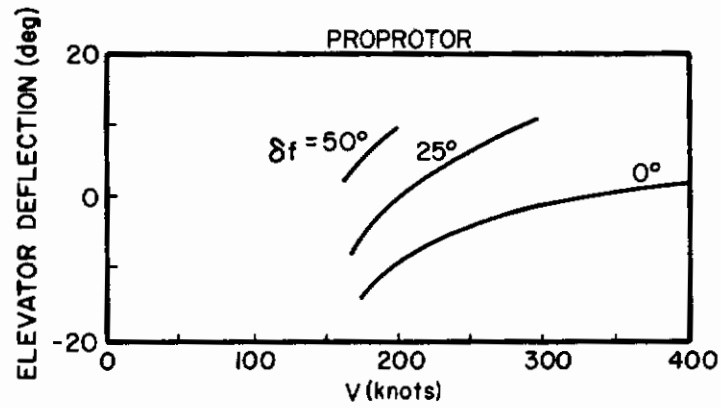

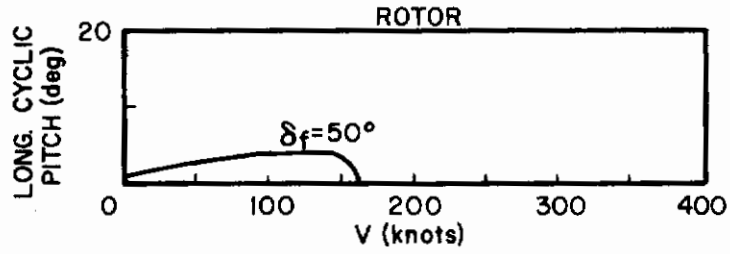

Figure 16. Trim Longitudinal Control Requirements

6. STABILITY DERIVATIVES EJECTOR WING CONFIGURATION

The linearized equations of motion describing transient behavior about the above trimmed flight conditions are:

$$\begin{aligned} \dot{u} + g\theta &= X_u u + X_\delta \delta \\ \dot{w} - V\dot{\theta} &= Z_u u + Z_w w + Z_\delta \delta \\ \ddot{\theta} &= M_u u + M_w w + M_q \dot{\theta} + M_\delta \delta \end{aligned} \tag{2}$$

where the force derivatives are divided by vehicle mass m and the pitching moment derivatives are divided by vehicle inertia I_{yy}.

Note that X_w, X_q, $X_{\dot{w}}$, $Z_{\dot{w}}$, and Z_q derivatives have been excluded from the force equations. These derivatives are not significant for single and tandem helicopters, 2 and 4 propeller tilt proprotor and tilt wing V/STOLs, or for the Bell X-22A tilt duct configuration (Reference 9). In addition, $M_{\dot{w}}$ has been excluded from the pitching moment equation because experimental data is insufficient to evaluate this derivative for V/STOLs. Experimental techniques usually measure the combined total of $(M_q + M_{\dot{w}})$. Curtiss (Reference 9) suggests that the $M_{\dot{w}}$ contribution may be small and that the measured data for the combination of $(M_q + M_{\dot{w}})$ reflects the M_q contribution above. This study is preliminary however, and these derivatives may need to be evaluated for an in-depth study.

These equations including relevant assumptions are discussed in Appendix I, together with the derivation of the stability derivatives from the aerodynamic model of the ejector wing configuration. The

results of the analysis are shown in Figures 17 through 22. The above equations are written in the stability axis system. This system coincides with the body axis system (Figure 5) when $\alpha=\theta=0$, or for $V \leq 150$ knots in the transitional flight schedule.

The u and w derivatives were analytically determined for the unaugmented ejector wing configuration; let us compare these to the derivatives of other V/STOLS to get an indication of how the ejector wing configuration might behave in transition. If these derivatives were similar to those of a helicopter, we might expect similar transitional flight behavior and similar problems in terms of handling qualities; thus the means used in overcoming these problems for the helicopter may also be applicable here. At least, an indication could be obtained as to what type of SAS might be used to improve the handling qualities of the ejector wing configuration and what types of feedback loops might be exercised.

The results of the comparisons are shown in Figure 17 through 21. Data for the other V/STOL concepts was obtained from Reference 9 and the results were corrected to reflect a 58,500 lb. configuration. The results represent a single rotor helicopter, a tandem helicopter, a quad-ducted propeller aircraft, a two-propeller tilt-wing transport, a four-propeller tilt-wing transport, and the VZ-2 research aircraft. The data was obtained from wind tunnel tests, flight tests, and model tests at the Princeton Long Track.

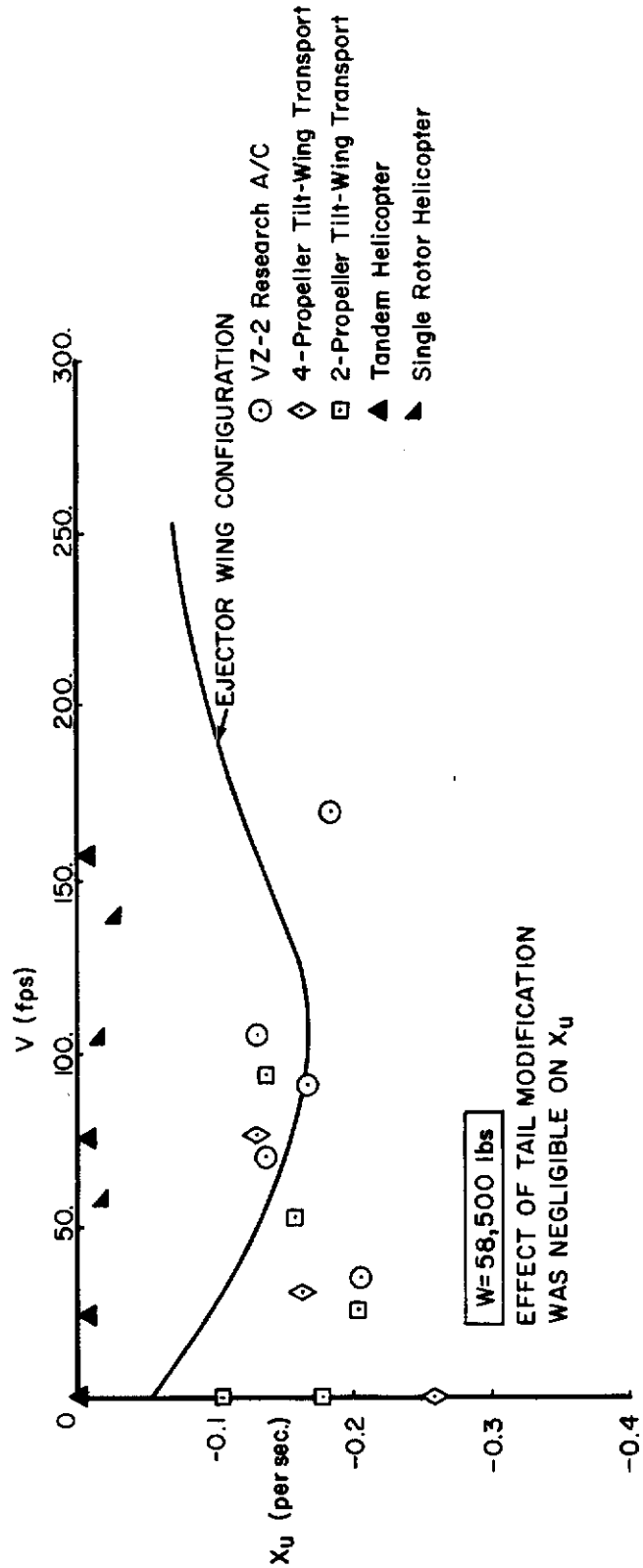

Figure 17. Variation of X_u Through Transition

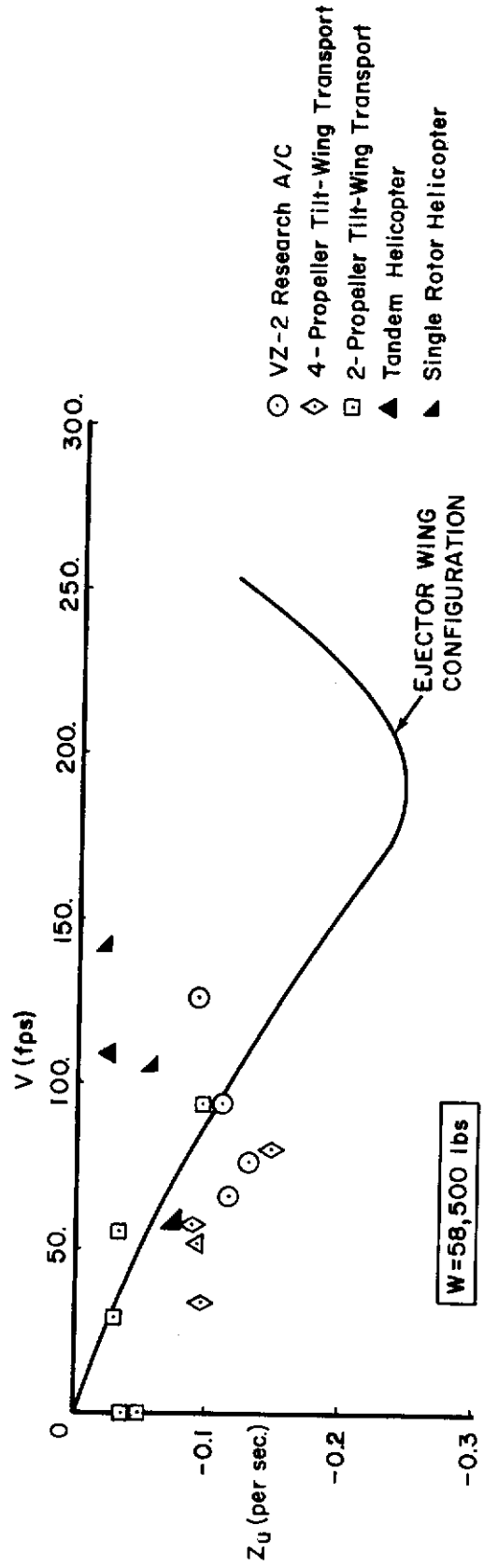

Figure 18. Variation of Z_u Through Transition

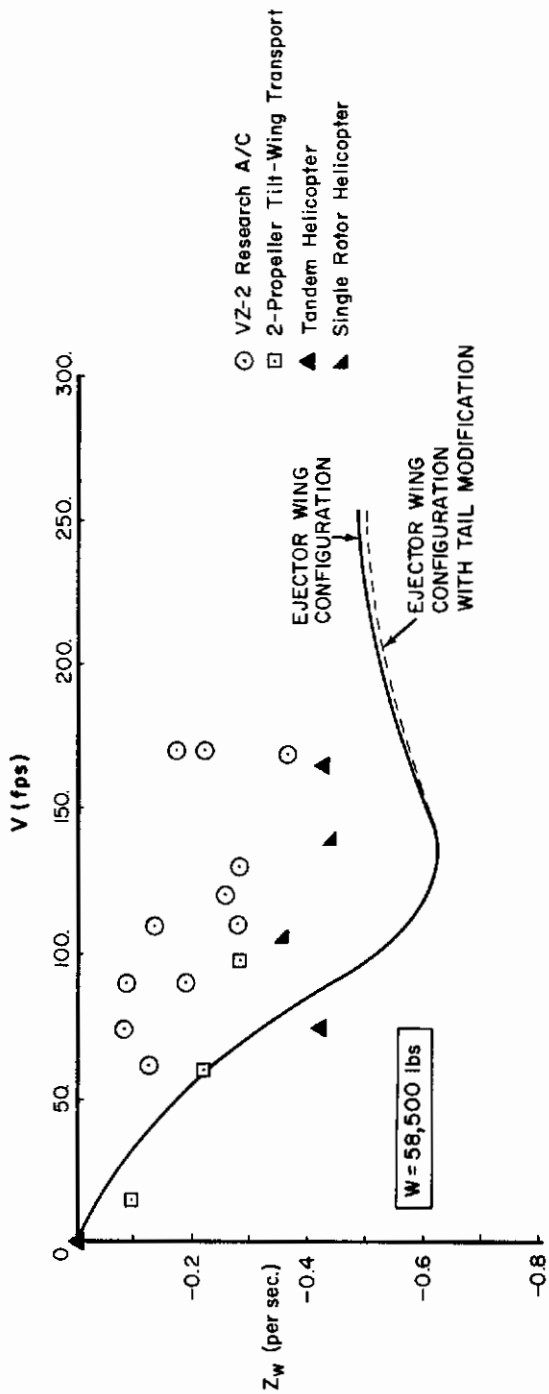

Figure 19. Variation of Z_w Through Transition

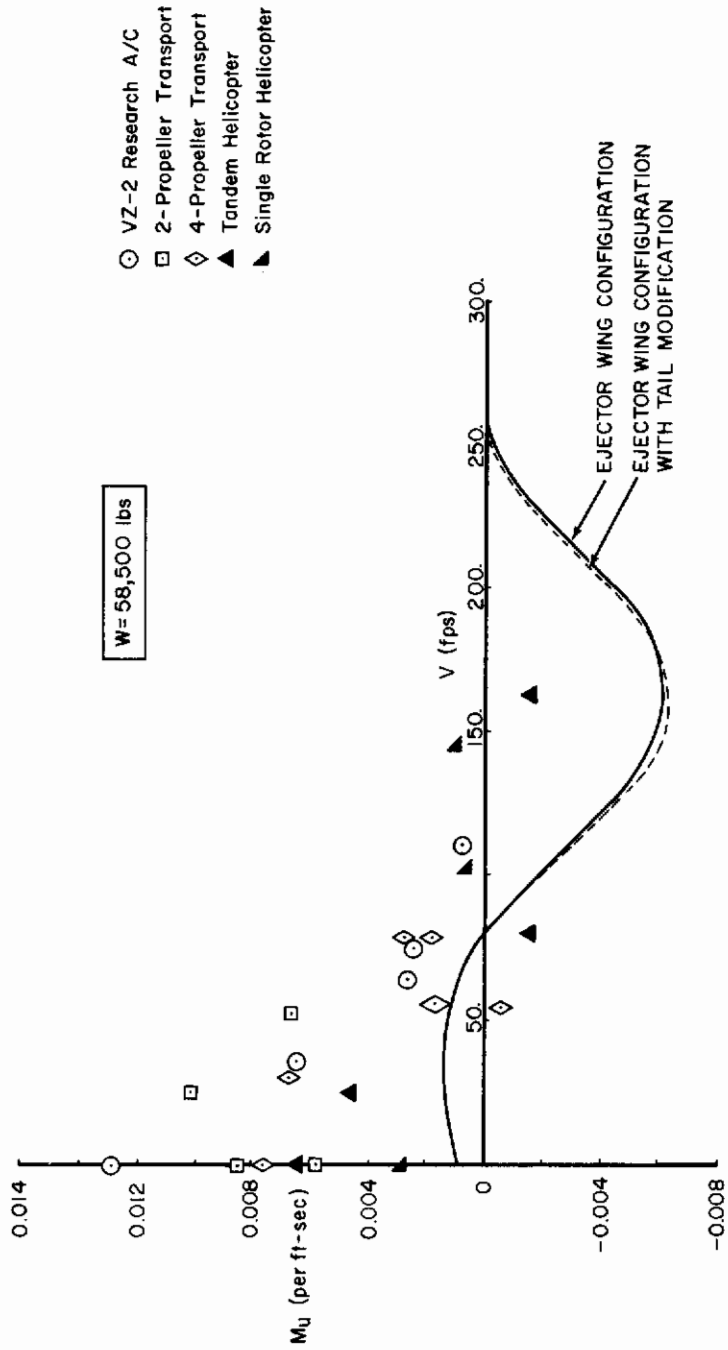

Figure 20. Variation of M_u Through Transition

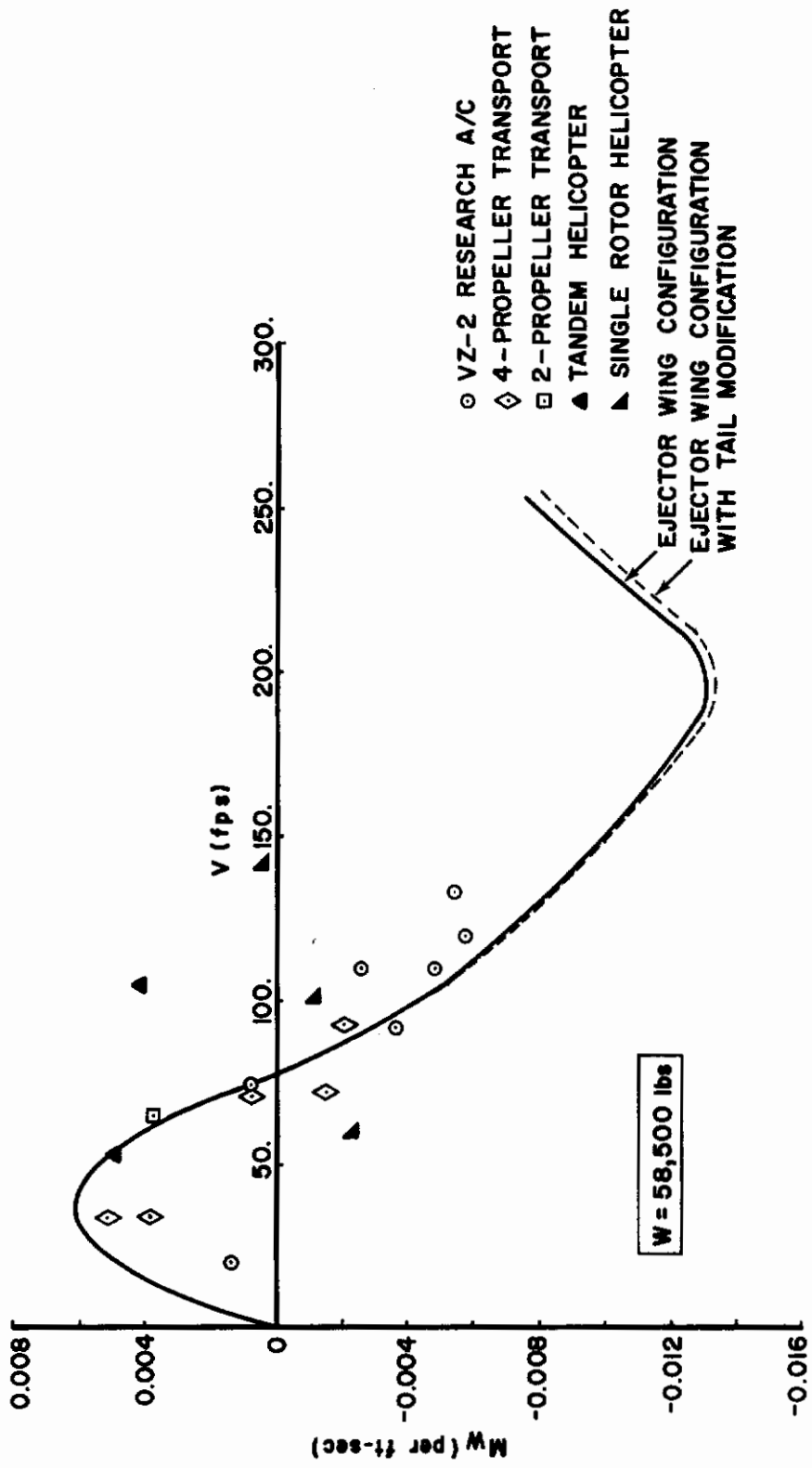

Figure 21. Variation of M_w Through Transition

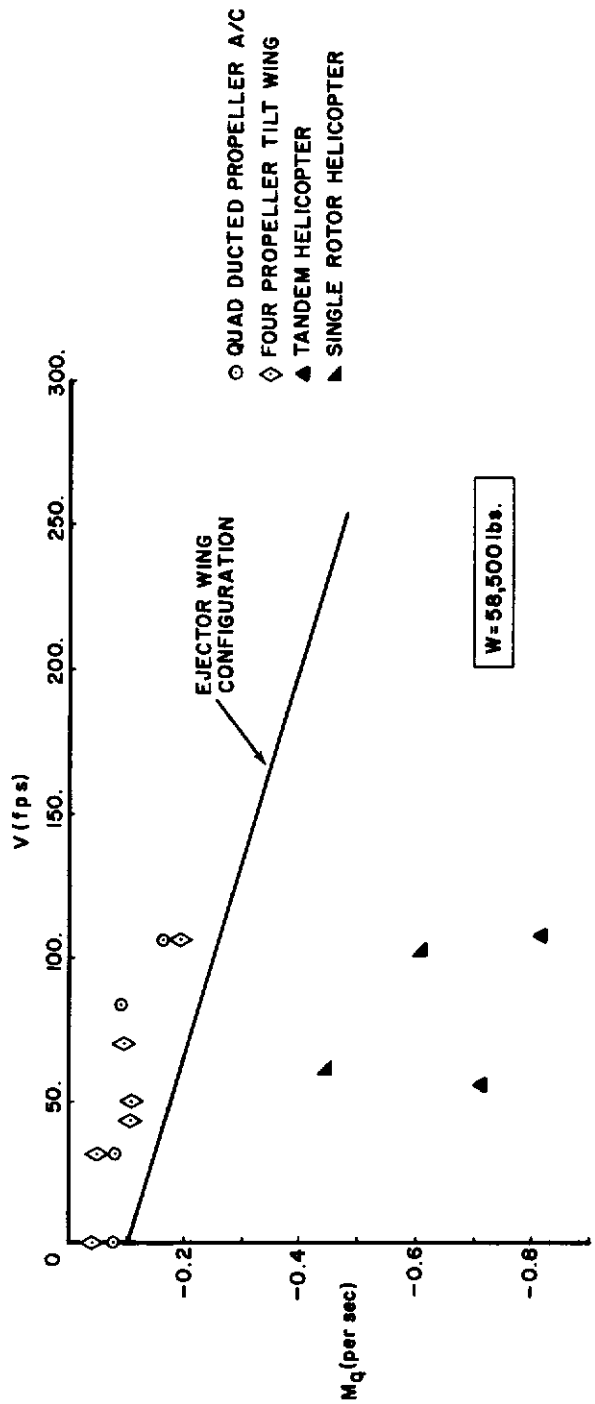

Figure 22. Variation of M_q Through Transition

Figures 17 through 19 provide comparisons for the force derivatives. The results suggest that the characteristics of the ejector wing configuration may be similar to those of a two-propeller tilt wing transport. The unaugmented moment derivatives M_w and M_u are shown in Figures 20 and 21. The fact that M_w and M_u can be both positive and negative, as shown in these figures, suggested that a speed instability may occur during transition, when the function formed by $(M_w Z_u - M_u Z_w)$ becomes negative. A test for this instability was performed and the results indicated that the unaugmented wing ejector configuration can have an unstable regime for the transitional velocity range of $71.0 \leq V \leq 186.0$ fps. This indicates that this vehicle requires some form of Stability Augmentation System (SAS).

Again, the results for pitching moment derivatives suggest that the ejector wing configuration may have characteristics similar to those of a two-propeller tilt-wing transport. Thus, handling qualities problems occurring on two-propeller tilt-wing transports may also occur here, in addition to many other problems unique to the ejector wing configuration.

The derivative M_q for this vehicle is shown in Figure 22. No reliable theory exists for estimating this derivative at low forward transitional speeds, and test data giving M_q for this type of vehicle are nonexistent. A value was used during transition that was representative of several V/STOLs of the approximate size and weight

of the ejector wing configuration. The M_q derivative was determined from data of Reference 9 and engineering judgment; the results are shown in Figure 22.

7. STABILITY DERIVATIVES, STOWABLE ROTOR CONFIGURATION

The X_u, Z_w, M_u, M_w, and M_q derivatives for the unaugmented stowable rotor configuration are shown in Figures 23 and 24. These derivatives were determined in Reference 2 for the nominal transition indicated in Figures 14 through 16. The Z_u derivative was not given in Reference 2, and we assume that Klingloff took this derivative to be $Z_u = 0$. Finally, the derivatives for the unaugmented ejector wing configuration are given in Figures 23 and 24 for comparison.

In general, the derivatives for the ejector wing configuration seem to be more nonlinear with forward speed than the derivatives for the stowable rotor vehicle when $V < 130$ knots. The nonlinear behavior of the ejector wing vehicle derivatives with V seems to be exhibited, to some extent, by the derivatives for other V/STOLs (Figures 17 through 21 and Reference 9). No further comments can be made concerning these nonlinearities or lack of them since the extent of the analytical procedures used in deriving these results for the Sikorsky stowable rotor vehicle have not been described in detail (Reference 2).

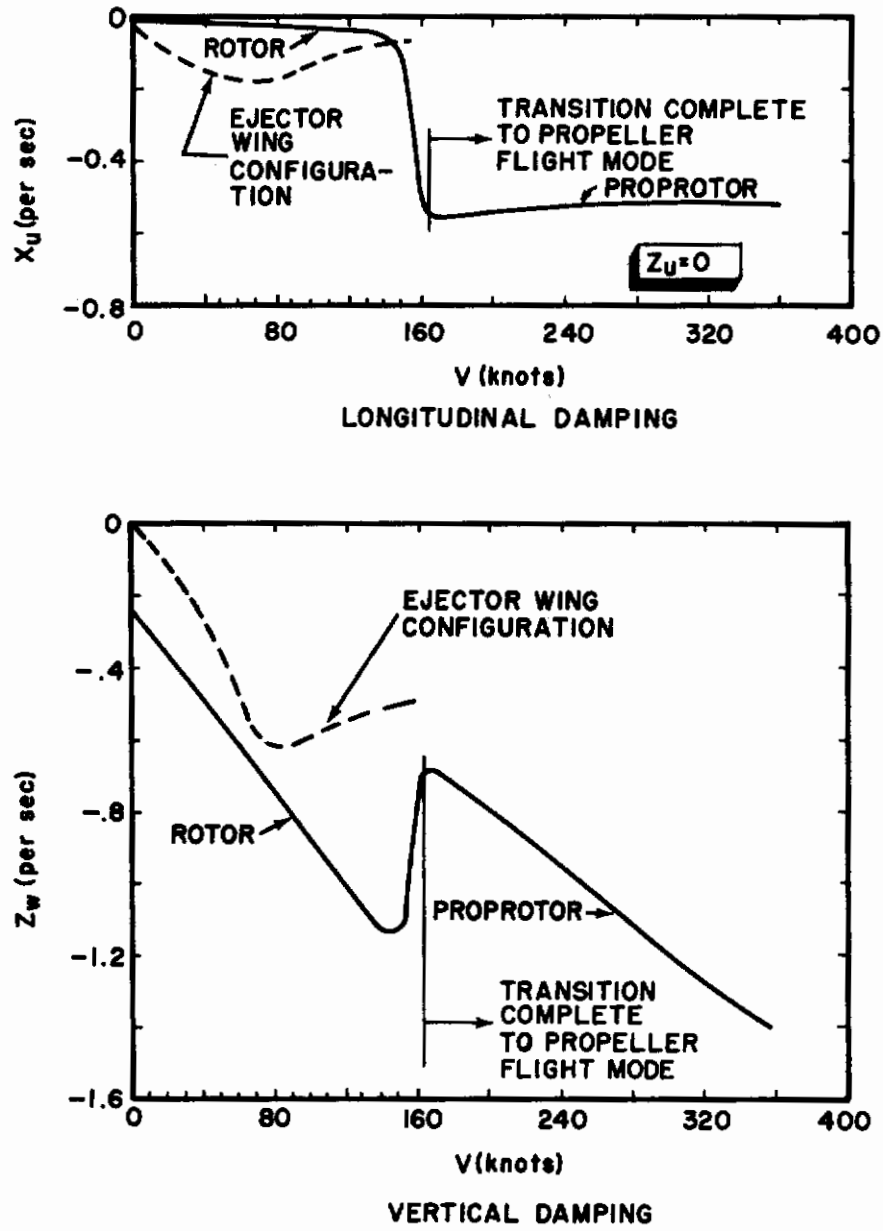

Figure 23. Variation in Force Derivatives With Airspeed, Stowable Rotor Configuration

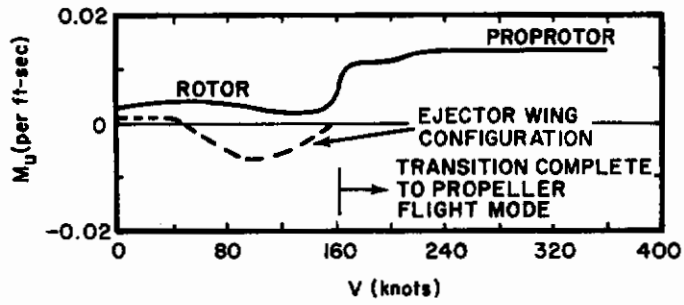

SPEED STABILITY

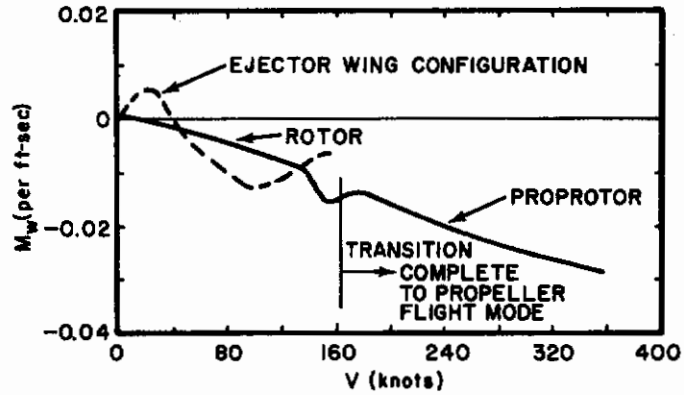

ANGLE OF ATTACK STABILITY

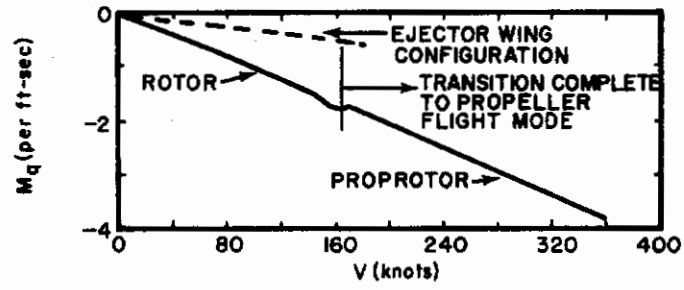

PITCH DAMPING

Figure 24. Variation in Moment Derivatives With Airspeed, Stowable Rotor Configuration

With the above aerodynamic representation, the Sikorsky stowable rotor configuration does not seem to exhibit speed instability during transition. With $Z_u = 0$, as was assumed, an unstable speed stability occurs when the function formed by $M_u Z_w$ becomes greater than zero. Since M_u is always positive and Z_w is always negative throughout transition to the propeller flight mode (Figures 23 and 24), speed instability cannot occur within the context of the linear analysis used here. The unaugmented ejector wing configuration, on the other hand, tends to be unstable with respect to speed stability for $71.0 \leq V \leq 186$ fps. Also, other V/STOLs such as the helicoper have shown a speed instability for some range of low forward flight speed when the SAS was inoperative.

8. CONTROL DERIVATIVES, EJECTOR WING CONFIGURATION

The $X_\delta\delta$, $Z_\delta\delta$, and $M_\delta\delta$ terms in equations (2) reflect control contributions to the forces and moments exerted on the vehicle. These control contributions for the ejector wing configuration consist of inputs to i_p, V_{Jp}, i_T, V_J, λ, and T_N to perturb the vehicle from the equilibrium flight path. These derivatives are shown in Figures 25 and 26 as a function of door angle λ. The quantity δ equals the particular control of interest. For example, $\delta = V_{J_p}$ for an increase in thrust to the propulsive engines. The details necessary to determine these derivatives can be found in Appendix I.

These derivatives could not be compared with those from another V/STOL. They are a function of the type of propulsion

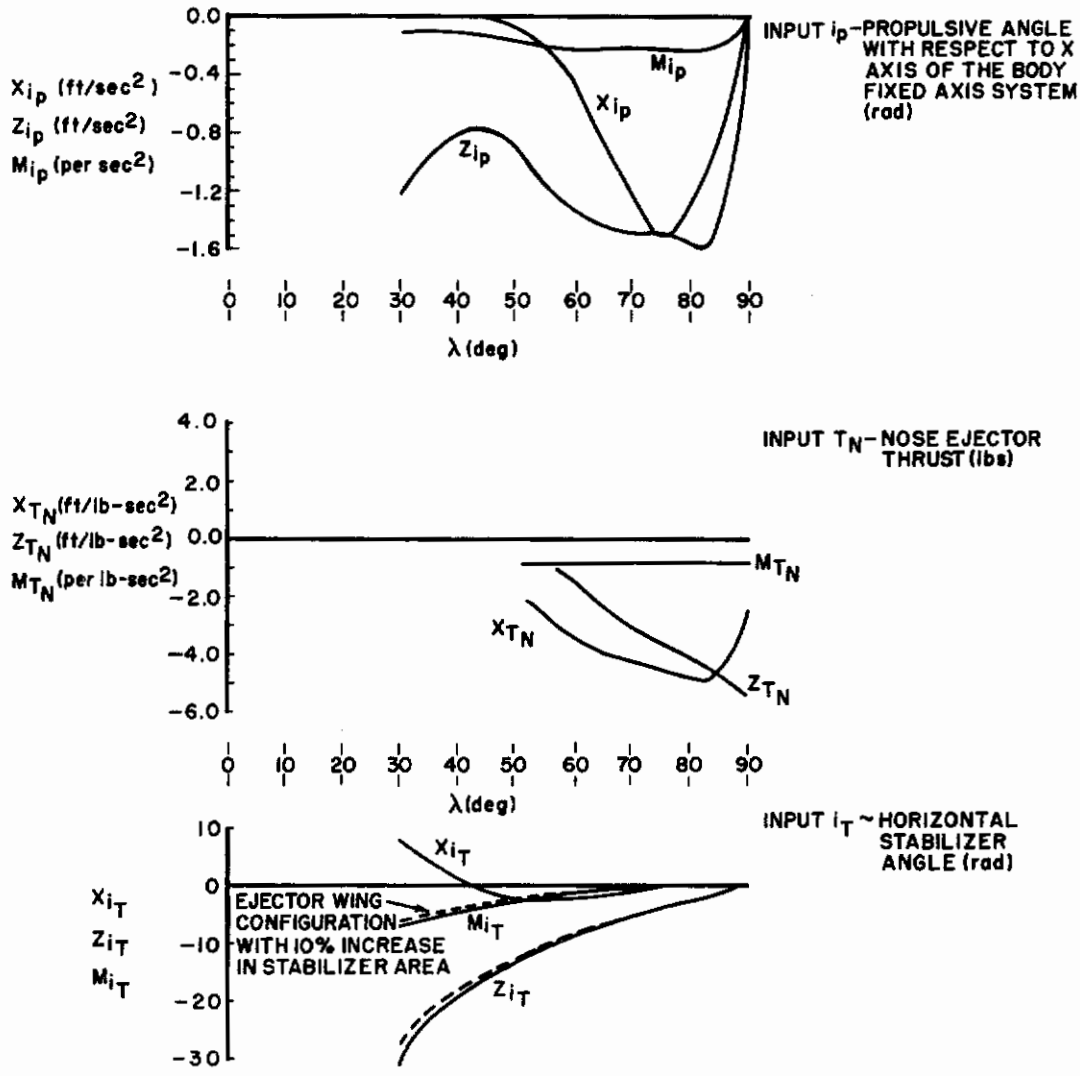

Figure 25. Control Derivatives i_p, T_N, i_T

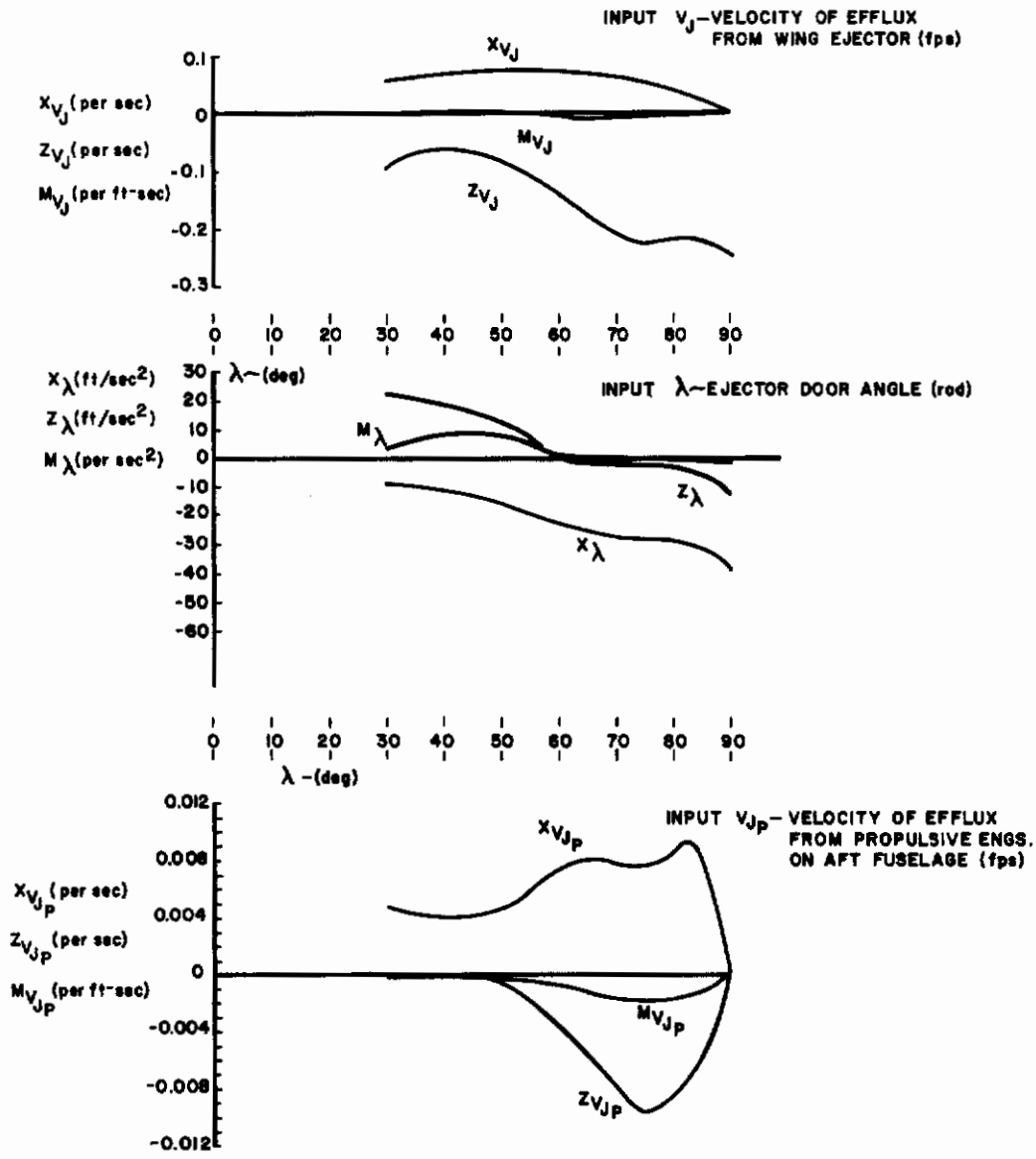

Figure 26. Control Derivatives V_J, λ, V_{JP}

system used to provide the vertical takeoff capability; the ejector wing configuration is unique in that it is the only wing ejector vehicle among all of the V/STOLs.

Further discussion of these control derivatives is reserved for the handling qualities evaluation, where we remark on the design of the cockpit control system.

9. THE MODIFIED EJECTOR WING CONFIGURATION

As mentioned above, we have analyzed a configuration with a modified ejector wing and a horizontal tail surface area that was increased by 10% to see whether a significant improvement could be made in the static speed stability of the concept in the mid to high transitional speed range. The results, shown in Figures 6 through 13 and 17 through 21, indicate that this modification was not sufficient to significantly improve the stability of the vehicle as a whole throughout transition.

Further increasing the tail surface may lead to a significant improvement in the stability of the aircraft. Such an increase, however, would increase vehicle weight and could eventually cause severe and possibly catastrophic torsional loads on the wing. Figures 1 and 2 show that the horizontal surfaces are positioned on the wing booms; the torsional moment about the wing elastic axis could be quite high for large horizontal tail loads. Thus, attempting to improve vehicle stability be increasing the horizontal tail of the ejector wing configuration does not seem appropriate.

SECTION III

HANDLING QUALITIES EVALUATION

Appendix II provides details on the manner in which Equation 2 was analyzed to provide the data necessary for performing the transient studies required for this evaluation. In addition, Appendixes II and III include input preparation and digital computer listings for new programs used during this investigation.

1. EQUILIBRIUM CHARACTERISTICS WITH CHANGING TRIM

Reference 1, Section 3.2.1.1 requires that the local slope of the equilibrium altitude-speed relationship shall not exceed 0.6 degrees per knot for speed perturbations of at least 10 knots in either direction about the trim speed. The configuration and trim may be different at each trim condition but they must remain fixed while determining the altitude-speed variations about the trim condition. These requirements shall be satisfied at all forward trim speeds and at backward trim speeds up to the limits of the Service Flight Envelope or 35 knots, whichever is less. These requirements are established to prevent divergences in airspeed and attitude which may not be noticed by a pilot who is busy on other mission tasks.

Calculations were performed to find the local slope of the equilibrium attitude-speed relationship for the ejector wing configuration with a 10-knot speed perturbation to the trim schedule shown in Figures 6 through 13. The results of these calculations shown in

Figure 27, indicate that the ejector wing configuration fulfills this criterion even when V > 35 knots. The quantity $(\Delta\theta/\Delta V)_M$ or the maximum θ change for a 10-knot increment on trim velocity is always negative because a positive ΔV to the trim speed requires a nose-down pitch attitude change to reestablish trim at the same constant altitude. A pitch-up change was considered to be positive, while a pitch-down change was taken to be negative, as is conventional.

An analysis could not be performed to see whether the Sikorsky stowable rotor configuration fulfilled this criterion. Details of the aerodynamic characteristics for this vehicle included in Reference 2 were not sufficient to perform trim calculations.

2. COCKPIT CONTROL GRADIENTS

Sections 3.2.1.3. and 3.3.1 of Reference 1 state that for the Level 1 category, the variations of cockpit control force and control position with airspeed must be smooth and the local gradients stable or zero for pitch cockpit controls. The gradients shall be essentially linear with no objectionable changes in the slope of force or position with speed. Stable pitch control gradients means that incremental pull forces and aft displacement of the cockpit control are required to maintain slower or more rearward airspeeds, and the opposite to maintain faster or more forward airspeeds. The term gradient does not include that portion of the control force or control position versus airspeed curve within the preloaded breakout force or friction band.

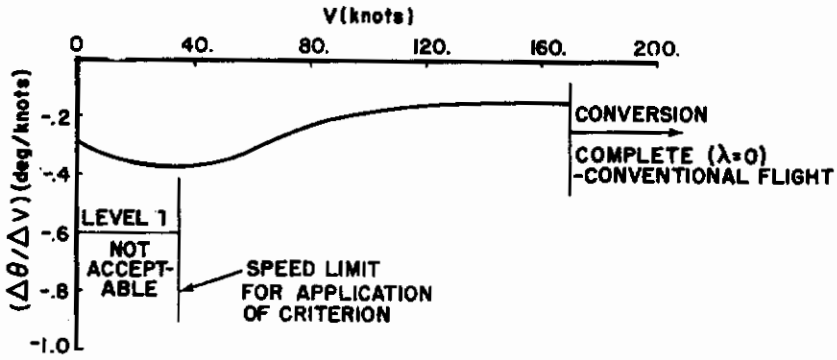

Figure 27. Trim Change Due to Velocity Perturbation, Ejector Wing Configuration

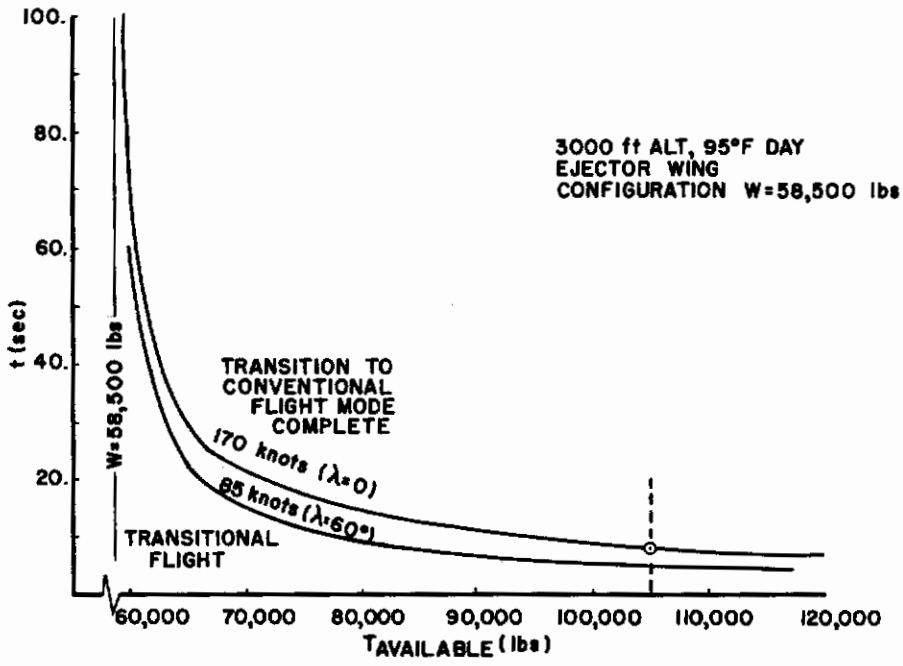

Figure 28. Acceleration From Hover Through Transition, Ejector Wing Configuration

This analysis is not to design a cockpit control system for the ejector wing configuration, but to indicate what modification may be necessary for the ejector wing configuration to meet requirements of a Level 1 aircraft. Therefore, potential problem areas that may affect the design of the cockpit system should be discussed.

Figures 25 and 26 present the control derivatives as a function of wing ejector door angle λ. As can be seen, the vehicle can be perturbed from longitudinal trim by 6 control inputs. Obviously, there must be control phasing and mix, since the pilot could not handle all of these simultaneously. A potential problem area in the design of the cockpit system may occur where reversals occur in the gradients of the control derivatives. For example, reversals in gradient exist in the derivatives M_{V_J}, M_λ, Z_λ, X_{ip}, and X_{i_T} in the $40° \leq \lambda \leq 90°$ range for ejector door angle λ setting. The control system designer must ensure that these reversals in gradient do not cause objectional changes in the slope of force or position with speed of cockpit pitch controls.

3. ACCELERATION TIME THROUGH TRANSITION

Reference 1 has no criteria for the time required by a V/STOL to complete acceleration or deceleration through transition; the procuring activity indicates this when specifying the mission. This aspect is important for the V/STOL required to hover in a hostile environment.

Reference 10 provides a discussion of maneuverability and energy considerations. The formulation given for accelerating through transition is

$$t = \int_0^{V_c} \frac{m\ V}{550\ HP_{excess}}\ dV \qquad (3)$$

based upon these energy considerations. The quantity m is the mass of the vehicle, while HP_{excess} is the excess horsepower available that can be converted to acceleration. The integration is performed from V=0, or from hover to V_c or that speed when the transition has been completed. For the ejector wing configuration, we assumed that the pilot manipulated the throttle to maintain a constant thrust level during the dash through transition. The flight path pitch angle, altitude, and control settings as a function of forward speed were assumed to correspond to the schedules shown in Figures 6 through 13. The results are shown in Figure 28.

The use of these results is illustrated as follows. If the total available thrust on board the aircraft is $T_{available}$ = 105,000 lbs, the dash from hover, through transition, and to the conventional mode of flight would be accomplished in approximately 8 seconds. On the other hand, if $T_{available}$ equals exactly 58,500 lbs or the maximum weight of this V/STOL, there is no excess thrust to be converted to acceleration and it will take an infinite amount of time to dash through transition. That is, the V/STOL cannot accelerate at all and the dash

through transition cannot be accomplished unless some other transitional flight schedule than the one shown in Figures 6 through 13 permits the pilot to do this.

An analysis was performed to determine the time required to accelerate through transition for the Sikorsky stowable rotor concept. The horsepower required to perform the nominal transition shown in Figures 14, 15, and 16 was determined in Reference 2 and is shown in Figure 29. The results of the analysis are given in Figure 30. Conversion to the propeller flight mode was assumed to be made at 160 knots. The results indicate that conversion to the conventional flight mode takes approximately 8 seconds for the stowable rotor configuration. As indicated previously, the ejector wing configuration requires a $T_{available}$ of 105,000 lbs on board the aircraft to accomplish the dash through transition in the same time interval.

No attempt was made to determine the optimum transitional flight path from hover to the conventional flight mode, or vice versa. Many paths exist within the permissible flight corridors for transition, and the above acceleration times reflect only one such flight schedule for each vehicle investigated. More analysis is required before acceleration or deceleration times through transition can be defined clearly.

4. VELOCITY LIMITATIONS UPON THE LINEAR THEORY

All of the discussion given in the section below is contingent upon use of the linearized equations of motion and the resulting time

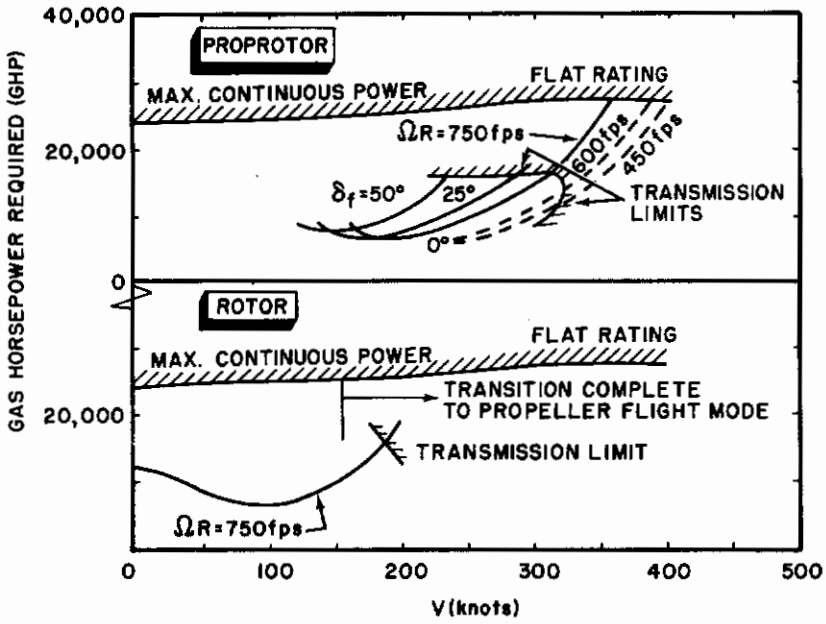

Figure 29. HP Required During Transition, Stowable Rotor Configuration

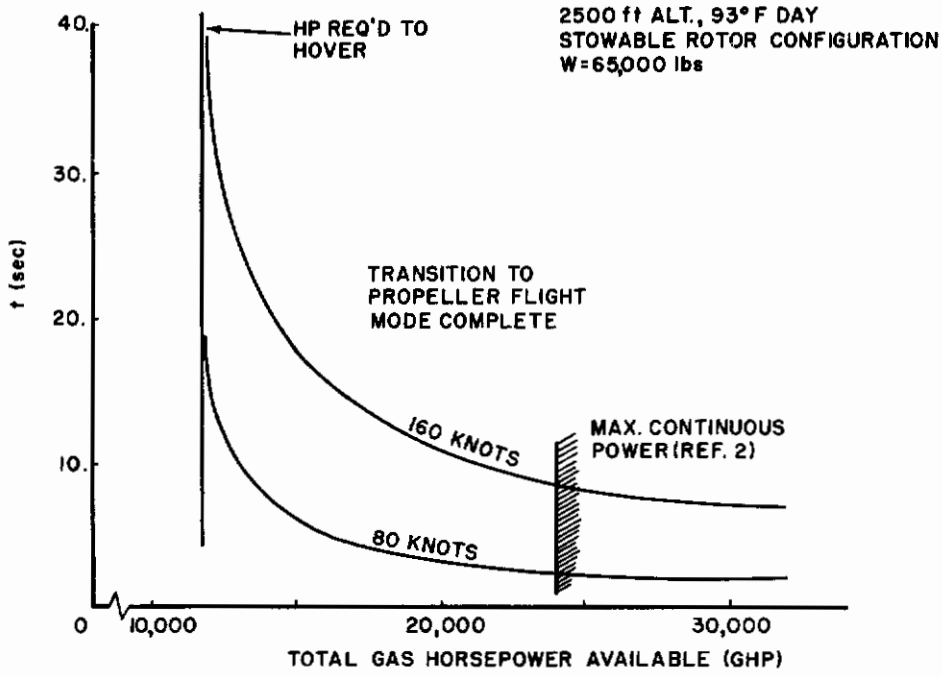

Figure 30. Acceleration From Hover Through Transition, Stowable Rotor Configuration

histories. It is therefore important at this point to emphasize some velocity considerations when the linearized theory is used for analysis.

The theory applies to cases of small perturbances, that is, $\frac{u}{V} << 1$ and $\frac{w}{V} << 1$. These assumptions work quite well in the equations of motion for the conventional flight mode. The velocity V is relatively high so that a limitation of $\frac{u}{V} < 0.3$, say, still permits a fairly large excursion in forward flight speed. For example, if trim speed is 300 fps, then a velocity excursion of 90 fps on either side of this trim speed falls within the requirement of $u/V \leq 0.3$. On the other hand, the first trim speed used in this analysis is V=1 fps at $\lambda=90°$. Applying the above limitation directly means that a velocity perturbation greater than u=0.3 fps falls outside the validity of the analysis. Therefore, caution must be exercised when applying this theory to V/STOLs near hover to ensure that the final results fall within the limitations of the initial assumptions.

To limit the validity of the analysis, it is assumed that $\frac{u}{V} < 0.3$ and $\frac{w}{V} < 0.3$. All velocity perturbations generated in excess of these limits must be subject to question.

5. LONGITUDINAL DYNAMIC RESPONSE

The longitudinal dynamic response criteria are obtained from two sections in the V/STOL specification: Section 3.2.2.1 applies to hover and low speed flight phases where the forward speed is less than 35 knots; and Section 3.3.2 applies to equilibrium flight or maneuvering

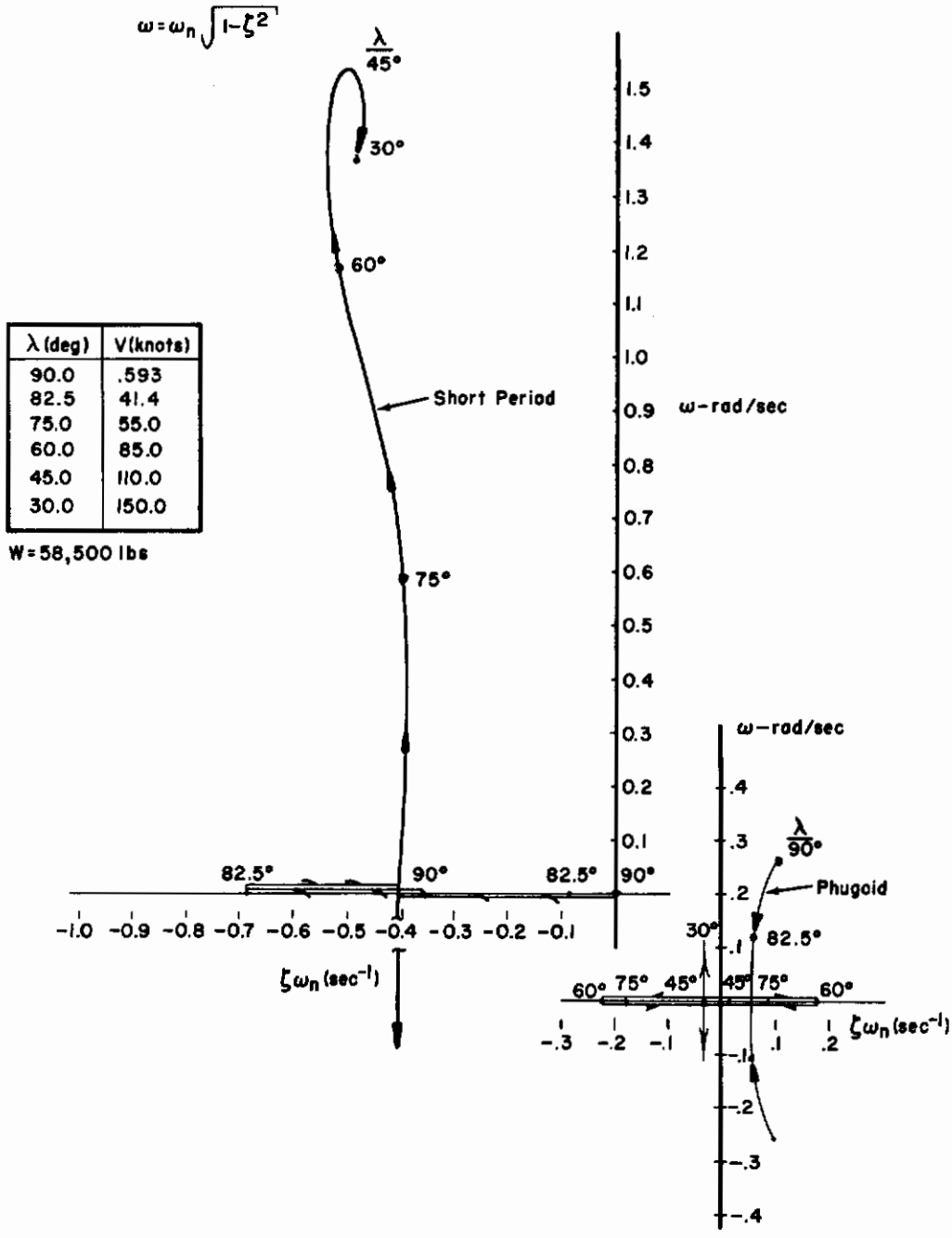

Figure 31. Root Loci for Unaugmented Ejector Wing Configuration

in the speed range of 35 knots to V_{con}, where V_{con} is that speed where the vehicle can be considered as flying as a conventional aircraft. At speeds in the vicinity of V_{con}, it is desirable that the handling characteristics and dynamic response blend in with the requirements of MIL-F-8785B (Reference 11). At speeds near 35 knots, it is desirable that the handling characteristics and dynamic response of the configuration fulfilling Section 3.2.2.1 for forward speeds below 35 knots blend in with the requirements of Section 3.3.2 of Reference 1. As indicated above, Section 3.3.2 applies to speeds greater than 35 knots.

The characteristic equations for the ejector wing configuration and the transfer functions were obtained from the Griffin digital computer program (Reference 12). The root loci are shown in Figure 31. Instabilities exist in the characteristic equation of the ejector wing vehicle since some loci are to the right of the vertical axis. The short period modes are basically stable but the phugoid or long period modes are definitely unstable. The phugoid mode is both lightly and negatively damped, which means that a divergent oscillating response would occur to a disturbance or control input. The unaugmented vehicle, then, fails to meet Level 3 requirements due to this instability.

An analysis of the characteristic equations at each trim point discussed above indicated that a simple longitudinal SAS loop incorporating feedback signals on q and w to modify the derivatives M_q and M_w could be used to make the vehicle sufficiently stable to be within the criteria of Reference 1. The feedback gains were estimated by analysis of the characteristic equations at each trim point

and the feedback system was incorporated into this evaluation. Figure 32 illustrates the effect of the SAS upon the M_q and M_w derivatives. No consideration was given to the actual mechanical design of this SAS or to what controls must be actuated to provide these changes in the moment derivatives. Such an analysis was beyond the scope of this study.

The roots of the augmented characteristic equations are shown in Figure 33. The main effect of the longitudinal SAS was to force the phugoid mode to be stable; that is, the roots lie to the left of the vertical axis where they are positive, lightly damped modes. The root locus of the augmented ejector wing configuration is typical of existing V/STOL aircraft. At hover and low speeds ($\lambda \simeq 90°$), the short period and phugoid modes are very close and almost inseparable. As the forward speed increases and approaches conventional flight, the roots separate and become distinct from each other as for a conventional aircraft.

Returning to Section 3.2.2.1 of Reference 1, for $V \leq 35$ knots, the requirements apply to the dynamic responses of the aircraft when the cockpit controls are free and when they are fixed following an external disturbance or an abrupt pitch control input in either direction. The requirements apply for responses of any magnitude that might be experienced in operation. If oscillations are nonlinear with amplitude, the oscillatory requirements shall apply to each cycle of the oscillation. For Level 1 acceptability, all aperiodic responses (real roots of the longitudinal characteristic equation) shall be stable. In

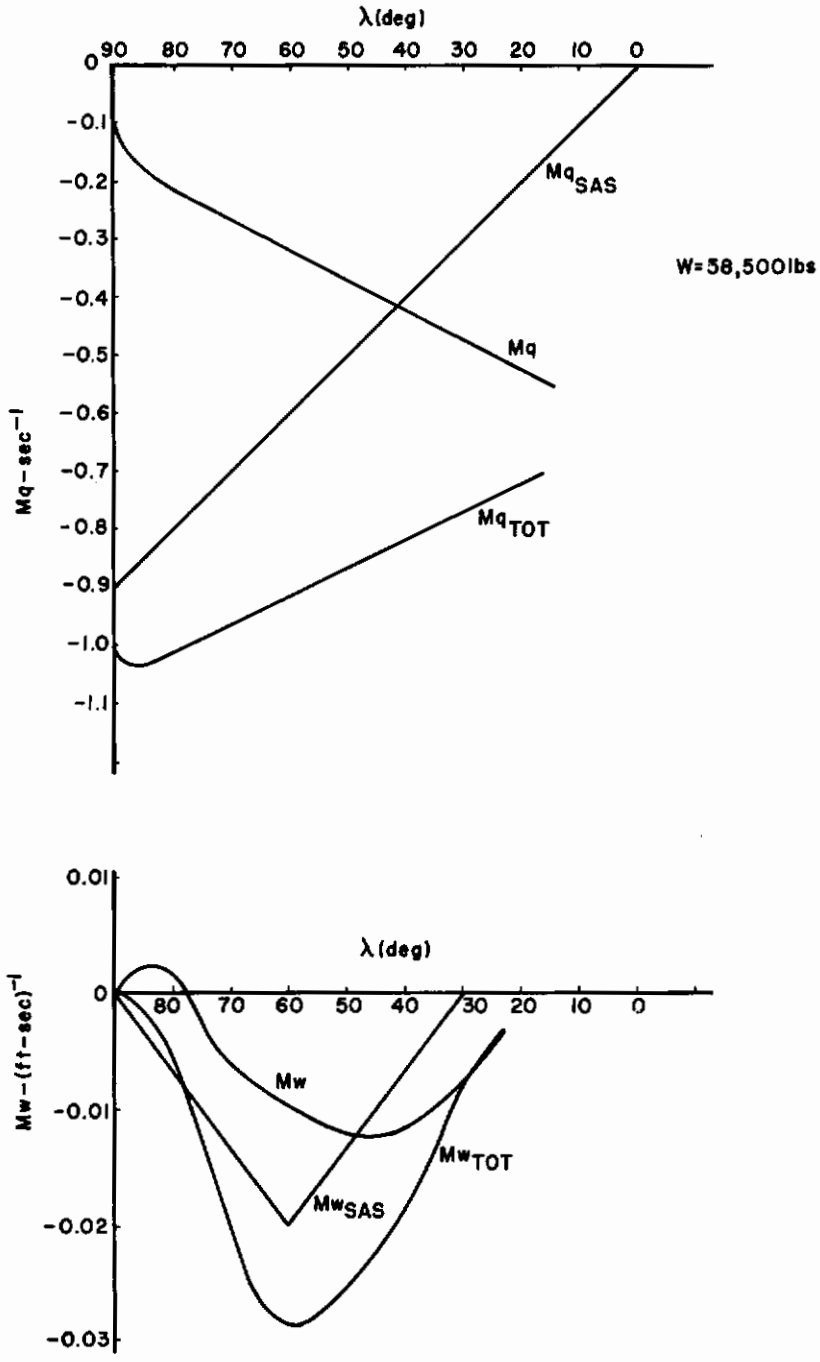

Figure 32. SAS for Ejector Wing Configuration

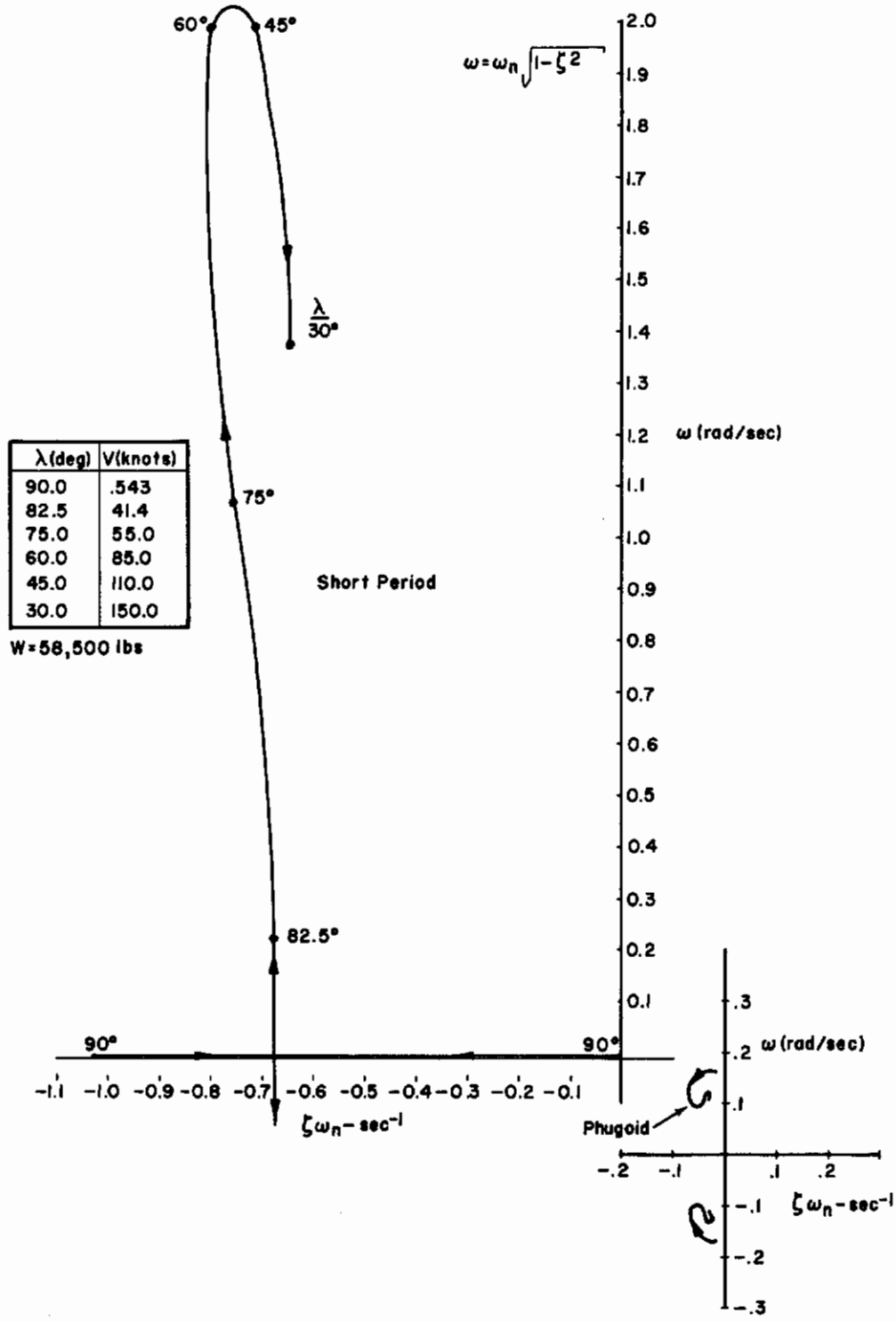

Figure 33. Root Loci for Augmented Ejector Wing Configuration

addition, for Level 1 flying qualities, the oscillatory modes of frequency greater than 0.5 radians/second shall be stable. Oscillatory modes with frequency less than or equal to 0.5 radians/second may be unstable provided the damping ratio instability is less than -0.10. Oscillatory modes of frequency greater than 1.1 radians per second shall have a damping ratio of at least 0.3. As seen by the results shown in Figure 33, the short period and phugoid roots of the augmented ejector wing configuration (SAS on) meet the requirements of this criterion insofar as stick fixed operation is concerned. Stick free conditions could not be evaluated since the control system mix and phasing has not, as yet, been defined.

Section 3.3.2 of Reference 1 considers the longitudinal dynamic response at forward speeds greater than 35 knots. The requirements apply to the dynamic response of the aircraft with the pitch control free and with it fixed. These requirements apply following a disturbance in smooth air, and following abrupt pitch control inputs in each direction, for responses of any magnitude that might be experienced in operational use. If the oscillations are nonlinear with amplitude, the requirements apply to each cycle of the oscillation. For Level 1 acceptability the roots of the longitudinal characteristic equation of the aircraft must be stable. In addition, the undamped natural frequency, ω, and damping ratio ζ of the second-order pair of roots (real or complex) that primarily determine the short-term response of angle of attack following an abrupt pitch control input must meet the Level 1 requirements of Figure 34. The figure illustrates clearly that the augmented roots of the ejector wing configuration (that is, the bare airframe

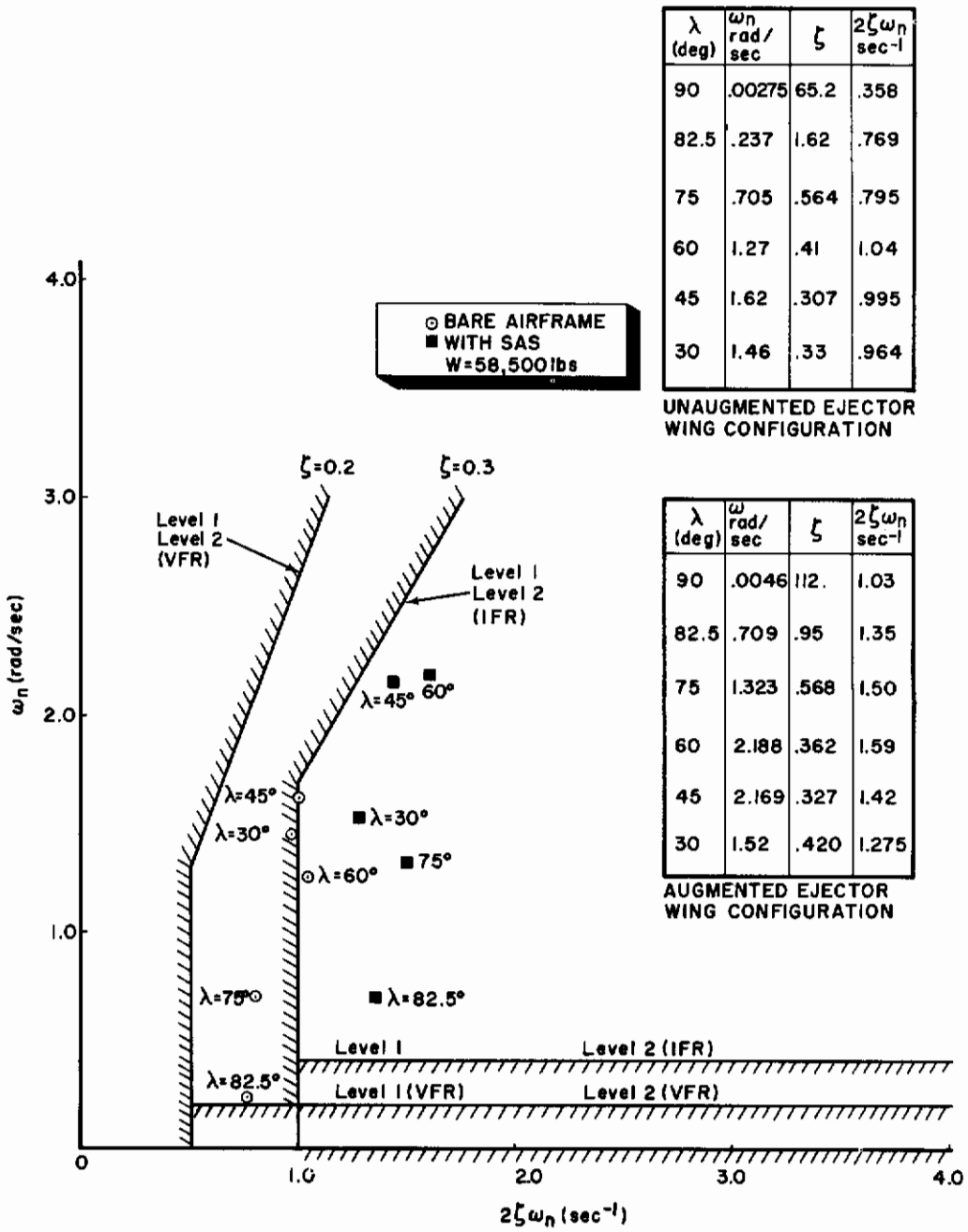

λ (deg)	ωn rad/sec	ζ	2ζωn sec-1
90	.00275	65.2	.358
82.5	.237	1.62	.769
75	.705	.564	.795
60	1.27	.41	1.04
45	1.62	.307	.995
30	1.46	.33	.964

UNAUGMENTED EJECTOR WING CONFIGURATION

λ (deg)	ω rad/sec	ζ	2ζωn sec-1
90	.0046	112.	1.03
82.5	.709	.95	1.35
75	1.323	.568	1.50
60	2.188	.362	1.59
45	2.169	.327	1.42
30	1.52	.420	1.275

AUGMENTED EJECTOR WING CONFIGURATION

Figure 34. Short Period Dynamic Response (V>35 Knots)

roots with a stability augmentation system incorporated) meet the Level 1 IFR requirement for damping ratio and natural frequency. The above concerns stick fixed operation. Stick free conditions could not be evaluated since the control system mix and phasing has not, as yet, been defined.

An evaluation was made of the dynamic response for the Sikorsky stowable rotor configuration. The transitional trim schedule and stability derivatives reflecting perturbed flight about this trim schedule have been discussed above. The results are shown in Figures 14 through 16 and Figures 23 and 24. The characteristic equations for the stowable rotor configuration, along with the transfer functions, were obtained from use of the Griffin digital computer program (Reference 12). The velocity trim points at which these computations were performed corresponded closely to the velocity trim points used in analyzing the dynamics of the ejector wing configuration (see table in Figure 31).

The roots for the unaugmented stowable rotor configuration (SAS off) during transition are shown in Figure 35. An instability exists in the phugoid mode of motion since the loci of the phugoid roots passes into the region where $\xi\omega_n > 0$ when forward speed exceeds approximately 100 knots. The presence of this instability means that the criteria of Section 3.3.2 for Level 1 handling characteristics cannot be met by the unaugmented stowed rotor vehicle.

The feedback gains shown in Figure 36 were then used to include a longitudinal SAS system into the analysis. The M_{qSAS}

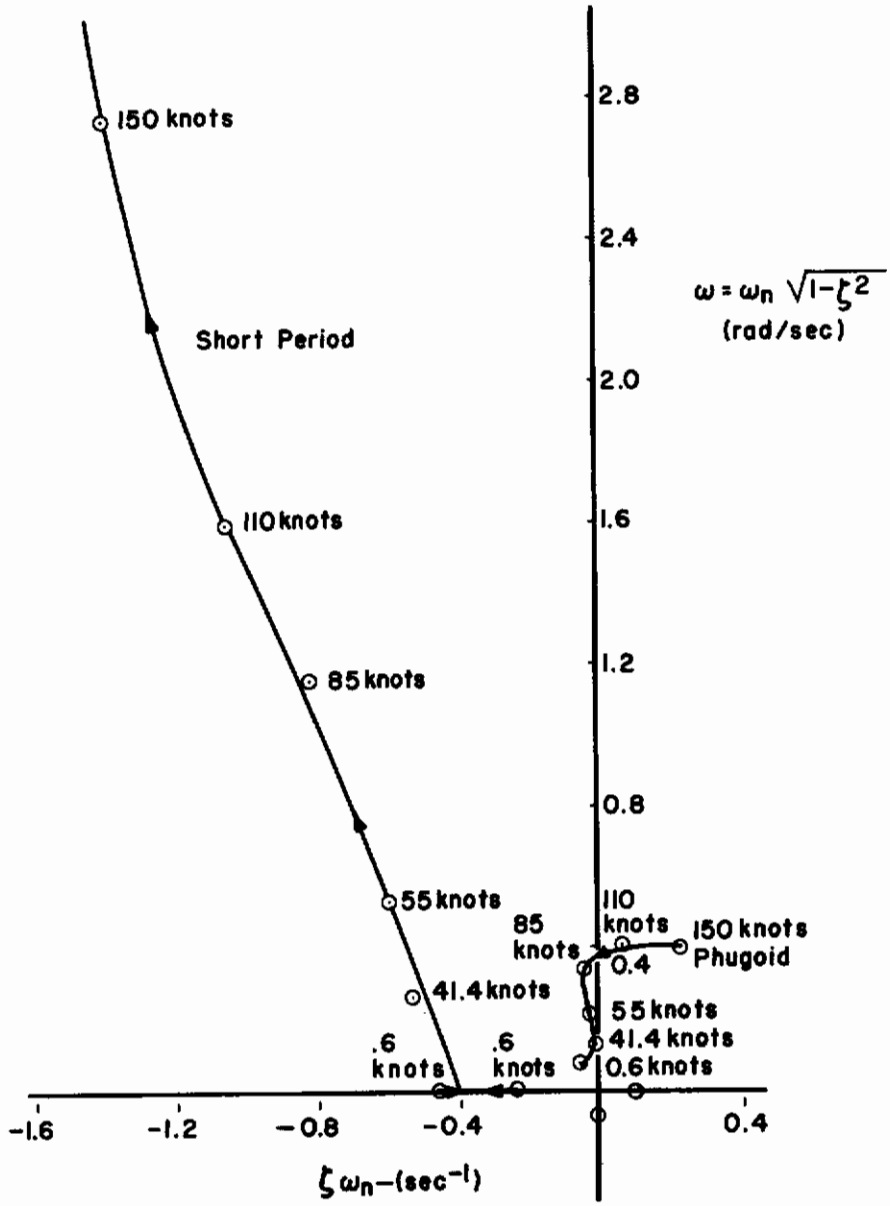

Figure 35. SAS Off Roots of Stowable Rotor Configuration

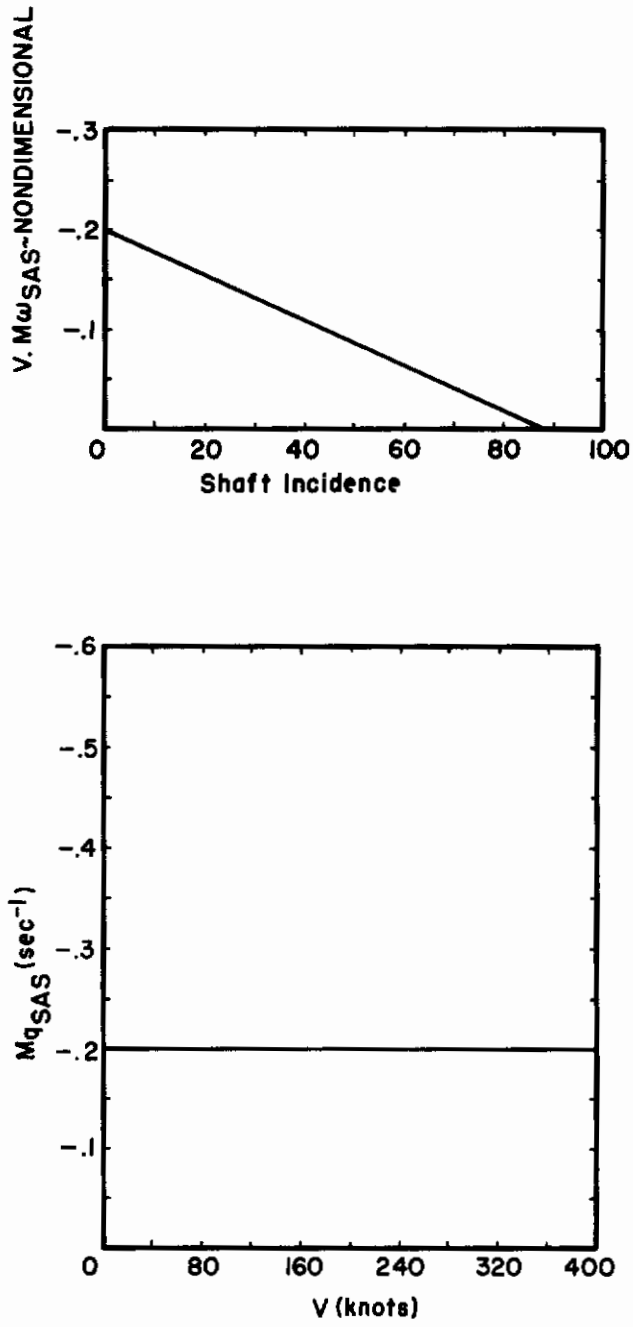

Figure 36. Stability Augmentation System Gain Schedule, Stowable Rotor Configuration

contribution shown in Figure 36 is equivalent to the M_q gain used in Reference 2, while M_{wSAS} requires further discussion. Klingloff (Reference 2) made use of a θ instead of a w feedback during his analysis of the dynamics of this configuration. The use of this gain would have meant that the digital computer program (Reference 12) used during this evaluation needed major modifications. These modifications were avoided by assuming that $VM_{wSAS} = M_\theta$ where M_θ is equivalent to the gain used by Klingloff. The variation of VM_{wSAS} with rotor shaft tilt angle could then be determined from the data presented in Reference 2; the results are shown in Figure 36.

The loci of the roots for the Sikorsky stowable rotor configuration with SAS on are shown in Figure 37. The phugoid mode is stable for the complete nominal transition from hover to the propeller mode of flight.

The results in Figure 35 were compared with the data presented in Reference 2 for SAS/off operation of the stowed rotor configuration. The correlation was excellent for both the short period and phugoid root loci through transition. The excellent correlation suggested that the Z_u derivative was taken to be $Z_u = 0$ in Reference 2. The stability derivatives for the stowable rotor configuration are discussed in Section II of this report.

The results shown in Figure 37 were compared with the data presented for SAS on operation of this vehicle in Reference 2. Good correlation existed for the short period root loci during transition

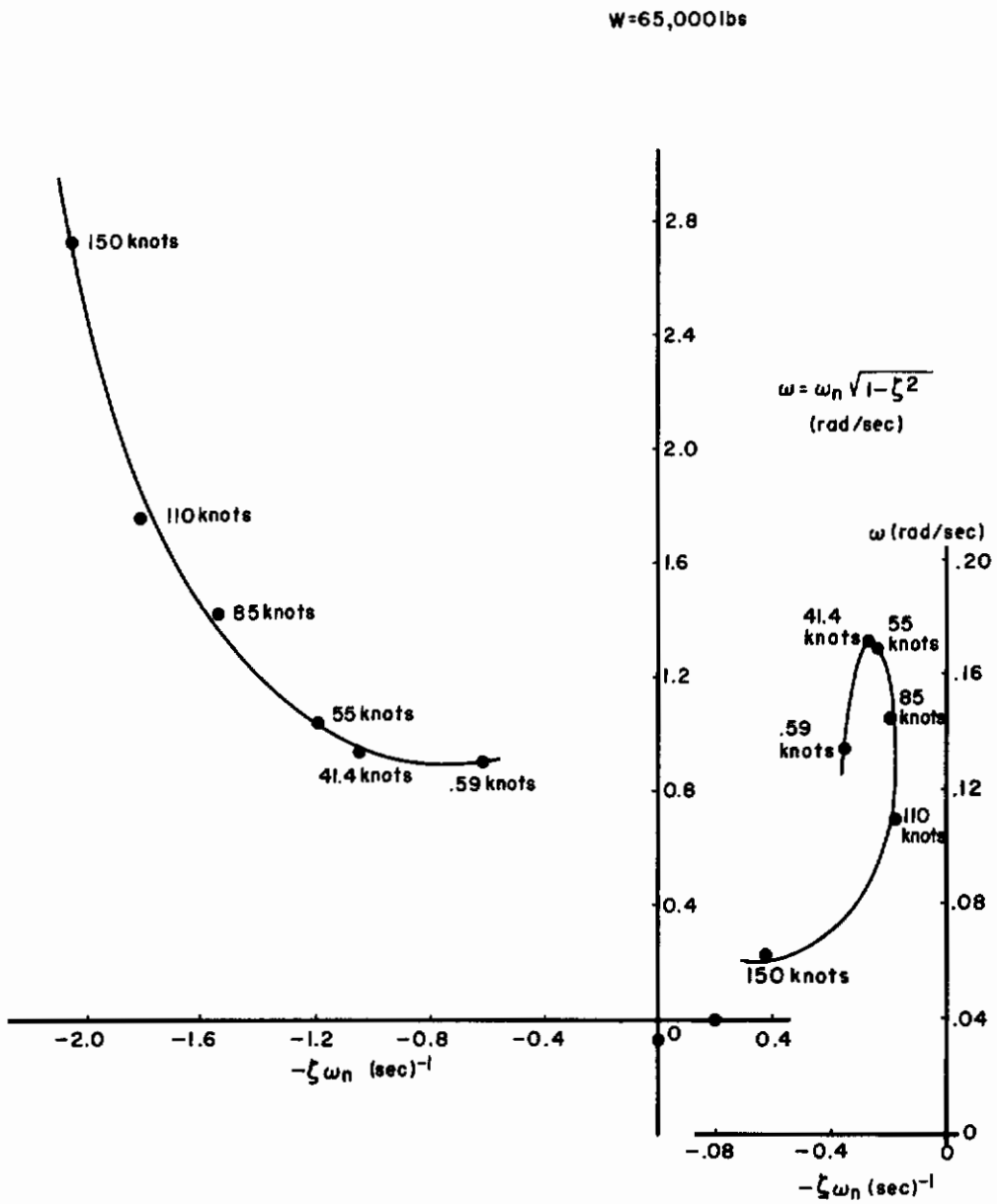

Figure 37. SAS On Roots of Stowable Rotor Configuration

while differences were evident on comparing the phugoid roots. These differences could be attributed to the use of a $M_{w_{SAS}}$ w feedback contribution to the equations of motion in the analysis presented in this report. Klingloff, on the other hand, used a pitch angle feedback loop as part of his SAS.

The results given in Figure 37 indicate that the Sikorsky stowed rotor configuration with SAS on fulfills the criteria given in Section 3.2.2.1 of Reference 1 for Level 1 handling characteristics when $V \leq 35$ knots and with the stick fixed. Sufficient data was not given in Reference 2 for evaluating the stick-free dynamic responses of this configuration.

Section 3.3.2 of Reference 1 was used in considering the longitudinal dynamic responses of the stowable rotor configuration at forward speeds greater than 35 knots. As discussed above, the roots of the longitudinal characteristic equation of the vehicle must be stable for Level 1 acceptability. Also, the short-term response following an abrupt pitch control input must meet Level 1 requirements shown in Figure 38. These results indicate that the roots of the Sikorsky stowed rotor configuration with SAS on meet the Level 1 IFR requirement for damping ratio and natural frequency.

6. CONTROL POWER CHARACTERISTICS FOR $V \leq 35$ KNOTS

The control power required to meet the handling qualities specifications may be considered as consisting of trimming, maneuvering, and stabilizing power contributions. Reference 1 indicates that

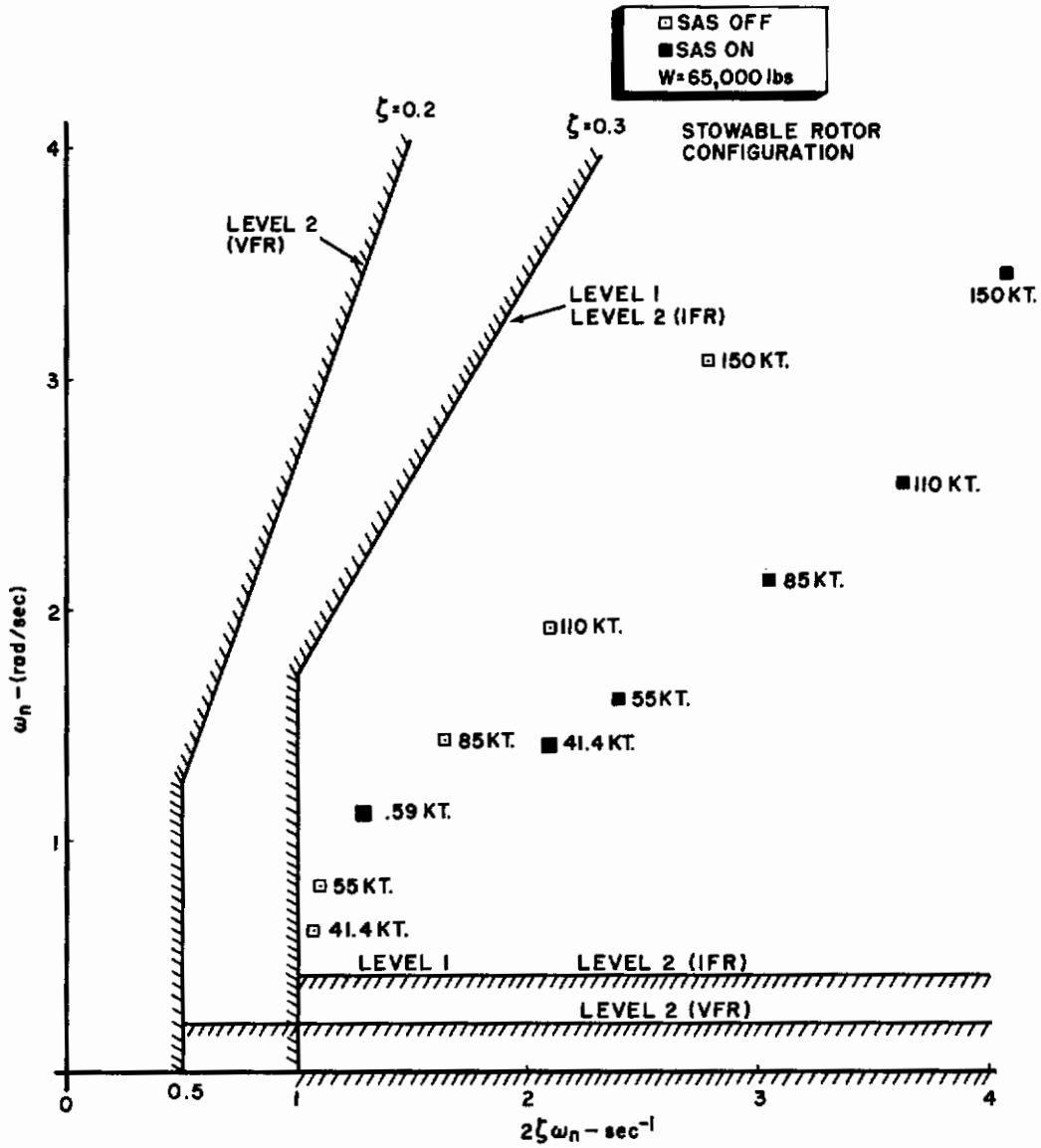

Figure 38. Short Period Dynamic Response (V>35 Knots)

further experimentation and analysis is required before it can be established that total control power is the simple addition of these individual contributions. Nevertheless, such an addition is performed here for want of a better definition. The additional thrust required to fulfill the maneuvering criteria of the specification during transition is determined. The longitudinal SAS is assumed to be operative during the maneuver transient so that the additional thrust necessary for the SAS system can be calculated. The sum of the individual control power needs is then formed to estimate the total longitudinal power requirement for the ejector wing and Sikorsky stowable rotor configurations. Stabilization in rough air should also be considered, but this consideration was beyond the scope of this study.

Sections 3.2.3 and 3.2.4 of Reference 1 state that sufficient power must be available on a Level 1 aircraft so that simultaneous and abrupt application of pitch, roll, and yaw controls in the most critical combination produces at least $\theta = \pm 3.0^\circ$, $\phi = \pm 4.0^\circ$, and $\psi = \pm 6.0^\circ$ within one second from the initiation of control force application. This attitude change must be made by a 1-inch stick deflection for pitch, a further 1-inch stick deflection for roll, and a 1-inch rudder pedal deflection for yaw. The specified simultaneous application of controls is important here because the ejector wing configuration may use engine compressor bleed air to power the SAS and wing ejector. The use of a common source for control power means that the moment available about one vehicle axis can depend upon the moments being used to provide control about the other axes. In addition, the control lags must be such

that the angular acceleration response in the commanded direction shall be developed within 0.1 second after the initiation of step displacements of the pitch, roll, and yaw pilot controls. This means that all valves in the ejector wing configuration and/or control devices which divert engine compressor bleed and/or bypassed air must provide the necessary jet momentum flux changes at the vehicle ejector systems within 0.1 second of the pilot inputs to the controls.

The vertical flight characteristics necessary near hover for a Level 1 category vehicle are described in Section 3.2.5 of Reference 1. These characteristics must be met while maintaining in reserve the attitude control power requirements discussed above. Starting from a steady descent rate of not greater than 4 fps, sufficient control power must be available to produce upward vertical accelerations of not less than 0.1 g following a step input to the thrust control, and the thrust to weight ratio shall be $T/w \geq 1.05$. The thrust control system shall be designed so that 63% of the commanded incremental thrust of $\Delta T = 0.05W$ shall be achieved in not more than 0.3 second following an abrupt step input to the thrust control. This requirement must be satisfied for the nominal thrust settings corresponding to a steady descent rate of between 5 and 10 feet per second. In addition, the ratio of maximum rate of climb occurring within the first second, to the magnitude of the cockpit control input in inches, shall not be less than 100. This latter requirement pertains to hovering in still air and for thrust inputs up to the maximum permissible. Finally, the translational height damping in vertical flight

(i.e., the vertical force proportional to vertical velocity) shall not be in the unstable sense. All of the above control requirements as given in Reference 1 are thought to be sufficient to provide the vehicle with moderate maneuvering capability. These criteria apply up to the limits of the Service Flight Envelope or 35 knots, whichever is less.

The results for hover or near hover (V = 0.6 knots) for the ejector wing are given in Figure 39. The wing ejector was used to obtain the desired climb rate while the nose ejector provided the necessary pitching moment to fulfill the pitch angle criteria of the specification. The horizontal stabilizer was not used to perturb the vehicle near hover because its effectiveness is minimal here. A time lag of 0.1 second was assumed to exist between control actuation and actual change in the jet momentum flux at the wing and nose ejectors, which is the maximum allowable lag according to the specification. The input perturbing the vehicle from the equilibrium flight condition was taken to be the classical step function 1(t).

The results indicate that a 12.5 fps change in V_J was required to effect a climb acceleration equal to or in excess of 0.1 g, as specified for a Level 1 category vehicle. This change corresponds to a 5130-lb increase in jet momentum flux from the wing ejector. An additional 2110 lbs of down thrust was required at the nose ejector and 707 lbs was expended for the SAS system to effect a positive 3-degree rotation in pitch within the first second after the initial

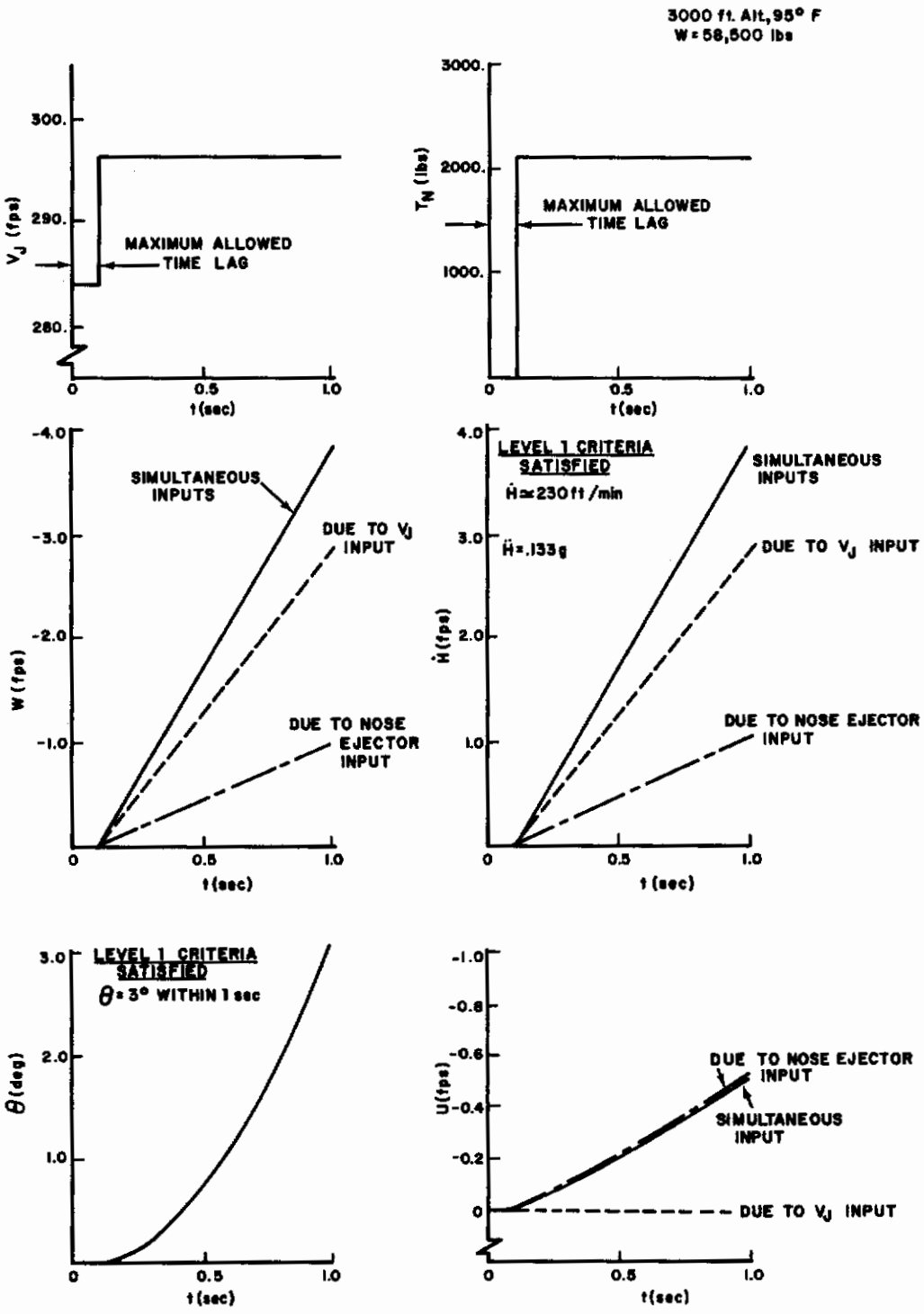

Figure 39. Transient for Ejector Wing Configuration
(λ=90°, V=.593 Knots)

input by the pilot. No additional thrust was used to fulfill the height damping criteria in vertical flight (i.e., the vertical force proportional to vertical velocity) since the derivative Z_w was negative, tending to make the plunging motions stable. No pitch change occurred in performing climb so that the same expenditure of thrust as given above would be required to effect a $\theta = -3°$ within one second.

The transients resulting from throttle and stick inputs were combined to give the maneuver resulting from simultaneous actuation of pilot controls. It was the combined transients that were used in determining the reserve thrust necessary for fulfilling the specification. In addition, the variation of θ and w with time for simultaneous control input were used in estimating the thrust required by the SAS system. The total thrust required to meet the Level 1 criteria was then estimated by the simple addition of all individual control power contributions and the results indicate that a thrust-to-weight ratio of $T/w = 1.14$ is required for hover to satisfy these criteria. Further discussion on total thrust requirements is reserved until later.

Note that the u perturbation is negative in Figure 39. A nose-up pitch rotation causes a rearward reaction, and the vehicle slows down from its forward flight trim speed of 1 fps. Also note that $\frac{\dot{h}}{V}$ and w/V exceed 0.3 when $t \geq 0.16$ sec. Thus, the validity of the assumption made in deriving the linearized equations of motion

is subject to reservations, as discussed previously. The criteria used here for determining maneuverability requirements for a Level 1 ejector wing configuration apply only to the speed range between hover and 35 knots. Sections 3.3.5 and 3.3.6 of Reference 1 must be used when the maneuvering requirements for V > 35 knots are of interest during the transitional flight path. A smooth blend in the characteristics of the VSTOL between these two speed regimes is desirable. To aid in establishing this smooth blend for the ejector wing configuration, we decided to apply the criterion for V < 35 knots, as discussed above, to the third trim point indicated in the table shown in Figure 33. The results of this application are shown in Figure 40.

Analysis showed that the horizontal stabilizer can be used to provide the ± 3 degree pitch rotation within the first second after pilot control actuation at approximately 47 knots. Therefore, the use of the nose ejector may not be necessary for attitude maneuvering for flight speeds above 47 knots. In terms of the transients shown in Figure 40, a step input of 5130 lbs to the wing ejector system was necessary to meet the Level 1 climb criteria; also, the SAS system expended 437 pounds of additional thrust when the horizontal tail was actuated to obtain 3 degrees of pitch within one second of pilot input. Since $\lambda = 75°$, there is a component of wing ejector thrust directed along the positive X stability axis of the vehicle. Therefore, forward speed u increased with increase in wing ejector thrust. The quantities u/V and $\frac{\dot{h}}{V}$ fall within the small velocity perturbation assumptions made in deriving the linearized equations of motion

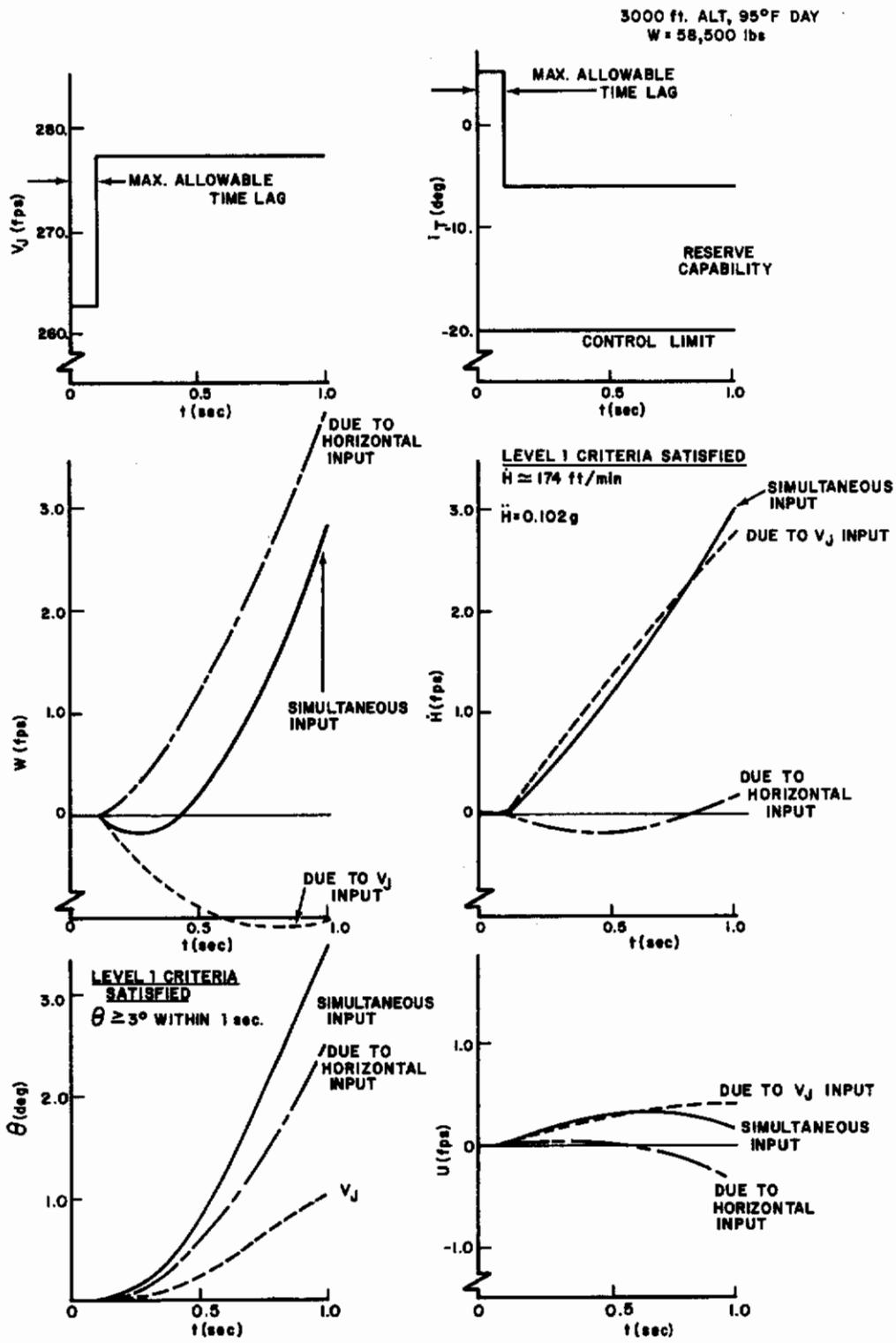

Figure 40. Transient for Ejector Wing Configuration (λ=75°, V=55 Knots)

as discussed previously. The facts that the aerodynamic coefficients in these equations of motion vary as a function of velocity as the ejector doors are closed during transition and that the aerodynamics are nonlinear are still a subject for discussion.

An analysis was made for the installed thrust necessary to fulfill the criteria specified in Sections 3.2.3, 3.2.4, and 3.2.5 of Reference 1 for the Sikorsky stowable rotor configuration in hover (reference Appendix III.) A comparison was made to the thrust-to-weight requirements for the ejector wing configuration. The results are shown in Table V.

TABLE V

THRUST-TO-WEIGHT RATIO IN HOVER
(Longitudinal Mode Only)

	Ejector Wing Configuration	Sikorsky Stowable Rotor Configuration
1. Vehicle Design Gross Wt. (lb)	58,500.	65,000.
2. Wing Download Due to Rotor Downwash During Hover (lb)	0.	5,470.
3. Thrust Required for SAS Operation (lb)	707.	0*
4. Thrust Required for Pitch Maneuvering (lb)	2,110.	0*
5. Thrust Required to Fulfill Climb Requirements (lb)	5,130.	6,040.
Total Installed Thrust Required	66,450.	76,510.
T/W	1.14	1.18

* Additional thrust not required; SAS feedback on θ and q vehicle motions. SAS and pitch maneuvering controlled by blade cyclic which offsets thrust vector from shaft axis. There is a horsepower expenditure when blade cyclic is used.

The drag incurred because of a wing and pylon immersed at right angles to the slipstream of the lift propulsor was estimated. The velocity in the slipstream of the rotors was determined from the analysis presented in Appendix III. This velocity was modified to reflect slipstream contraction below the rotor disc plane. Strip theory was then used for that portion of the wing immersed in the slipstream to estimate wing drag. Cross flow drag concepts were used to estimate the drag on the pylon immersed in the slipstream (Reference 4). The results of these calculations are given in Item 2 of Table V. This drag penalty amounts to 8.42% of the vehicle weight in the case of the Sikorsky stowable rotor configuration. If the wing had been tilted to be aligned at zero angle of attack to the axial flow component of the slipstream, the drag penalty would be approximately 60 lb. There is no such penalty for the ejector wing configuration because lift propulsion is generated from within the wing itself.

The thrust expenditures for the operation of the SAS system and for providing maneuvering capability in vehicle pitch (i.e., $\theta = \pm 3^\circ$ in 1 second) are presented in Items 3 and 4 of Table V. These operations necessitate the expenditure of thrust at the nose ejector of the ejector wing configuration to provide the required pitching moments about the vehicle c.g. In the stowable rotor configuration, on the other hand, SAS operation and vehicle pitch maneuverability are achieved by the use of cyclic control at the rotors. This causes the rotor thrust vector to shift either forward or aft from the rotor shaft axis

and creates the necessary pitch moments about the vehicle c.g. No additional thrust is required. Additional shaft horsepower is expended with the use of cyclic control.

The thrust expended in meeting the climb requirements as specified in MIL-F-83300 are given in Item 5 of Table V. The 6040 lb thrust increment for the Sikorsky stowable rotor configuration includes the additional download on the wing that is incurred when the rotor disk loading is increased to achieve the necessary climb rate as discussed above.

The data suggests that the T/W ratio in hover is 1.18 for the Sikorsky stowable rotor configuration, as compared to 1.14 for the ejector wing vehicle. The major contributor in making the T/W of the Sikorsky vehicle so high is the download on the wing. For example, if the wing were tiltable to zero angle of attack relative to the rotor downwash of this vehicle, T/W = 1.08. This implies that the T/W for a tilt wing configuration of the same weight as the Silorsky vehicle may be of the order of $1.08 \leq 1.10$ for control over the longitudinal modes of flight.

Basing hover performance on only the thrust-to-weight ratio may lead to erroneous conclusions in the sense that horsepower requirements should be considered as well. The T/W ratio does not reflect power expenditures. For example, a comparison of the air

horsepower requirement yields

$$\frac{\text{Air HP Required by ejector wing vehicle in hover}}{\text{Air HP Required by Sikorsky stowable rotor vehicle in hover}} \approx 3$$

at an altitude of 3000 ft on a 90°F day. This means that the air horsepower required and specific fuel consumption is, theoretically, three times greater for the ejector wing vehicle than for the Sikorsky stowable rotor configuration in hover.

7. CONTROL POWER CHARACTERISTICS FOR 35 KNOTS < V ≤ V_{con}

The criteria of Reference 1, Section 3.3.5, state that when the aircraft is trimmed in unaccelerated flight at any speed and altitude within the Operational Flight Envelope, it shall be possible to develop at the trim speed the limiting attitude or angle of attack of the Operational Flight Envelope. In addition, when automatic stabilization and control equipment or devices are used to overcome an aperiodic instability, both the magnitude of the instability and the installed control power shall be such that at least 50 percent of the nominal control moment is available to the pilot in the critical direction through the use of the pitch control. This requirement applies throughout the Service Flight Envelope within ±15 knots TAS or 15 percent of the trim speed, whichever is greater. Also, the aircraft dynamic characteristics, together with the effectiveness and response times of the pitch, thrust magnitude, and thrust angle controls, shall be such that adequate control of the flight path and airspeed can be maintained at all permissible angles of attack and load factors.

The Operational Flight Envelope defines the boundaries in terms of speed, attitude, and load factor within which the V/STOL must be capable of operating to fulfill its mission. The Service Flight Envelope contains the Operational Flight Envelope and defines the aircraft structural and operational limits. These envelopes have not been defined, as yet, for the ejector wing configuration. Furthermore, only one flight path through transition was investigated above. Many possibilities exist between the flight corridors within transition from hover to forward flight, and vice versa. The more critical of these flight paths must be defined before the control power characteristics of the ejector wing configuration can be evaluated fully with regard to the above criteria.

The maneuverability of the ejector wing configuration can be demonstrated by an evaluation of the control power necessary to cause vehicle transients about one trim path, such as the one shown in Figures 6 through 13. For example, analysis has shown that horizontal stabilizer deflection can provide sufficient pitch moment change to cause a 3 degree rotation in vehicle attitude within 1 second of the input perturbation for $V > 47$ knots (reference the previous section of this report and Figure 40). This vehicle's capability to fulfill the above criteria is indicated, at least, by the reserve control power available from the stabilizer after this surface has been deflected from its trim position to cause the above transient, since this reserve control power could be put to use for fulfilling the criteria.

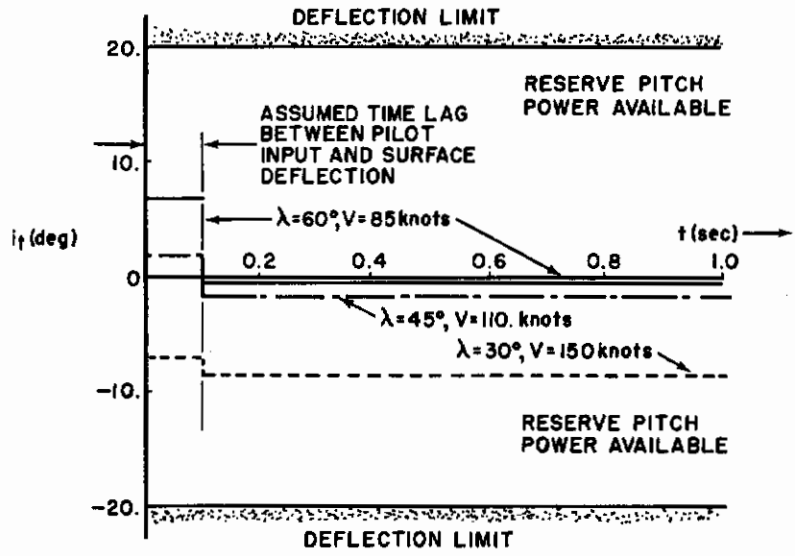

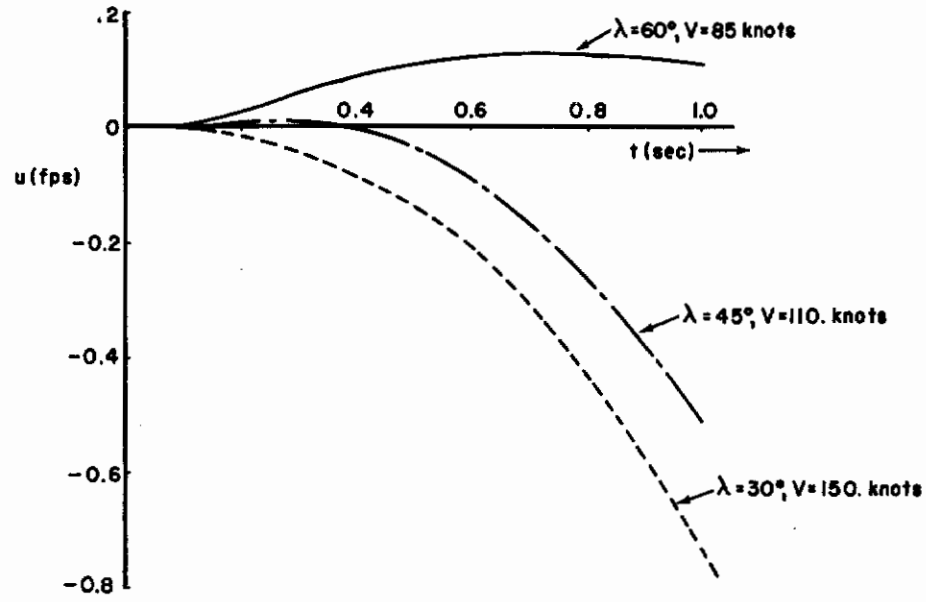

Figure 41. Perturbed Flight for Ejector Wing Configuration (i_T & U for λ=60°, 45°, and 30°)

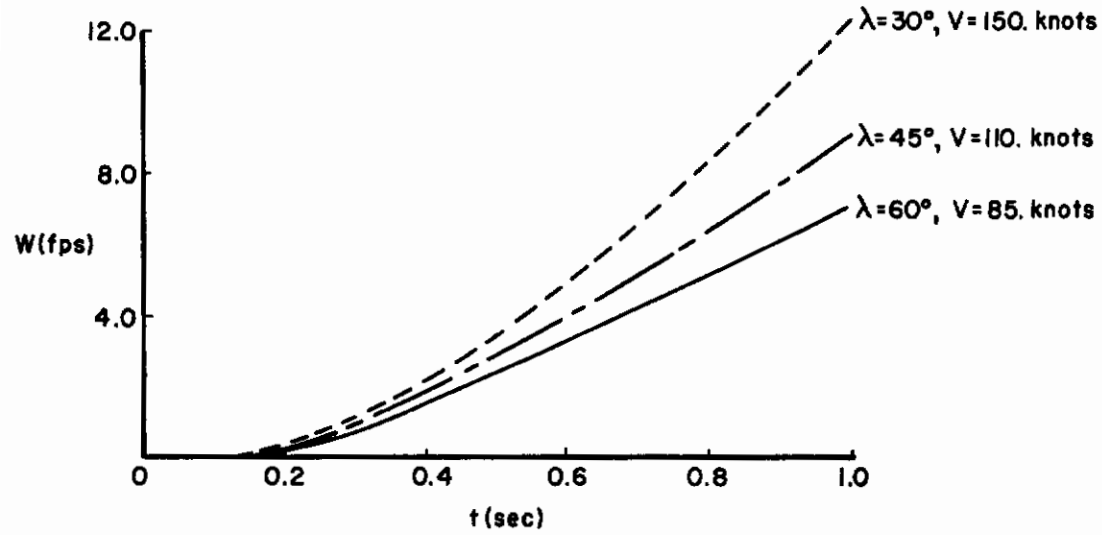

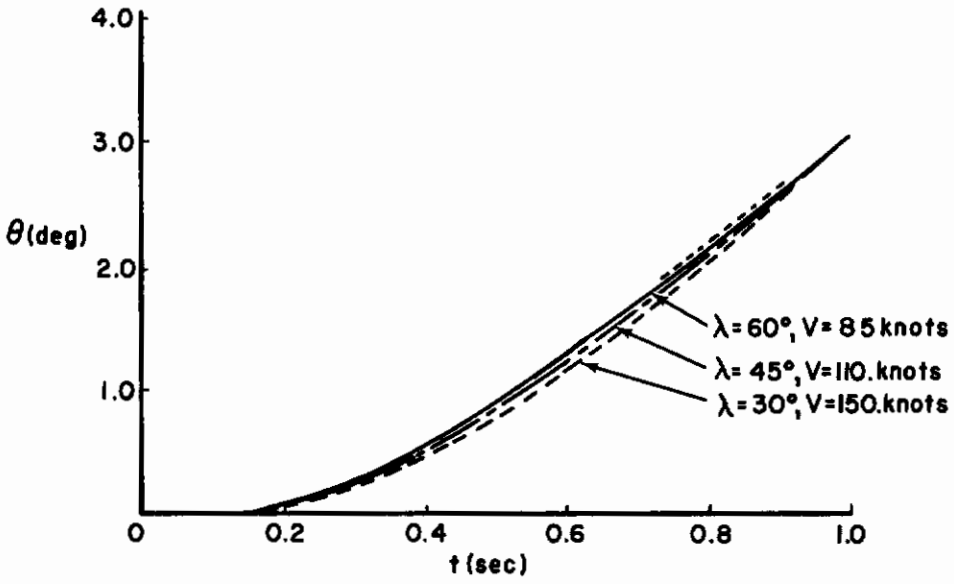

Figure 42. Perturbed Flight for Ejector Wing Configuration (ω & θ for λ = 60°, 45°, and 30°)

The results are shown in Figures 41 and 42. The trim velocities about which the transients take place correspond to the trim velocities for λ = 60°, 45°, and 30°, as given in the table in Figure 33. It was assumed that the SAS pitch moments were provided by the nose ejector system and that the horizontal stabilizer alone was used for maneuvering or for changing the trim condition from the nominal given in Figures 6 through 13. In addition, a 0.1 second time lag was used between the pilot's actuation of the stick and the initial input to the horizontal tail. As indicated in Figure 41, plenty of reserve stabilizer power is available for attitude control after perturbing the vehicle by θ = 3° in 1 second (Figure 42). From Figure 9, the trim horizontal tail setting for λ=60° or V=85 knots is 6.9°. An up horizontal deflection to $i_T \simeq -0.5°$ means that the horizontal surface drag contribution has been reduced. Consequently, forward speed increases, as indicated in Figure 42 where $u > 0$. The trim stabilizer setting for λ = 30° is $i_T = -7.0°$. Up deflection of the horizontal causes an increase in the absolute value of the horizontal deflection angle causing a corresponding increase in vehicle drag. Thus, a decrease in forward flight speed occurs, as indicated in Figure 42, when $u \leq 0$. In all cases, an up deflection in horizontal causes a decrease in vehicle lift so that the vehicle loses altitude initially ($w \geq 0$). The greater loss occurs at the higher forward flight trim speed since the dynamic pressure $1/2\ \rho V^2$ is higher here.

The control power available for the ejector wing configuration should blend smoothly between the criteria given in the

last section for $V \leq 35$ knots and that given above (35 knots $< V \leq V_{con}$). In addition, a smooth blend should exist between the criteria requirements discussed here and those given in Reference 11 for conventional flight ($V > V_{con}$). Since the control power necessary to meet the criteria for $35 < V \leq V_{con}$ could not be defined clearly, no effort was made to establish engineering judgments as to what the ejector wing vehicle's control blend should be between the criteria of the three speed regimes. In particular, the control power criteria for 35 knots $< V \leq V_{con}$ were not applied to vehicle perturbations about a trim point where $V < 35$ knots or for $V > V_{con}$ so that these engineering judgments could be formed.

The ejector wing and Sikorsky stowable rotor configurations are not compared for 35 knots $\leq V \leq V_{con}$ since requirements for the ejector wing configuration have not been established.

8. CONSIDERATIONS ON THRUST-TO-WEIGHT RATIO

The thrust-to-weight ratio for $V = 0.593$ knots has been discussed for the ejector wing configuration. The total thrust necessary in fulfilling the Level 1 criteria for $V < 35$ knots was determined and the thrust-to-weight ratio required was $T/W = 1.14$ for control over the longitudinal mode of flight. The reserve thrust needed to perform a vertical acceleration of 0.1 g and a climb rate of at least 100 fpm was determined for the trim speeds used in Figures 41 and 42. These

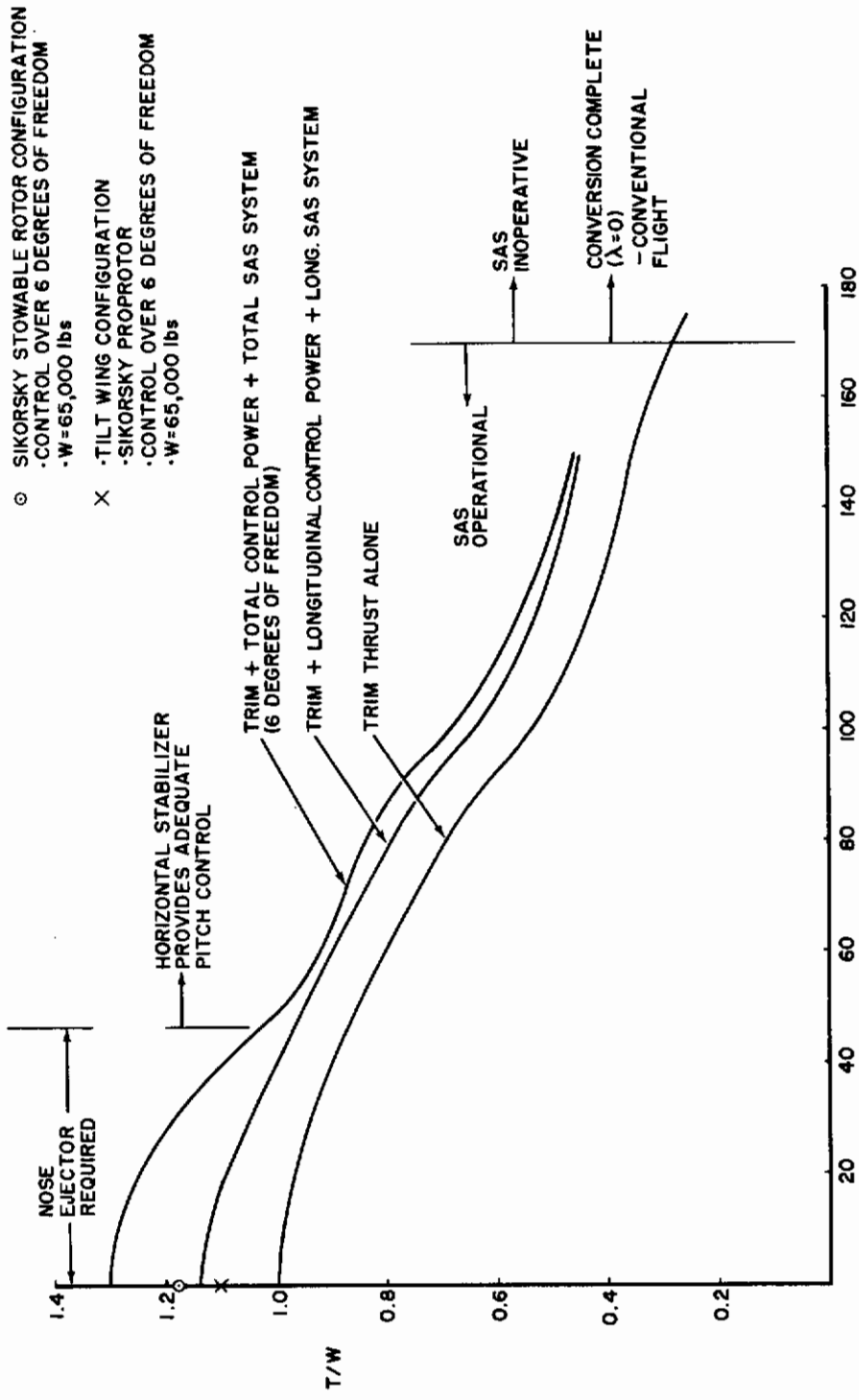

Figure 43. Thrust-to-Weight Ratio for the Ejector Wing Configuration

thrust increments were added to the thrust required to operate the SAS system at these trim speeds and to maintain trim forming an estimate of the total control thrust necessary for 35 knots < $V \leq V_{con}$. The results of these calculations including the thrust-to-weight ratio for V = 0.593 are shown in Figure 43.

The data for trim alone and for controlling the longitudinal motions of the ejector wing configuration are a result of the evaluation discussed above. The results shown in Figure 43 for controlling the full six degrees of freedom, however, warrant further discussion. The total thrust necessary to control all of the degrees of freedom for $0 \leq V \leq 35$ knots consists of the longitudinal total thrust as described above plus an additional amount to control the roll and yaw modes of flight. These modes require SAS control about the X and Z body axes and a reserve thrust contribution which can be used to give $\phi = \pm 4°$ and $\psi = \pm 6°$ within 1 second after the controls are actuated. Now, the sum of $T_{SAS} + T_N$ gives the thrust required (T_{SAS}) for the SAS actuations controlling vehicle dynamics about the Y body axis and the additional thrust necessary (T_N) to provide 3 degrees of pitch in 1 second. An estimate for reserve thrust required to control roll may then be $\frac{4I_{xx}}{3I_{yy}} (T_{SAS} + T_N)$ for the ejector wing configuration if it is assumed that similar SAS power expenditures as that for the longitudinal are required to control the roll mode and that a wing tip ejector system is used to provide the 4 degrees of roll rotation. The factor of $4I_{xx}/3I_{yy}$ is just the ratio of the amount of rotation necessary about the X-body axis to meet the specification as

compared to that necessary about the Y body axis. The feedback loops controlling roll motions might be actuated by β and p as opposed to w and q as in the longitudinal SAS loops. Similarly, an estimate for the power required to control yaw by means of a separate yaw ejector system may be $6I_{zz}/3I_{yy}$ $(T_{SAS} + T_N)$ where 6 degrees of yaw rotation are required within the first second to meet the specification and β and r actuate the SAS feedback loops for control about the Z-axis. This means that the additional thrust necessary to control the roll and yaw modes of the ejector wing configuration is $\frac{1}{3I_{yy}}$ $(4I_{xx} + 6I_{zz})(T_{SAS} + T_N)$. However, the wing ejector could be programmed to provide some roll and yaw control power. Presumably, differential door angle in the wing ejector system might be used to provide some yaw control. Similarly, differential thrust between the left and right wing ejector systems could give some roll control. It is assumed that the wing ejector system is programmed to provide 25% of the lateral-directional SAS feedback and that the additional thrust necessary to control the roll and yaw modes is $\frac{.75}{3I_{yy}}$ $(4I_{xx} + 6I_{zz})(T_{SAS} + T_N)$. This additional thrust contribution was added to the longitudinal thrust required for the ejector wing configuration to yield the results shown in Figure 43 for control over the full six degrees of freedom.

The results given in Figure 43 indicate that a thrust to weight ratio of between 1.14 and 1.30 is required for the ejector wing configuration at hover to meet the specification as defined in Reference 1. No additional thrust reserve was used to fulfill the height damping criteria in vertical flight (i.e., the vertical force proportional to vertical velocity) since the derivative Z_w was negative,

tending to make the plunging motions stable. No reserve was included for accelerating from hover at a constant altitude. In addition, no accounting was made of losses due to inefficiencies of the ejector systems and propulsive engines, the existence of ducting air leaks, and frictional losses in the ducting systems between engines and the ejector systems.

Also shown in Figure 43 are the thrust-to-weight ratios required for the Sikorsky stowable rotor configuration and tilt wing configuration in hover. The data indicates that T/W = 1.18 is required for the stowable rotor vehicle, and T/W $\leq$ 1.10 for the tilt wing aircraft. Discussions following Table III indicate the analysis of thrust-to-weight required in hover for these configuration.

The upper value of T/W = 1.3 for the ejector wing configuration in hover includes the effects of an additional ejector system to control roll and another to control yaw motions. That is, the wing ejector in not programmed fully to provide roll or yaw control power. If full implementation were possible, such that the wing ejector provided all of the roll and yaw control, the thrust-to-weight ratio for the ejector wing configuration (6 degrees of freedom) would be close to T/W = 1.14.

SECTION IV

SOME CONSIDERATIONS ON DOWNWASH

1. PROBLEMS WITH DOWNWASH

In performing a rescue mission with an ejector wing configuration or helicopter, the downwash from the lifting system becomes an important consideration. Downwash can cause personnel on the ground to experience difficulty such as loss of footing, injury due to debris or broken foliage, loss of body heat to a rescuee in shock, and swinging and entanglement in the rescue hoist. In addition, the ejector wing configuration may encounter serious operational difficulties while in low-altitude hover. Since the disk loading of the ejector wing configuration is much greater than that of the conventional helicopter, its downwash velocity is significantly higher, which can generate excessive spray in hover over water or agitate sand in hover over land. This is unattractive not only from the point of view of detection, but can result in the loss of pilot visibility, harm to either equipment or personnel being rescued, and possible damage to the wing ejector system and engines due to spray or debris ingestion. Furthermore, the cavity formed below the vehicle and on the surface of water during hover may be of sufficient depth to change the induced flow pattern through the ejector system significantly. This could result in an unfavorable effect on hover performance and vehicle stability. Also, unsteadiness in cavity shape and longitudinal or lateral oscillations of the water cavity along the surface of the water may have an effect on the pilot's capability to maintain a stationary hover attitude. Thus, the workload

of the pilot could be significantly increased and the completion of the mission could be affected.

2. IMPACT PRESSURE

The impact or dynamic pressure of the jet flow issuing from the ejector wing system was estimated and the results are shown in Figure 44. The midmission weight was taken to be 75% of the design takeoff weight. For an ejector system, $\bar{q}$ is equal to the gross weight divided by twice the exit area of the diffuser since the downwash is fully developed at the ejector exit plane. Therefore, the quantity $\bar{q}$ equals one-half the disk loading for this kind of propulsive system.

The data indicates that $\bar{q}$ approaches 81.0 psf for the wing ejector vehicle weight of 58,500 lb. It was assumed here that the nose ejector was not used to provide propulsion and that the moment balance required to maintain the trimmed hover condition was achieved by the use of the hot core efflux from the jet engines at the rear of the fuselage. The minimum weight considered for performing a rescue is the midmission weight of 44,000 lbs, as established above. Here, $\bar{q}$ was estimated to be 45.5 psf if the nose ejector were used to provide thrust in maintaining hover during the rescue. Therefore, $\bar{q}$ should vary between 45.5 and 81 psf during any rescue operation, with the magnitude of impact pressure being a function of vehicle weight and use of the ejector system during hover, as shown in Figure 44.

Downwash impact pressures for several different VTOL aircraft were compared. Downwash characteristics of all of

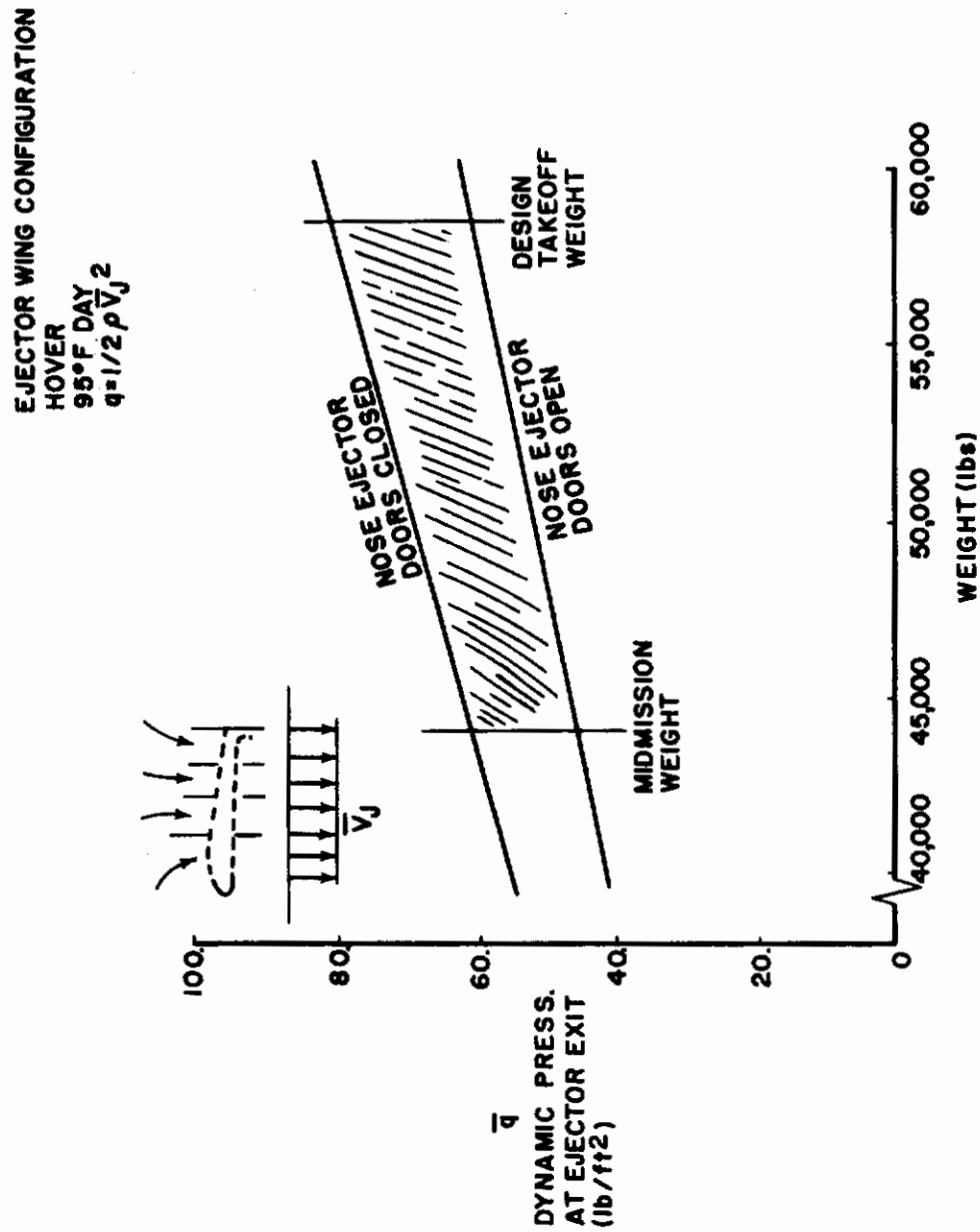

Figure 44. Dynamic Pressure of Ejector Exit Mass Flow

these aircraft have been evaluated experimentally and all have demonstrated feasibility for use in rescue operations, at least to some degree.

The downwash data for the XC-124A is considered to be most representative of the ejector wing configuration. The planforms of the XC-142A tilt wing VTOL and the ejector wing configuration are compared in Figure 45. The maximum dynamic pressure $\overline{q}$ in the downwash of the XC-142A is equal to the propeller disc loading because the effective area of the downwash of the propeller contracts to about 1/2 of the disc area. For the ejector wing, on the other hand, the downwash is fully developed at the diffuser exit plane, as discussed above. The maximum dynamic pressure just below the propulsive units of both the ejector wing and the XC-142A is also indicated in Figure 45.

3. IMPACT PRESSURE AT GROUND LEVEL

The maximum dynamic or impact pressure at ground level below the ejector wing configuration was estimated and the results are shown in Figure 46. The quantity H_E is the height above ground of the ejector wing system, and $\overline{q}_E$ is the dynamic pressure as measured along the center line of the downwash at the surface of the earth. It is the magnitude of $\overline{q}_E$ within the downwash field at ground level that causes problems on the ground.

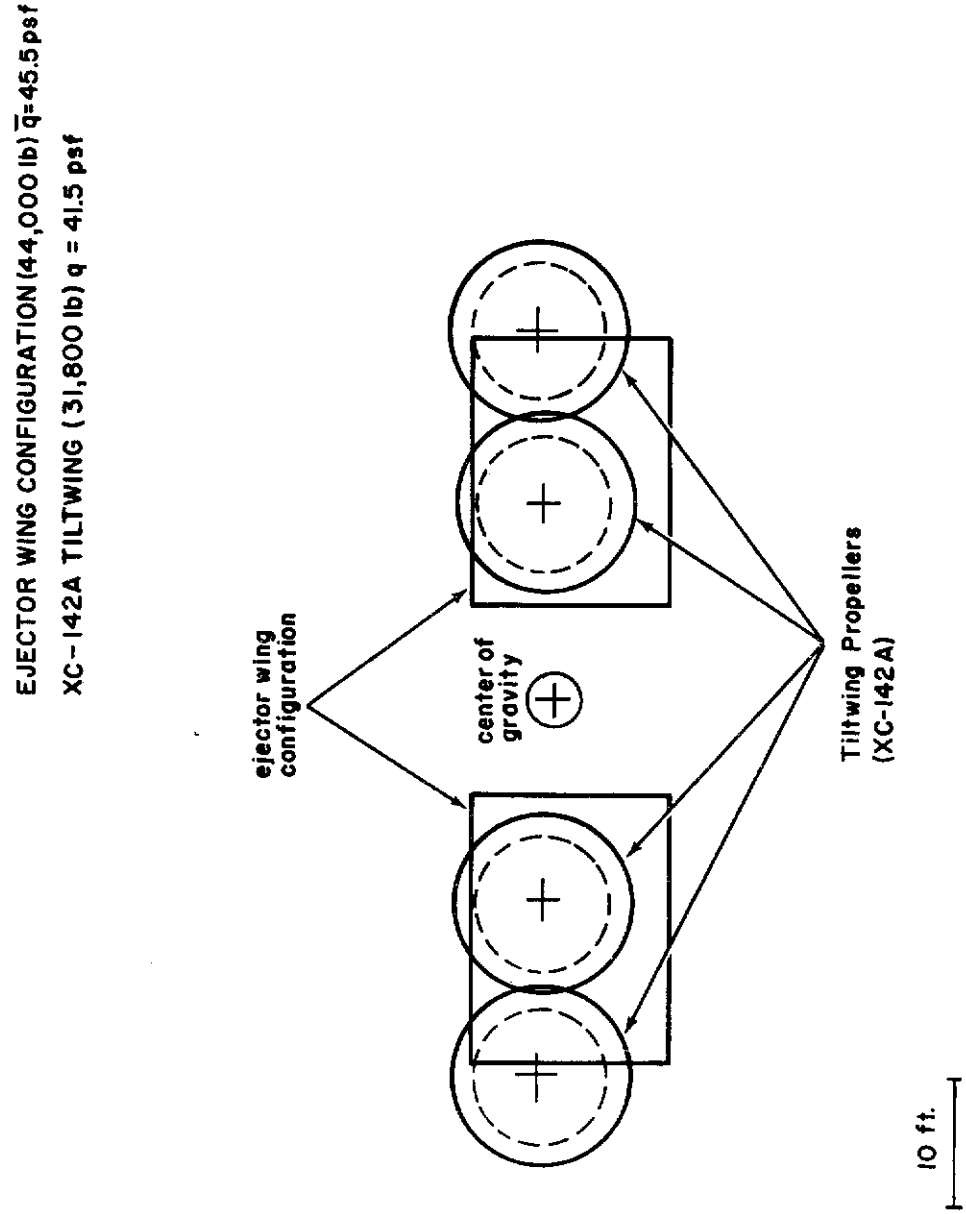

Figure 45. Comparison of Lifting Propulsion Planforms

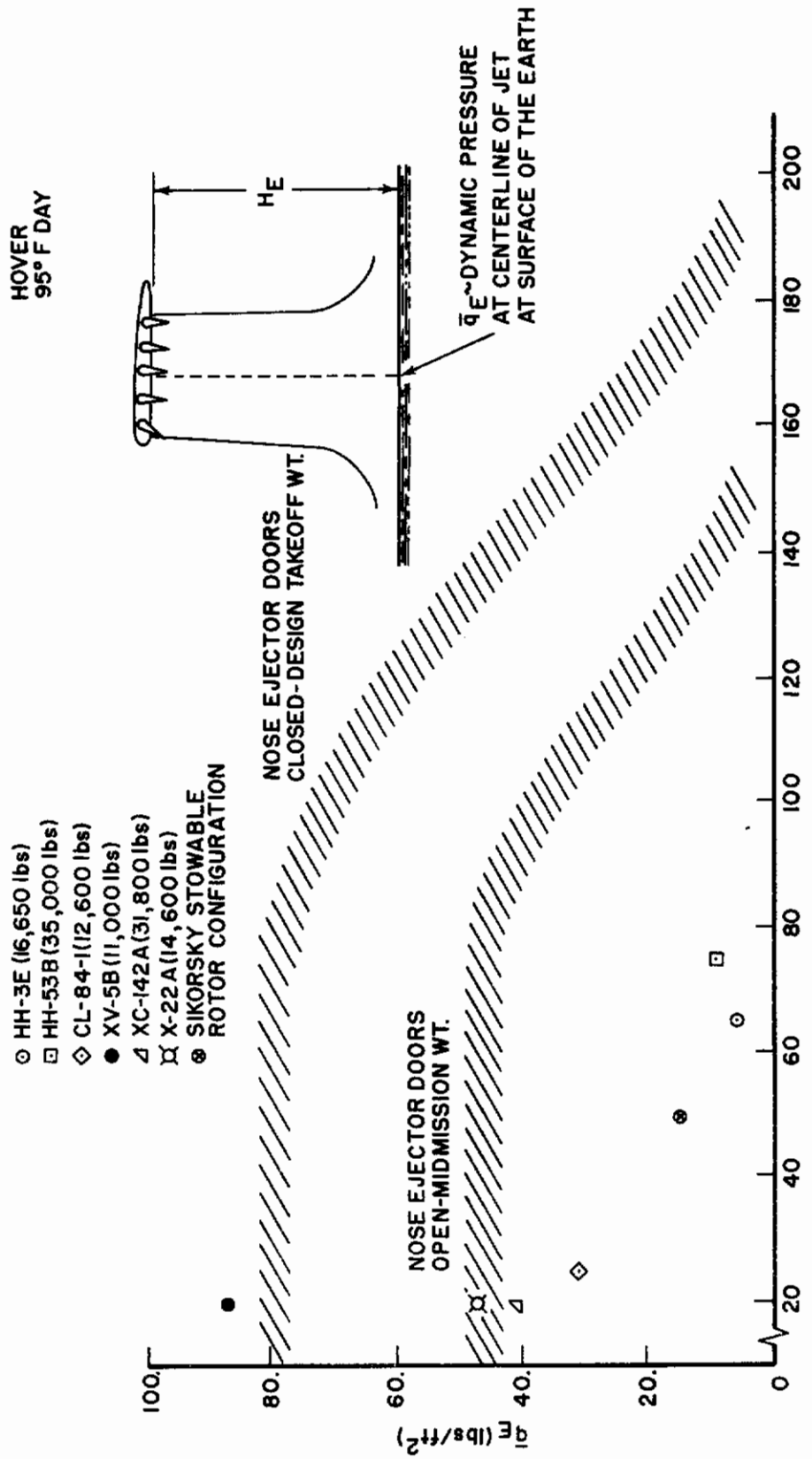

Figure 46. Dynamic Pressure in Downwash at Ground Level

The data indicates that $\bar{q}_E$ for the ejector wing configuration should lie in the range $45.5 \leq \bar{q}_E \leq 81$ psf for hovering altitudes below $H_E = 80$ ft. The higher impact pressure corresponds to an ejector wing vehicle design weight of 58,500 lbs with nose ejector doors closed, while the lower impact pressure corresponds to the midmission weight of 44,000 lbs with nose ejector doors open. Figure 46 also shows the downwash characteristics for other VTOLs, including the Sikorsky stowable rotor configuration. At low hovering altitudes and for the design takeoff weight, the strength of the downwash for the ejector wing configuration is comparable to that of the XV-5B. Therefore, we recommend that a vertical takeoff at the beginning of a mission with full gross weight be initiated from a prepared concrete site and that adequate precautionary measures be taken to ensure that ground personnel are not injured, ground equipment damaged, or the vehicle itself damaged through debris ingestion.

Impact pressure at the earth's surface decreases with altitude when $H_E > 80$ ft. This decrease is attributable to entrainment processes and viscous flow mixing within the downwash flow field. We recommend that a rescue operation be attempted from an altitude in excess of $130 \leq H_E < 140$ ft at the midmission vehicle weight, and at an altitude in excess of 175 ft if the vehicle weight is 58,500 lbs or the nose ejector is inoperative. At these altitudes, the strength of the downwash field at ground level should be comparable to that produced by the HH-3E, the Sikorsky stowable rotor configuration, and the HH-53B when hovering at one rotor diameter above ground level.

4. OPERATIONS OVER WATER

Figure 47 depicts a simplified representation of the spray that may be generated by the ejector wing configuration in low altitude hover over water. Several angular regions may be defined in terms of pilot visibility (Reference 13) and these indicate that:

a. Vision should be unimpaired if the interests of the pilot concern the region ζ_1.

b. In ζ_2, vision should be primarily affected by the spray enveloping the fuselage.

c. In ζ_3, a primary source of visibility deterioration would be due to spray which leaves the cavity tip; this region is designated as the region of severe spray activity. Vision in this region would be affected also by the spray enclosing the fuselage. Thus, this region may be considered as the one where pilot visibility would be most affected by spray.

The cavity structure on the surface of the water should have a relatively smooth center portion. Small white-crested waves should form near the center of the cavity, and these waves should increase in size and move radially outward from the cavity center. Most of the spray should originate from the white crests of these waves when they reached the lip of the cavity and the initial angle of spray projection should be approximately equal to the slope of the cavity at that point. The cavity depth, the quantity of white crested waves, and the slope near the cavity lip should increase with impact pressure $\bar{q}_E$. Correspondingly, more spray should be created, the spray projection angle should be increased and the spray-cloud dimensions should be increased with increase in disk loading.

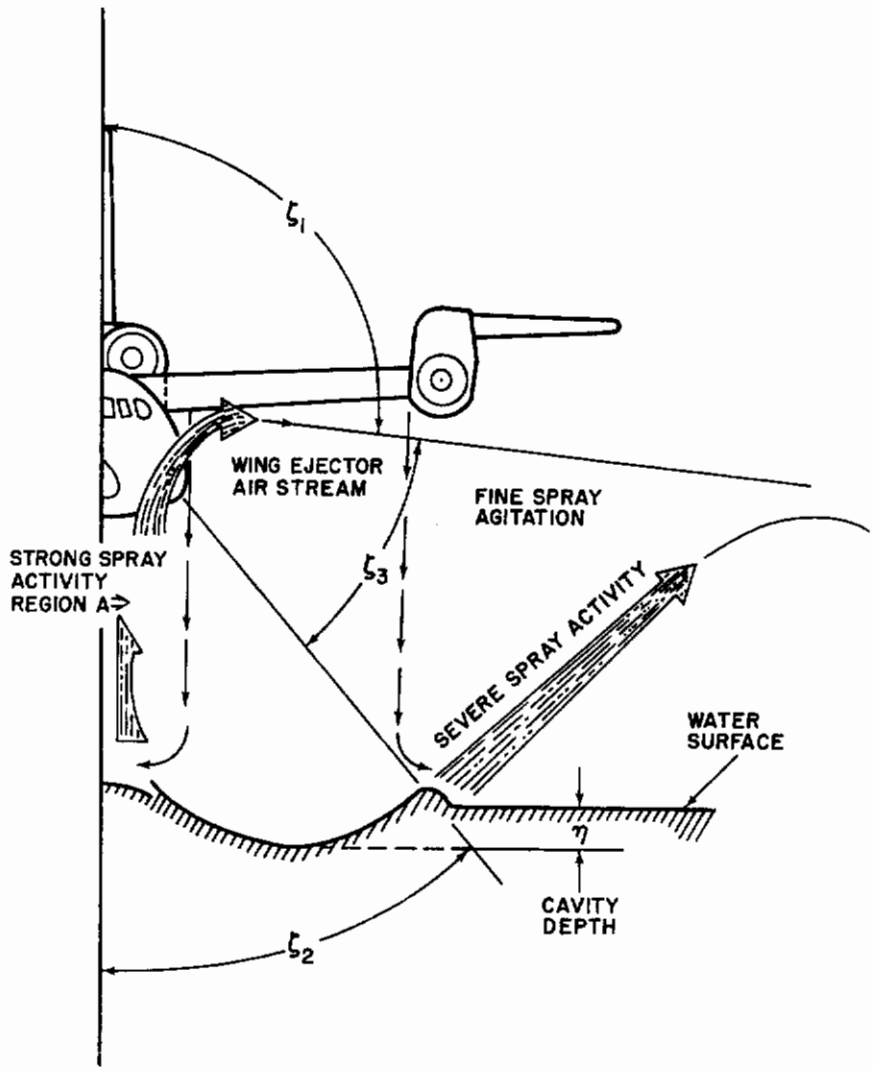

Figure 47. Water Spray Pattern of Ejector Wing in Hover

At low hovering altitudes, two distinct cavities should be formed under the ejector wing configuration and on the surface of the water. Their proximity should cause turbulent agitation in the region between these two cavities, designated Region A in Figure 47. The spray generated in this region would envelope the fuselage at low hovering altitudes and would severely hamper any rescue procedures.

From the point of view of the pilot and the safety of the vehicle, any sea rescue should be performed at hover altitudes above 140 ft so that strong spray activity cannot envelope the fuselage (Reference 13). This would clear region ζ_2 of some spray agitation and improve pilot visibility.

At hovering heights above 140 ft, the two distinct cavities below the vehicle may coalesce, forming a single elliptically shaped cavity. This would eliminate the turbulent agitation of Region A, significantly clear region ζ_2 of spray, and improve pilot visibility. In addition, buffet and spray damage would be significantly reduced. For safety, the equipment and/or personnel should remain close to the cavity center during the whole rescue operation, since buffet and spray damage is less in this area. It was estimated that the equivalent diameter of the coalesced cavity for the ejector wing configuration at a hovering height of 160 ft would be of the order of 80 ft.

SECTION V

CONCLUSIONS AND RECOMMENDATIONS

This evaluation was performed using "stability derivatives" and classical linearized analyses. The validity of such an approach is limited. The aerodynamic forces and moments exerted on a V/STOL can be highly nonlinear near hover or at low transitional flight speeds, and angle of attack and sideslip excursions of ±90° are possible even for modest perturbations in w and u. The aerodynamic coefficients in the equations of motion vary with time as conversion progresses, so that the use of constant coefficients in a linear analysis does not fully represent the character of the motion. Also, large accelerations can be experienced by the V/STOL in transition, and the vehicle is rarely in a state of equilibrium during this mode of flight. Therefore, a rigorous application of linear analyses that is limited to small departures from the equilibrium trimmed flight condition is subject to question. The results of the stability derivative approach presented in this report should be validated by the use of nonlinear equations of motion including a nonlinear aerodynamic representation.

The results of this evaluation are based upon the aerodynamic formulations described in Appendix I. Engineering judgment was used to modify the results of the wind tunnel test program so that the aerodynamic data would represent a 58,500 lb configuration. Certain corrections could not be made. For example, no correction could be made for Reynolds number effects when scaling up the wind-tunnel data.

Insufficient data exists at this time for making this modification for a wing ejector type system. The argument that an increase in Reynolds number may be beneficial since lift and stall characteristics should improve in going to full scale is not valid at and near hover, since the conventional definition of Reynolds number $\left(R_e = \rho \frac{VD}{\mu}\right)$ is difficult to determine under these flight conditions. Interference between ejector mass flow air and the airframe plays a large role near and at hover, and especially when the vehicle is in ground effect. It is difficult, then, to prescribe the correct velocity and the significant characteristic length (D) that should be used in the definition of Reynolds number.

If the ejector wing configuration is to be a viable aircraft in the Air Force, further wind tunnel testing must be performed. The test model should be large and closely resemble the baseline configuration. A vehicle in flight rarely operates in the smooth air environment of a wind tunnel or laboratory, where tests are usually conducted; an operational aircraft is subjected to a number of indignities. The test program should include sensitivity studies to establish the effects of such disturbances as gusts, turbulence, nonuniform inflow, and ingested debris. The test program should also consider the question of duct losses between the propulsive units and the ejector system(s).

Only one flight path through transition was investigated during this evaluation for both the ejector wing and the stowable rotor configurations. Many possible flight paths exist during transition from hover to forward flight. An analytical study should

be performed to define the permissible flight corridors for acceleration from hover through transition and for deceleration from the conventional flight mode. Different acceleration and deceleration rates should be explored, and special emphasis placed upon the mix and phasing of the controls. The application of energy methods for investigating the time required to complete transition should be a valuable aid in defining the optimum transitional flight path, if such exists. This analysis indicates that the Sikorsky stowable rotor configuration requires approximately 8 seconds to perform a transition from hover to the propeller mode of flight at 160 knots. The ejector wing configuration requires approximately 105,000 lbs of installed thrust capability on board the aircraft to accomplish the dash through transition in the same time interval. A search should be made for transitional flight schedules that do not drop bare-airframe handling qualities below the Level 3 category at any point during conversion to the conventional mode of flight.

The evaluation indicates that the ejector wing configuration can be made to meet the Level 1 criteria as specified in the military specification. A Stability Augmentation System is required to fulfill these needs, and the results indicate that a thrust-to-weight ratio of more than 1.14, and possibly as much as 1.3, is required in hover. This T/W ratio does not include any reserve for accelerating from hover at a constant altitude. No accounting was made of losses due to inefficiencies of the ejector systems and propulsive engines, ducting air leaks, and frictional losses in the ducting system between engines and the ejector systems. The time lag between pilot control actuation

and an actual change in the jet momentum flux at the wing and nose ejectors was assumed to be $\leq$ 0.1 second. Thus, all valves and/or control devices that divert engine compressor bleed and/or bypassed air must provide the necessary jet momentum flux changes at the vehicle ejector systems within 0.1 second of the pilot inputs to the control. This limit on time lag is a specification requirement, and an analysis should be performed to see whether it can be fulfilled.

The thrust/weight ratio of 1.14 was obtained by analyzing the longitudinal flight mode of the ejector wing configuration. This value reflects the amount of reserve thrust necessary for climb, pitch control, and SAS control about the Y-body axis only. The value of T/W = 1.3 is based upon the longitudinal mode results as to requirements for controlling the full six degrees of freedom. No evaluation was made of the lateral-directional characteristics of the ejector wing configuration. Therefore, a T/W = 1.3 for control of the six degrees of freedom must be regarded with some reservation. We recommend that the lateral-direction handling characteristics of this vehicle be evaluated, and that the evaluation include an analysis of the flight characteristics with coupled and nonlinear aerodynamics in 6-degree-of-freedom nonlinear equations of motion. The equations, therefore, cannot be solved analytically, but would have to be solved by a numerical integration scheme on a digital computer.

This evaluation indicates that the Sikorsky stowable rotor configuration can be made to meet the Level 1 criteria of the military specification. The T/W ratio in hover was 1.18 in the longitudinal

mode for the stowable rotor configuration, as compared to 1.14 for the ejector wing configuration. The T/W of the Sikorsky vehicle is so high mainly because of the download on the wing due to the two rotor slipstreams, which amounts to 8.42% of the vehicle weight. If the wing had been tiltable and aligned at zero angle of attack to the axial flow component of the rotor slipstream, the T/W ratio would be 1.08. Thus, a tilt wing of the same weight as the Sikorsky vehicle may have a T/W of the order of 1.08 $\leq$ 1.10 for control over the longitudinal mode of flight.

In the stowable rotor configuration, SAS operation and vehicle pitch maneuverability are achieved by cyclic control at the rotors. The rotor thrust vector is shifted from the rotor shaft axis, which creates the necessary pitch moments about the vehicle c.g. No additional thrust is required, but additional shaft horsepower is expended for cyclic control. Roll control is available without additional thrust by using differential collective, which causes a thrust differential between the left and right-hand mounted rotors. Similarly, yaw control is achieved by differential shaft tilt angle between the rotors, which requires some additional thrust. Nevertheless, the T/W ratio necessary to control the full six degrees of freedom for the stowable rotor configuration should be closer to 1.2 than the 1.3 projected for the ejector wing configuration.

Performance of a V/STOL should be based not only on the thrust-to-weight ratio but also on horsepower requirements, since the T/W ratio does not reflect power expenditures. For example, a

comparison of the air horsepower requirement yields:

$$\frac{\text{Air HP for Ejector Wing in Hover}}{\text{Air HP for Sikorsky Stowable Rotor in Hover}} \approx 3$$

The air horsepower required and also specific fuel consumption is three times greater for the ejector wing configuration than for the Sikorsky stowable rotor configuration in hover.

The downwash and spray characteristics for the ejector wing configuration in hover were evaluated. The results indicated that the dynamic pressure in the downwash could be as high as 80.5 psf at a vehicle weight of 58,500 lbs. A vertical takeoff with full gross weight should be made from a prepared concrete site, and adequate precautionary measures should be taken to prevent damage or injury to ground personnel, ground equipment, and the vehicle itself. Rescue operations should be performed at an altitude in excess of 175 ft if the vehicle weight is 58,500 lbs, which would create a downwash field at ground level comparable to that produced by the Sikorsky rotor configuration, the HH-3E, and the HH-53B when hovering at one rotor diameter above ground level.

APPENDIX I

AERODYNAMIC REPRESENTATION OF EJECTOR WING CONFIGURATION

The objective of this research was to investigate the longitudinal stability and control characteristics of the ejector wing configuration. This vehicle employs the wing ejector system for power, and has a vertical takeoff gross weight capability of 58,500 lbs. A wind tunnel test program (References 5, 6) was conducted in the NASA Langley tunnel to determine the aerodynamic forces and moments for a configuration incorporating the wing ejector system. The model was a 1/5 scale version of the ejector wing Research Test Vehicle, or RTV. This configuration has a gross weight capability of approximately 13,000 lbs in full scale.

The RTV wind tunnel data was scaled up to reflect the ejector wing configuration of interest. The scaling law used was that the loading for the model and full-scale wing be the same. No corrections were made for Reynold's number effects when scaling the wind tunnel data to full scale. Nevertheless, the aerodynamic representation was felt to be of sufficient accuracy for performing a preliminary analysis of the longitudinal stability and control characteristics of this vehicle.

1. AERODYNAMIC FORCES AND MOMENTS FOR TRIM

Figure 4 presents the wing cross section in model scale. The wing ejector tubes extend spanwise the length of the wing as shown in Figure 5. The first four ejector tubes are fixed and the inlet and exit doors move with respect to the tubes. The fifth tube is fixed

to the flap and the flap tube moves with respect to the other doors. Thus, the flap setting is established by the door open angle λ.

The quantity $\rho A_{e_\lambda} V_J^2$ is used in nondimensionalizing data presented in this Appendix. This quantity reflects the jet momentum flux from the wing ejector system, where V_J is the average velocity of the air issuing from the wing, and A_{e_λ} is the wing exit area measured in a plane normal to the mean diffuser flow. This quantity was determined during the wind tunnel test program (References 5,6) and is shown in Figure 48 as a function of door angle. This figure reflects model geometry and indicates a scale factor of 107.0 is necessary to obtain Ae_λ for the 58,500 lb ejector wing configuration. Again, the scale factor is based on keeping the wing loading constant between model scale and full scale.

The first contribution to lift, drag, and pitching moment is primarily from the wing ejector system. The formulations are:

$$L_1 = \rho A_{e_\lambda} V_J^2 [\hat{C}_L + \hat{C}_{L_\alpha} \alpha]$$

$$D_1 = \rho A_{e_\lambda} V_J^2 [\hat{C}_D + \hat{C}_{D_\alpha} \alpha] \qquad (4)$$

$$M_1 = \rho A_{e_\lambda} V_J^2 \bar{c} [\hat{C}_m + \hat{C}_{m_\alpha} \alpha]$$

where $\hat{C}_L$, $\hat{C}_{L_\alpha}$, $\hat{C}_D$, $\hat{C}_{D_\alpha}$, $\hat{C}_m$, and $\hat{C}_{m_\alpha}$ are shown in Figures 49 through 54; these reactions are measured about a point at 28% $\bar{c}$ of the model. The quantities $\hat{C}_L$, $\hat{C}_D$, $\hat{C}_m$ are the nondimensional aerodynamic coefficients reflecting ejector wing vehicle flight during

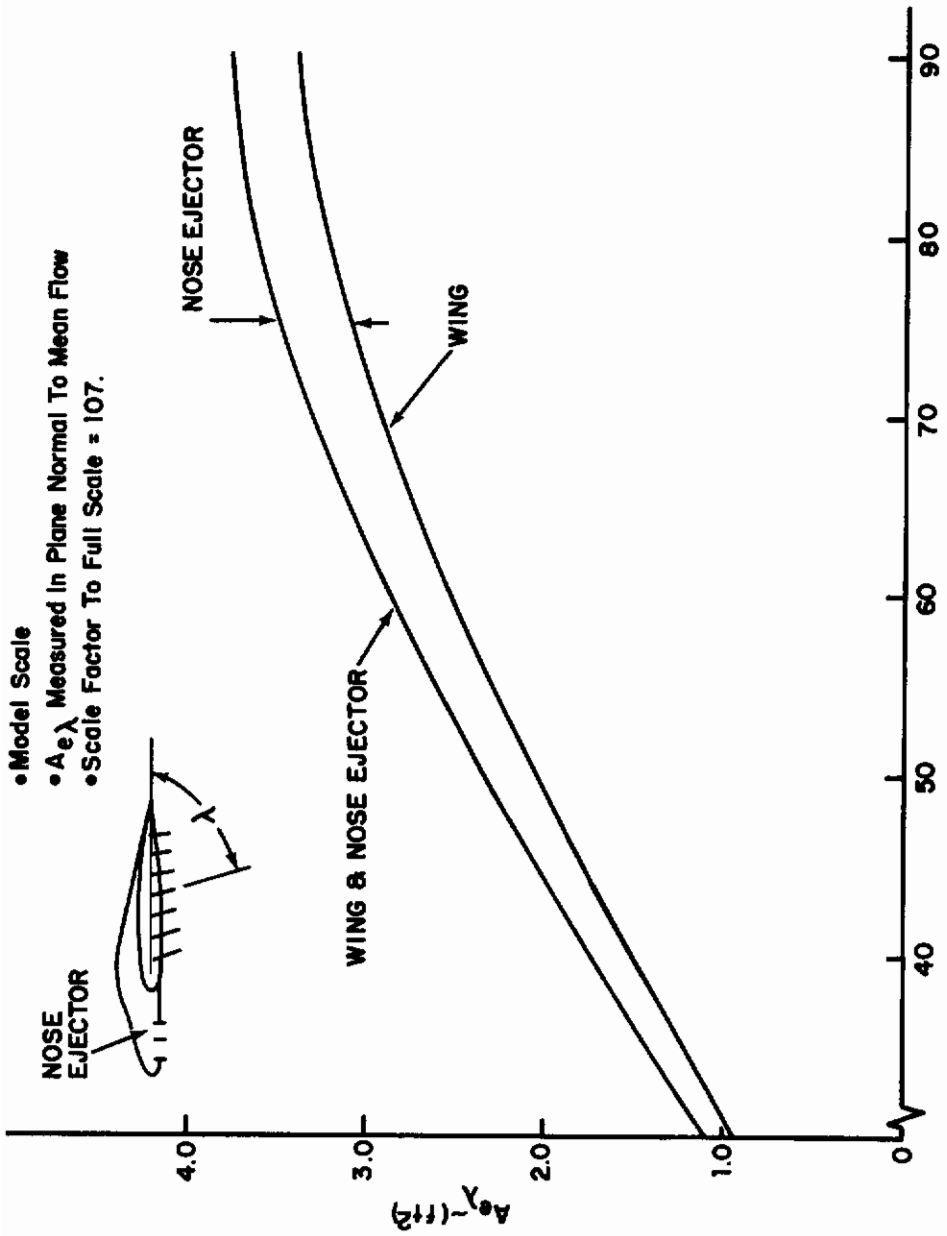

Figure 48. Effect of Door Angle on Ejector Exit Area

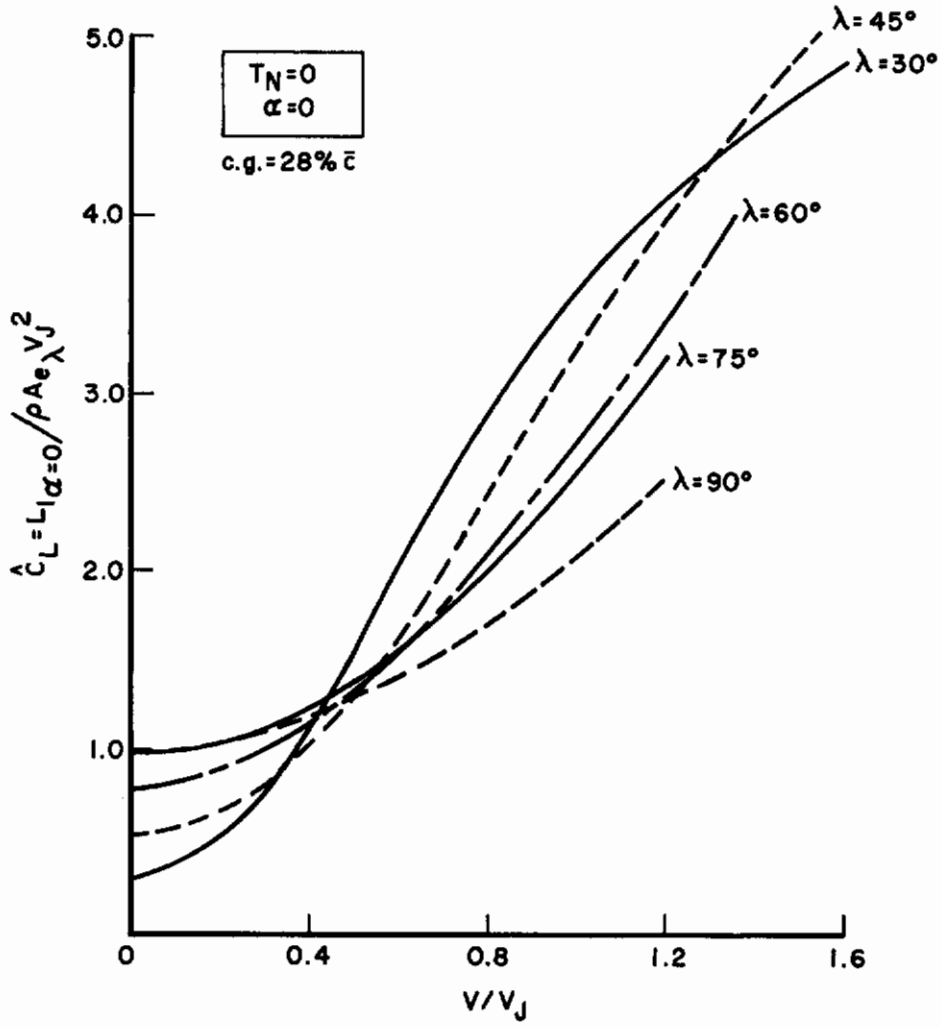

Figure 49. The Effect of Velocity Ratio on $\hat{C}_L$

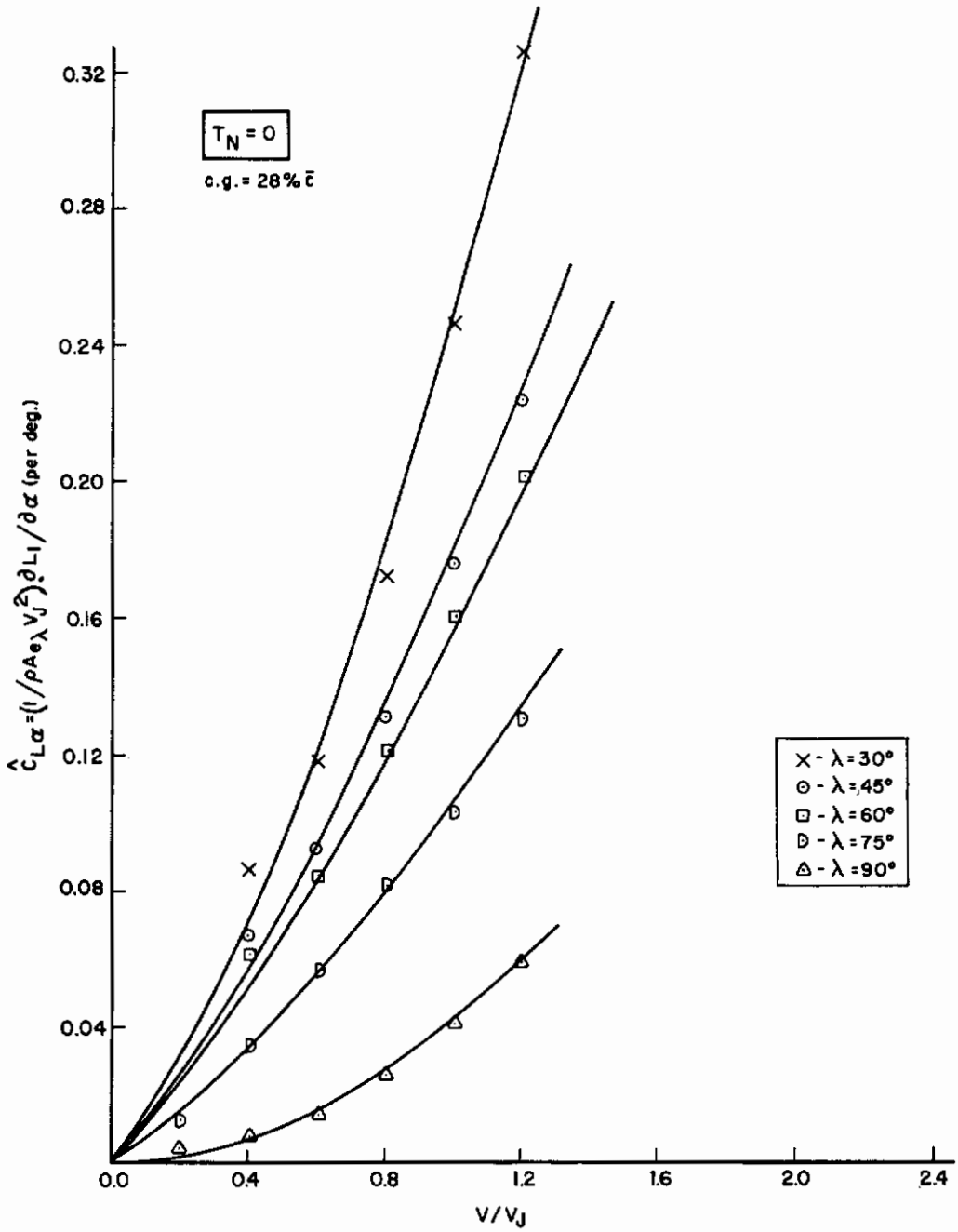

Figure 50. The Effect of Velocity Ratio on $\hat{C}_{L_\alpha}$

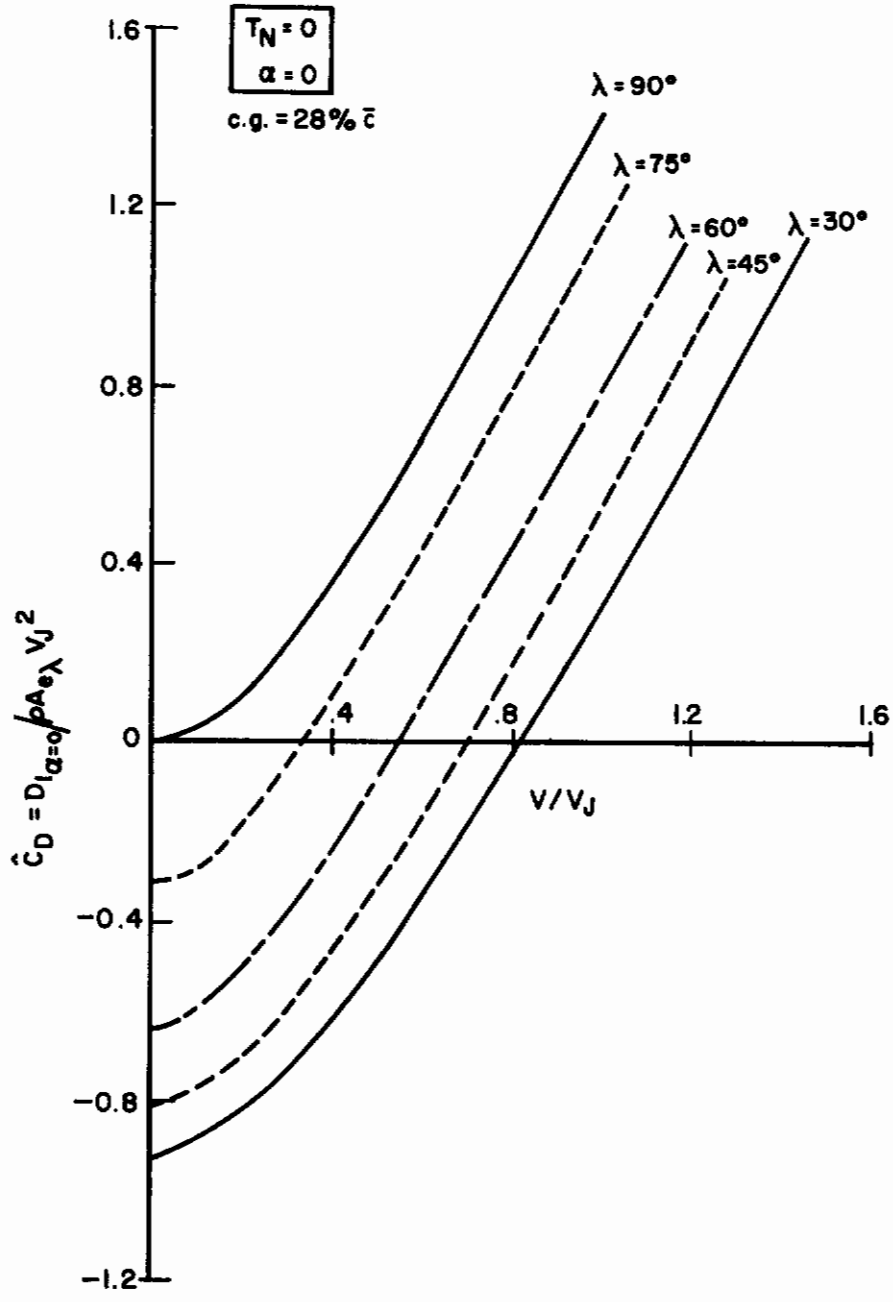

Figure 51. The Effect of Velocity Ratio on $\hat{C}_D$

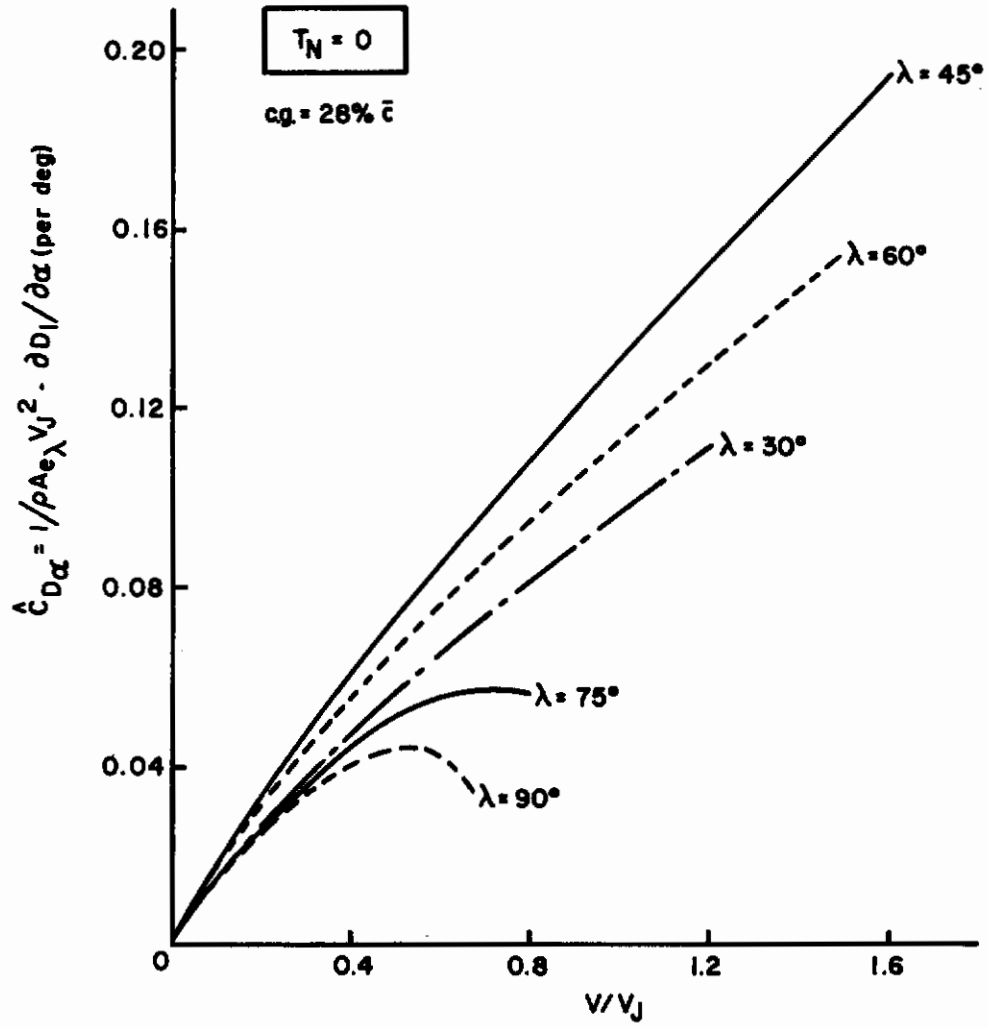

Figure 52. The Effect of Velocity Ratio on $\hat{C}_{D_\alpha}$

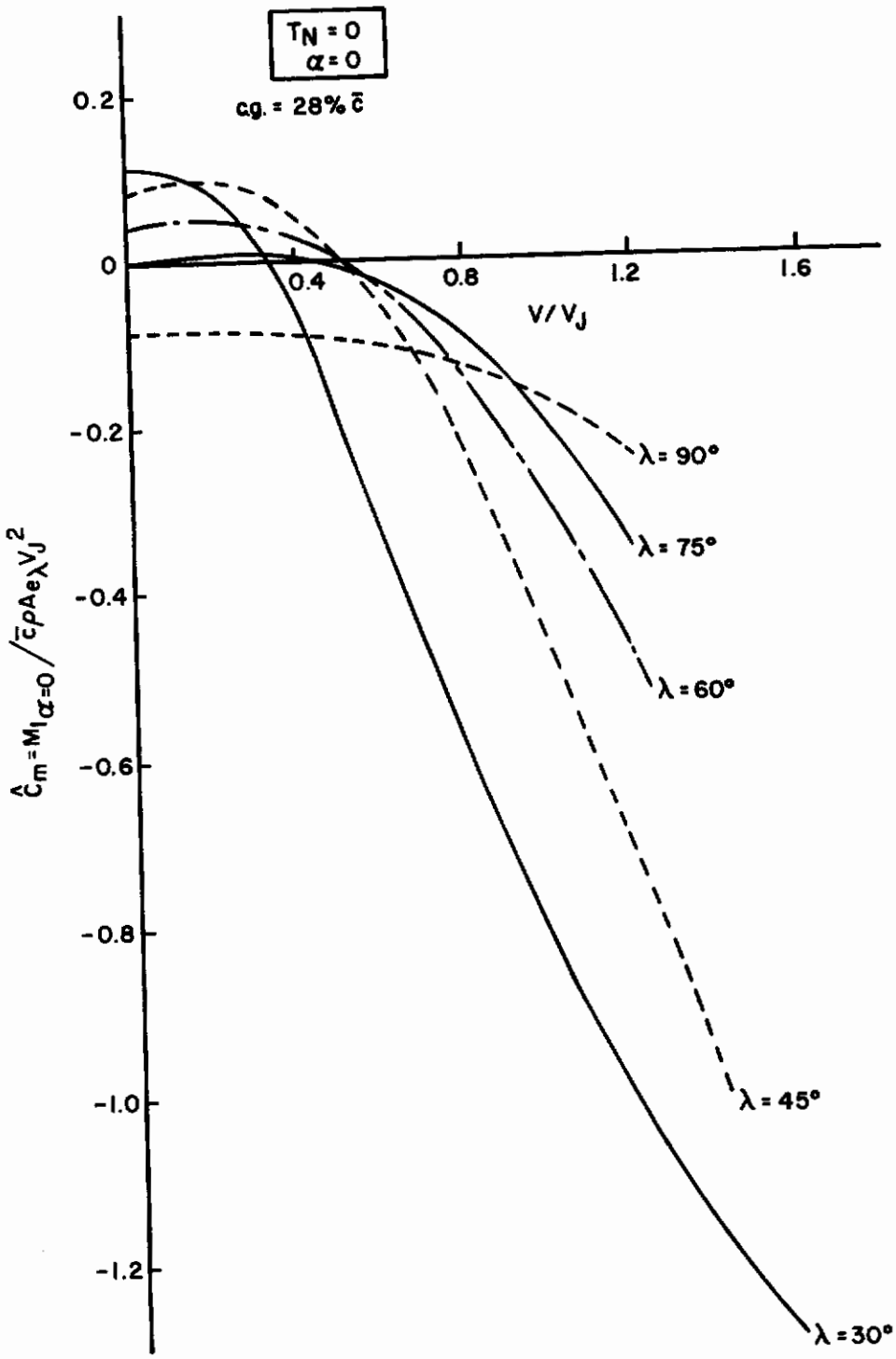

Figure 53. The Effect of Velocity Ratio on $\hat{C}_m$

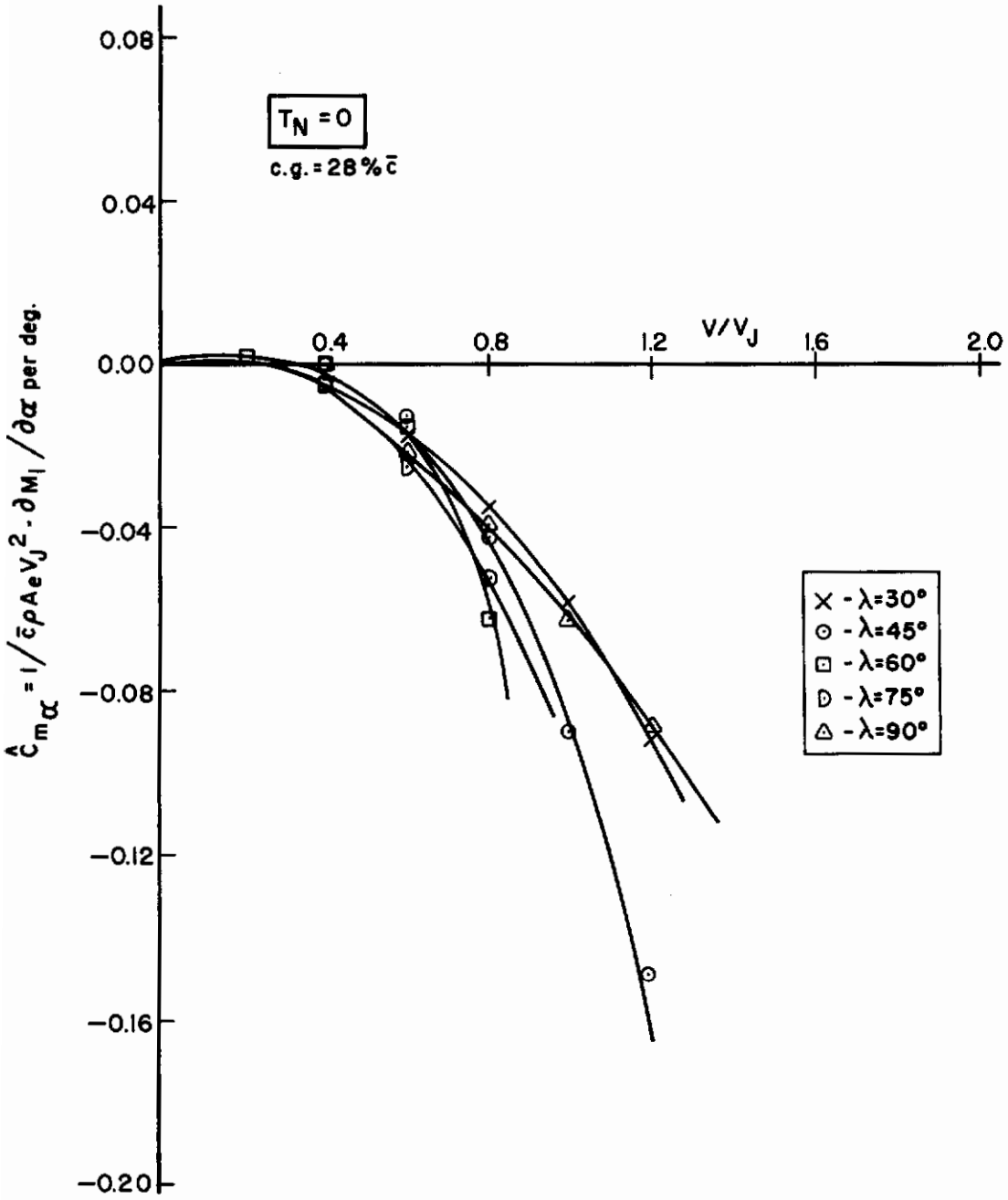

Figure 54. The Effect of Velocity Ratio on $\hat{C}_{m_\alpha}$

α = 0 while the terms containing $\hat{C}_{L_\alpha}$, $\hat{C}_{D_\alpha}$, and $\hat{C}_{m_\alpha}$ provide additional contributions to the aerodynamic forces and moments due to the effects of angle of attack. The L_1, D_1, and M_1 reactions co-align with the L, D, and M vectors shown in Figure 5. These data were generated from wind tunnel results and do not include stabilization effects such as from the nose ejector, pitching moment effects due to rear engine tilt, or rear engine propulsive effects; the engines mounted at the aft end of the fuselage in Figure 2 were not included in the wind tunnel model. Contributions due to the wing booms and horizontal tail for i_t = 0 are included (see Figures 1 and 2).

No attempt was made to separate thrust interference effects in these formulations because the information available was insufficient. The results plotted in Figures 49 through 54 reflect primarily the forces and moments due to the wing ejector system. For example, Figure 51 shows negative drag values for α = 0 at each λ or door angle setting except for $\lambda = 90°$. This negative drag reflects a positive thrust component from the jet momentum flux exiting from the ejector system.

The wind tunnel data in References 5 and 6 was analyzed to obtain the aerodynamic reactions due to the operation of the nose ejector. The results of the evaluation are

$$L_2 = T_N(1.0 - (3.0 - .0278\lambda)V/V_J)$$

$$D_2 = T_N(-1.05 + .0166\lambda + (-1.25 + .0416\lambda)V/V_J) \qquad (5)$$

$$M_2 = T_N\bar{c}/(1 - \frac{\Delta X_{cg}}{\ell_N})$$

where T_N is the nose ejector thrust in lbs, λ is the door angle in degrees, and ΔX_{cg} is the shift (in ft) of the center of gravity from the 28% $\bar{c}$ position. The dimension ΔX_{cg} is positive if the c.g. shift is in the X-direction of the body-fixed axis system. These expressions were derived by determining the difference in values for test data reflecting aerodynamic forces and moments with nose ejector on and nose ejector off. Consequently the expressions given in Equation 5 include mutual interference effects between nose ejector and fuselage, and nose ejector and wing ejector performance. The expressions for L_2 and D_2 are shown in Figure 55.

Some engineering judgment was necessary to extract this data from the results of References 5 and 6, which warrants further discussion. The nose ejector used on the wind tunnel model sucked secondary air through doors located on the upper surface of the fuselage nose (Figure 1). Therefore, this ejector system created large interferences on the pressure distribution of the fuselage. Note that the L_2/T_N plot of Figure 55 gives negative lift increments due to the nose ejector at the higher V/V_J ratios. This is possible if interferences upon the fuselage pressure distribution and on the wing

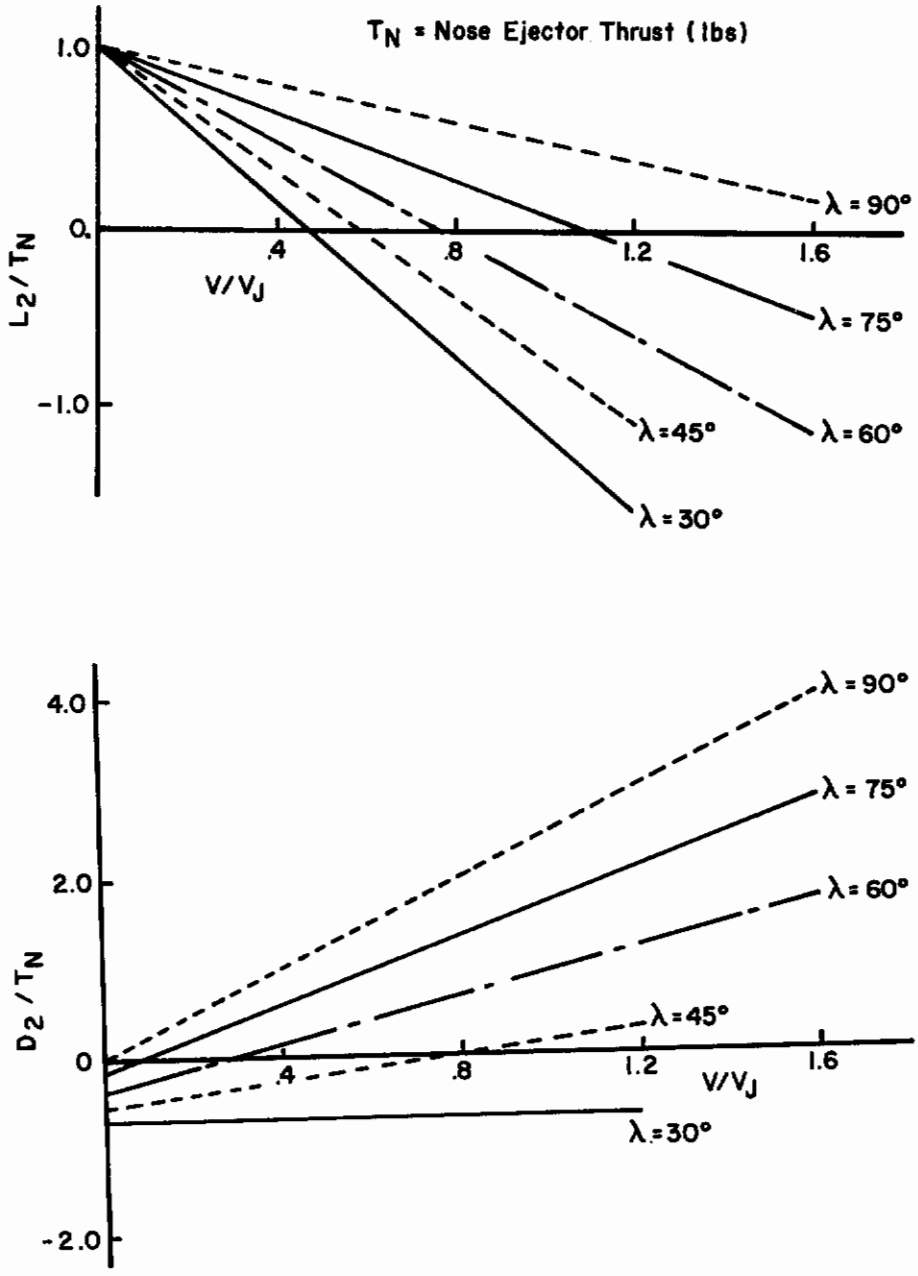

Figure 55. The Effect of Velocity Ratio on Nose Ejector Performance

ejector are sufficiently large to cause a forward shift of the net lift vector for the total system while reducing its overall magnitude. Also, a low pressure field appears to be over the nose of the fuselage, as suggested by the negative drag or positive thrust increment reflected by D_2/T_N when $\lambda = 30°$. A high pressure interference effect may exist on the lower surface of the fuselage aft of the nose ejector in conjunction with the low pressure distribution on the nose ahead of the ejector, and this could cause a pure nose-down couple which would reduce the overall pitching moment about the c.g. For example, a preliminary analysis was performed to find

$$\frac{M_2}{\bar{c}T_N}\left(1 - \frac{\Delta X_{cg}}{\ell_N}\right) = 1.07 \qquad (6)$$

if the nose ejector system did not interfere with the pressure distribution on the fuselage. Test data gives

$$\frac{M_2}{\bar{c}T_N}\left(1 - \frac{\Delta X_{cg}}{\ell_N}\right) = 1.0 \qquad (7)$$

indicating a 7% reduction in pitching moment control due to these interferences.

The third contribution to the total aerodynamic representation of the ejector wing configuration is that due to horizontal tail deflection i_t and to any changes in the area of this surface. A modification consisting of increasing the tail surface area by 10% was considered to improve the stability of the configuration in the mid to high transitional speed range.

In References 5 and 6, the horizontal tail surface of the wind tunnel model was used as a stabilizer with a deflection range of $|i_t| \leq 20°$. The elevator was geared to the horizontal stabilizer and deflected according to the following schedule in most of the wind tunnel runs.

$$\delta_e = 1.2 i_t \tag{8}$$

This angular deflection limit for i_t and the gearing ratio between horizontal tail and elevator were assumed to exist for the full scale ejector wing configuration.

The data in References 5 and 6 was evaluated to determine the stabilizer and elevator deflection contributions to the aerodynamics for the wind tunnel model; the results are shown in Figures 56 through 58. A best fit formulation for the aerodynamic contribution in each of these figures is also noted. Engineering judgment was used to form the following expressions for the horizontal tail contribution to the total aerodynamic representation of the ejector wing configuration.

$$L_3 = 1/2\ \rho V^2 S_w \left(.015 i_t \frac{S_{H_{modified}}}{S_H}\right) \tag{9}$$

$$D_3 = 1/2\ \rho V^2 S_w \left(i_t^2 / 3340\right) \frac{S_{H_{modified}}}{S_H}$$

$$M_3 = 1/2\ \rho V^2 \bar{c} S_w \left(\frac{S_{H_{modified}} \cdot \Delta C_m(i_t)}{S_H\left(1 - \frac{\Delta X_{cg}}{\ell_T}\right)}\right)$$

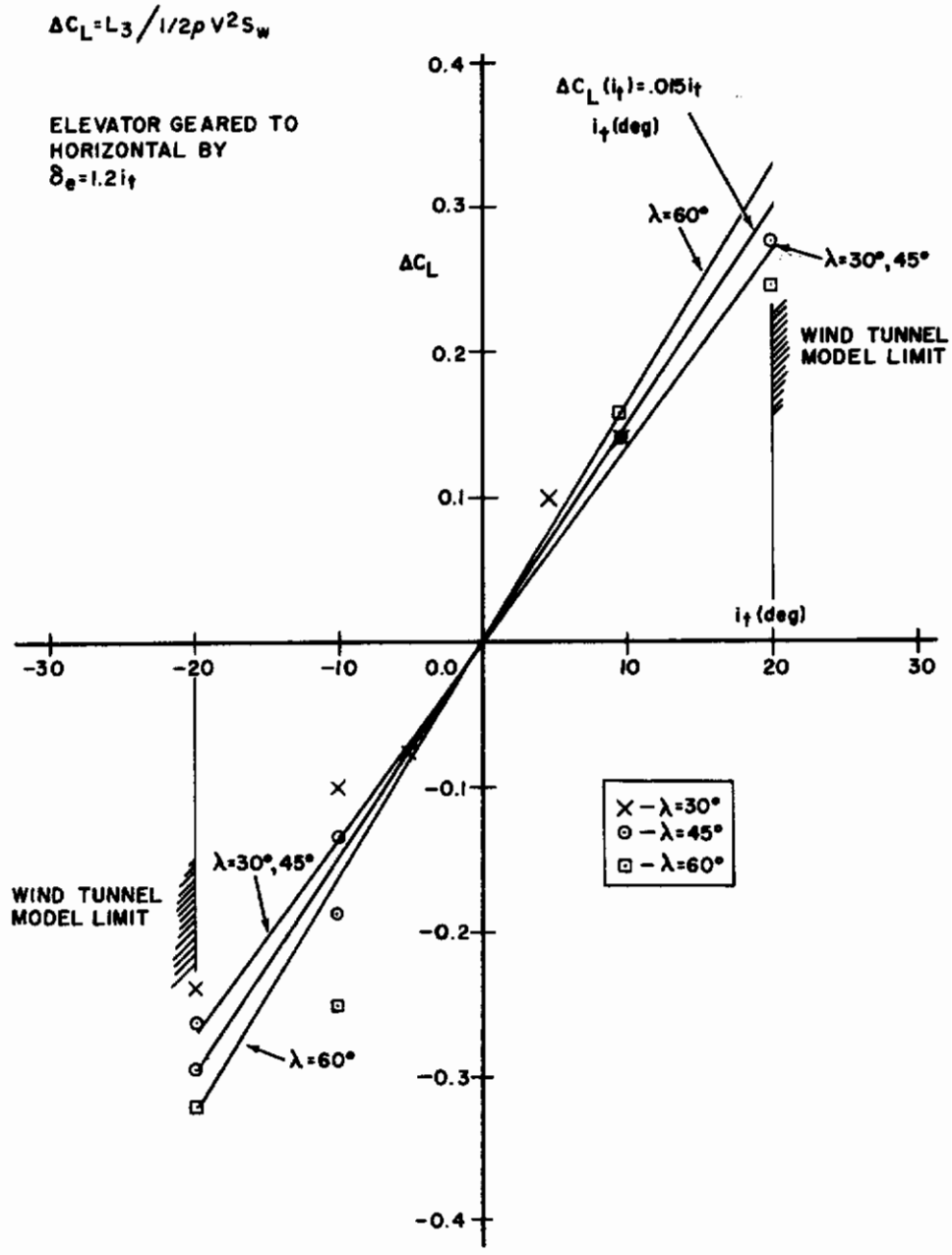

Figure 56. Tail Lift for Ejector Wing Configuration

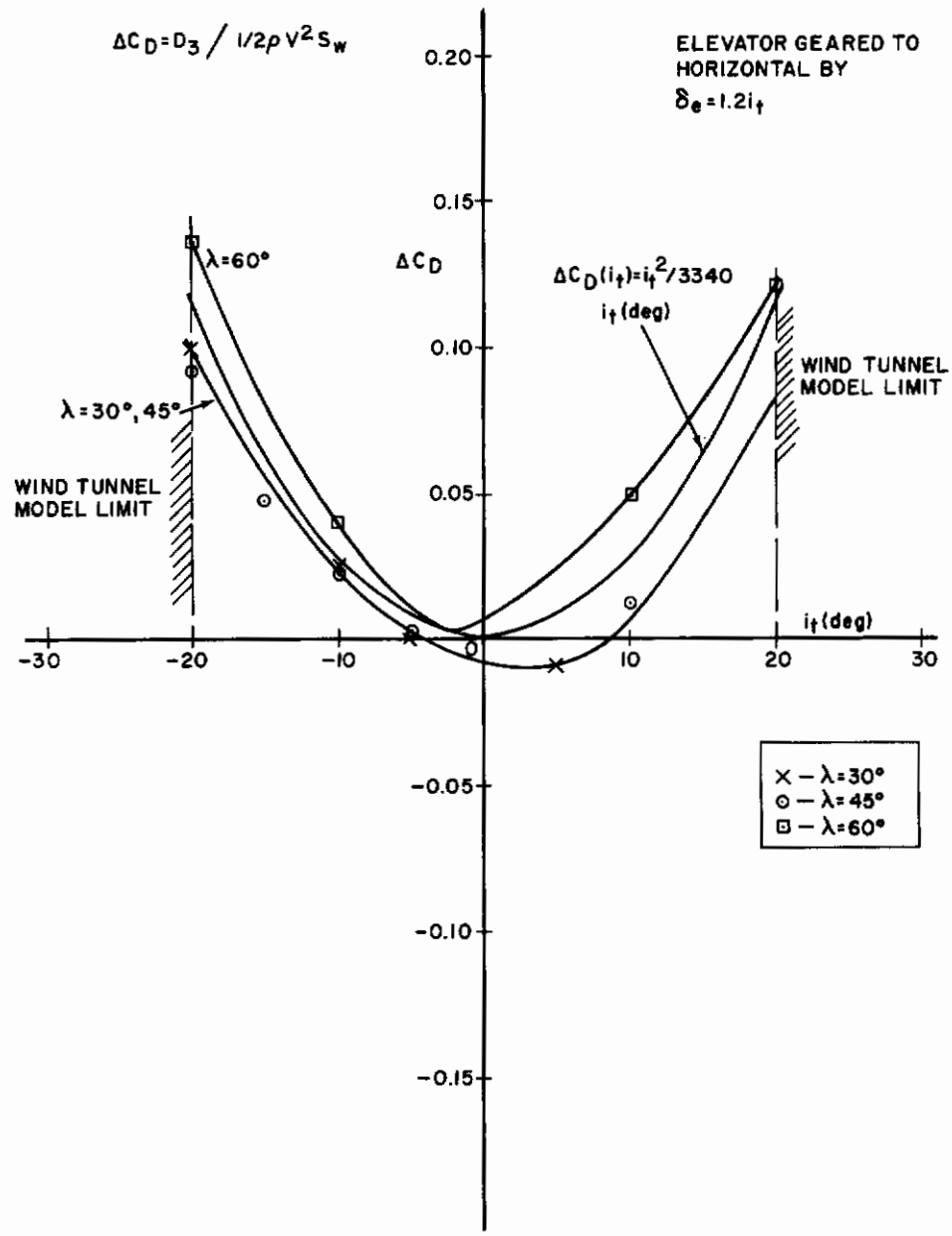

Figure 57. Tail Drag for Ejector Wing Configuration

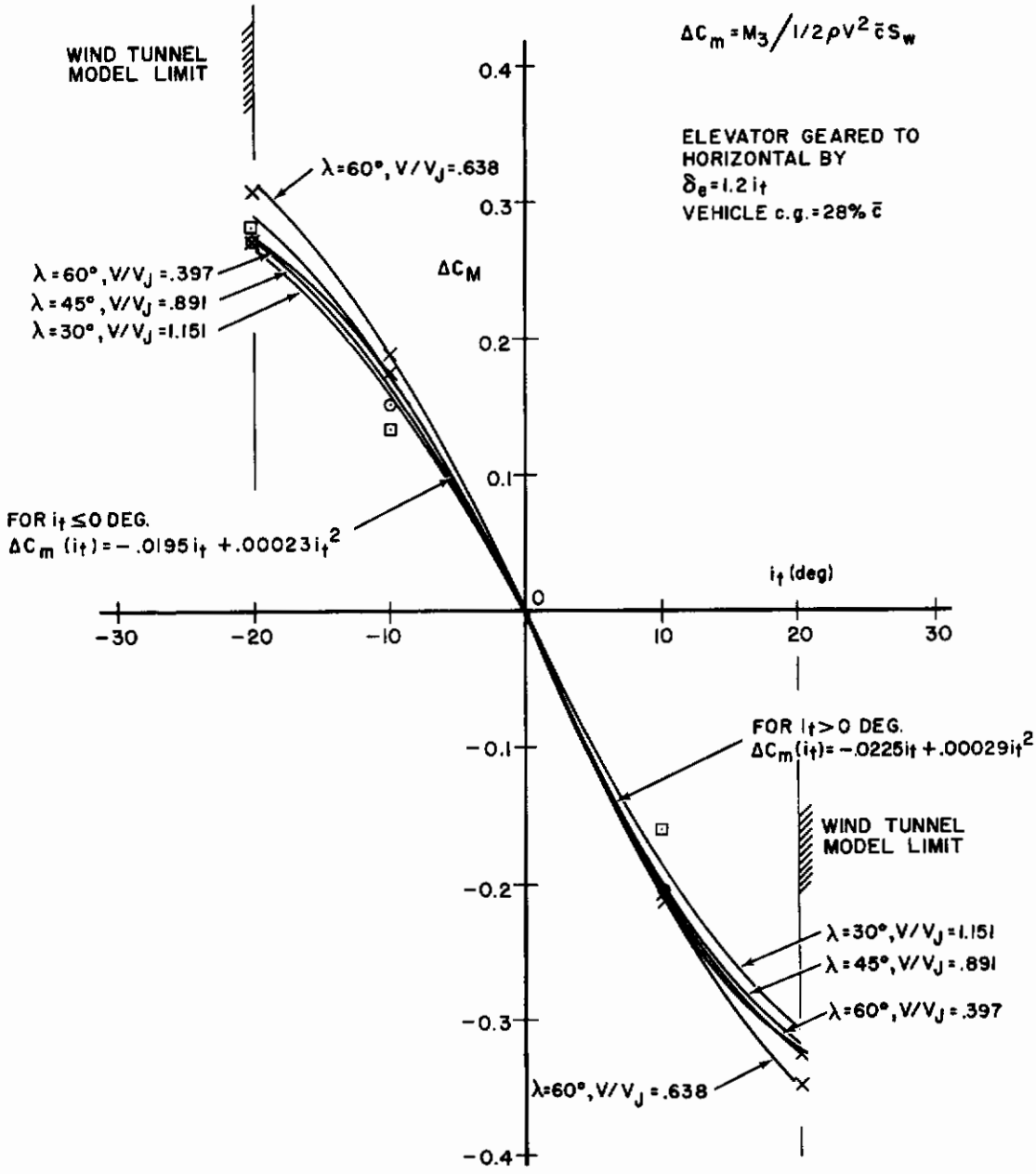

Figure 58. Tail Moment Contribution for Ejector Wing Configuration

where i_t is in degrees with

$$\Delta C_m\ i_t = -.0225 i_t + .00029\ i_t^2 \qquad i_t \geq 0 \text{ Degrees}$$
$$= -.0195 i_t + .00023\ i_t^2 \qquad i_t < 0 \text{ Degrees} \tag{10}$$

and where ΔX_{cg} reflects the shift in feet of the center of gravity from the 28% $\bar{c}$ position. This distance is positive if the shift is in the positive X direction of the body fixed axis system. The quantity $S_{H_{modified}}$ reflects a change in the area of the horizontal tail. This change was taken as a 10% increase over that of the baseline configuration. This modification was used to see whether an improvement could be made to the stability of the configuration in the mid to high transitional speed range. See Figure 7 through 11 for the trim analysis comparisons to the baseline configuration and Figures 17 through 21 for the effect of this modification upon the stability derivatives.

The two propulsive engines shown in Figure 2 at the aft end of the fuselage and nested on either side of the vertical fin were not included on the wind tunnel model. Momentum concepts were used to estimate the effect of these engines upon the forces and moments exerted on the full scale vehicle.

The thrust and normal force exerted on the engines are estimated by the following expressions:

$$T_p = \rho A_{e_p} V_{J_p} (V_{J_p} - V(\cos i_p - \alpha \sin i_p))$$
$$N_p = \rho A_{e_p} V_{J_p} V(\alpha \cos i_p + \sin i_p) \tag{11}$$

where it is assumed for simplicity that the normal force N_p acts at the engine inlet lip, as shown in Figure 2. The quantity A_{e_p} is the exit area of both engines (Figure 2) while V_{J_p} is the mean exhaust jet velocity. Small angle approximations were used for α but not for i_p. These engines may be used to provide trim moment to the vehicle, and i_p could be quite large near hover or in low speed transitional flight (see Figure 11). These forces can be resolved to yield

$$X_E = T_p \cos i_p - N_p \sin i_p$$
$$Z_E = -T_p \sin i_p - N_p \cos i_p \qquad (12)$$

in the body fixed axis system (Figures 2 and 5). The pitching moment contribution about the vehicle center of gravity is then

$$M_E = Z_p X_E - X_p Z_e \qquad (13)$$

where the distances Z_p and X_p are shown in Figure 2. These distances are positive in the positive direction of X and Z axes of the body fixed-axis system. Obviously, problems are involved with rotating the jet engines or deflecting the hot core gas of these engines to provide pitching moment control. An evaluation of these problems and the implementation required to mechanically rotate these engines were beyond the scope of this study.

The final contribution to pitching moment considered here is a correction to the wind tunnel data for a shift in center of gravity

position. All of the force and moment data given in References 5 and 6 were measured at the 28% $\bar{c}$ of the wind tunnel model. The study discussed in the main text of this report considered the c.g. to be at the 36%$\bar{c}$ position in the full scale ejector wing vehicle. A correction for this change was taken to be

$$M_4 = -\Delta X_{cg}(L_1 + L_3) \tag{14}$$

where ΔX_{cg} is the shift in feet of the c.g. location from the 28%$\bar{c}$ point. This dimension is positive if the shift is in the positive X direction of the body-fixed-axis system. The aerodynamic reactions from the nose ejector and the jet engines at the aft end of the fuselage already contain the correction for c.g. shift.

The total forces and moments about the vehicle c.g. are then

$$\begin{aligned} X &= (L_1 + L_2 + L_3)\alpha - (D_1 + D_2 + D_3) + X_e \\ Z &= -(L_1 + L_2 + L_3) - (D_1 + D_2 + D_3)\alpha + Z_E \\ M &= M_1 + M_2 + M_3 + M_4 + M_E \end{aligned} \tag{15}$$

where the L_i, D_i, M_i, X_E, Z_E, and M_E are given in the formulations above, and where the body-fixed-axis system is located at the c.g. of the vehicle as illustrated in Figure 5. It has been assumed throughout the above analysis that small angle approximations could be applied to angle of attack.

A part of this overall program consists of solving for longitudinal trim at a preselected trim speed V, altitude h, and pitch angle θ. We assumed that $\theta = \alpha$ and $\dot{h} = 0$ during this transi-

tional trim schedule for V < 150 knots. The trim equations are then

$$X - mg\theta = 0$$
$$Z + mg = 0 \qquad (16)$$
$$M = 0$$

where X, Z, and M are given in Equation 15.

2. AERODYNAMIC DERIVATIVES FOR PERTURBED FLIGHT

The linearized equations of longitudinal motion to describe transient behaviour about the trimmed flight conditions reflected in Equation 16 are:

$$\dot{u} + g\theta = X_u u + X_\delta \delta$$
$$\dot{w} - V\dot{\theta} = Z_u u + Z_w w + Z_\delta \delta \qquad (17)$$
$$\ddot{\theta} = M_u u + M_w w + M_q \dot{\theta} + M_\delta \delta$$

where the force derivatives are divided by vehicle mass m, the pitching moment derivatives are divided by vehicle inertia I_{yy}, and the forces and moments are resolved about the stability axis. These equations and relevant assumptions are discussed in References 3 and 12. Further discussion on the implementation of these equations is provided in Appendix II.

The X_w, X_q, $X_{\dot{w}}$, $Z_{\dot{w}}$, and Z_q derivatives have been excluded from the force equations. Analysis of single and tandem rotor helicopters, 2 and 4 propeller tilt proprotor or tilt wing V/STOLs, and the Bell X-22A tilt duct configuration

indicates that these derivatives are insignificant (Reference 9). $M_{\dot{w}}$ has also been excluded from the pitching moment equation because insufficient experimental data exists to evaluate this derivative for V/STOL configurations in general. Experimental techniques usually measure the combined total of $(M_q + M_{\dot{w}})$. Curtiss (Reference 9) indicates that $M_{\dot{w}}$ may be small for V/STOL vehicles and that the measured data for the combination of $(M_q + M_{\dot{w}})$ reflects the M_q contribution alone. This is the assumption we have used in this preliminary study. These derivatives would have to be re-evaluated for an in-depth study.

The $X_\delta\delta$, $Z_\delta\delta$, and $M_\delta\delta$ terms given in Equation 17 reflect control contributions to the forces and moments exerted on the vehicle. These control contributions are caused by i_p, V_J, λ, or V_{J_p} inputs to the X equation, λ, V_{J_p}, or i_p control changes to cause a force reaction in the Z equation, and finally, T_N, i_p, or V_{J_p} control inputs to cause a pitching moment change from equilibrium. In each case cited above, δ equals the particular control variable involved (i.e., $\delta = V_{J_p}$ for an increase in thrust to the jet engines used for propulsion).

Estimates for the relevant derivatives used in Equation 17 for a trim pitch angle of $\theta = \alpha = 0$ are given in Equation 18. The formulations are obtained from differentiation of equation 15 and other related expressions.

$$X_u = \frac{1}{m}\left[\frac{\partial X_E}{\partial u} - \left(\frac{\partial D_1}{\partial u} + \frac{\partial D_2}{\partial u} + \frac{\partial D_3}{\partial u}\right)\right]$$

$$Z_u = \frac{1}{m}\left[\frac{\partial Z_E}{\partial u} - \left(\frac{\partial L_1}{\partial u} + \frac{\partial L_2}{\partial u} + \frac{\partial L_3}{\partial u}\right)\right]$$

$$Z_w = \frac{1}{m}\left[\frac{\partial Z_e}{\partial w} - \left(\frac{\partial L_1}{\partial w} + \frac{\partial L_2}{\partial w} + \frac{\partial L_3}{\partial w}\right) - \frac{(D_1 + D_2 + D_3)}{V}\right]$$

$$M_u = \frac{1}{I_{yy}}\left[\frac{\partial M_1}{\partial u} + \frac{\partial M_2}{\partial u} + \frac{\partial M_3}{\partial u} + \frac{\partial M_4}{\partial u} + \frac{\partial M_E}{\partial u}\right] \qquad (18)$$

$$M_w = \frac{1}{I_{yy}}\left[\frac{\partial M_1}{\partial w} + \frac{\partial M_2}{\partial w} + \frac{\partial M_3}{\partial w} + \frac{\partial M_4}{\partial w} + \frac{\partial M_E}{\partial w}\right]$$

$$M_q = -.10 - .0015V \; ; \; V \leq 250 \text{ fps}$$

One may presume after a brief look at these derivatives that the thrust terms were not included, but this is not true. No attempt was made to separate the thrust effects, including interferences, from the test data of References 5 and 6. Therefore, D_1 reflects the sum total of forces in the drag direction for the ejector wing system. For example, Figure 51 shows negative drag values at each λ or door angle setting except for $\lambda = 90°$. This negative drag reflects a positive thrust contribution from the jet momentum flux exiting from the wing. In addition, X_E, Z_E, and M_E reflect the thrust effects from the jet engines situated at the aft end of the fuselage.

The above expressions are straightforward except for M_q. No reliable theory exists for estimating M_q for an ejector wing aircraft in low speed transition, and test data are nonexistent. A mean value for several V/STOLs of the same size as the ejector wing configuration was selected from data in Reference 9 for the quad-ducted propeller aircraft, 2 and 4-propellered tilt wing configurations, and single and tandem helicopters.

The derivatives shown in the brackets of Equation 18 are

$$\frac{\partial X_E}{\partial u} = \frac{\partial Z_E}{\partial w} = -\rho A_{e_p} V_{J_p}$$

$$\frac{\partial Z_E}{\partial u} = \frac{\partial X_E}{\partial w} = 0$$

$$\frac{\partial M_E}{\partial u} = Z_p \frac{\partial X_E}{\partial u}$$

$$\frac{\partial M_E}{\partial w} = -X_p \frac{\partial Z_E}{\partial w} \qquad (19)$$

$$\frac{\partial L_1}{\partial u} = \rho A_{e_\lambda} V_J \partial \hat{C}_L / \partial V/V_J$$

$$\frac{\partial D_1}{\partial u} = \rho A_{e_\lambda} V_J \partial \hat{C}_D / \partial V/V_J$$

$$\frac{\partial M_1}{\partial u} = \rho A_{e_\lambda} V_J \bar{c} \partial \hat{C}_m / \partial V/V_J$$

where $\partial \hat{C}_L / \partial V/V_J$, $\partial \hat{C}_D / \partial V/V_J$, and $\partial \hat{C}_m / \partial V/V_J$ are found by determining the slopes of $\hat{C}_L$, $\hat{C}_D$, and $\hat{C}_m$ at the trim V/V_J values in Figures 49, 51, and 53.

Note that $\partial X_E/\partial_u$ has been included. This derivative reflects the variation with u of thrust and normal force for the jet engines located at the aft end of the fuselage (Figure 2). Momentum concepts were used to obtain this contribution to the overall forces and moments exerted on the vehicle. This derivative is normally insignificant for conventional, jet-propelled configurations in cruise at altitudes greater than 10,000 ft (Reference 16) but

may be of significance near hover and at sea level. For completeness, the derivative $\partial Z_E/\partial w$ has been included as well.

The quantities $\partial L_1/\partial w$ and $\partial M_1/\partial w$ are found from

$$\frac{\partial L_1}{\partial w} = \frac{57.3\ \rho A e_\lambda}{V}\ V_J^2\ \hat{C}_{L_\alpha}$$

$$\frac{\partial M_1}{\partial w} = 57.3\ \rho \frac{A e_\lambda}{V}\ V_J^2\ \bar{c}\ \hat{C}_{m_\alpha} \tag{20}$$

where $\hat{C}_{L_\alpha}$ and $\hat{C}_{m_\alpha}$ are given in Figures 50 and 54 at the prescribed trim values for V/V_J. The factor 57.3 is included because the figures give $\hat{C}_{L_\alpha}$ and $\hat{C}_{m_\alpha}$ in units of deg^{-1}.

The derivatives relevant to the nose ejector system are

$$\frac{\partial L_2}{\partial u} = -\frac{T_N}{V_J}(3-.0278\lambda)$$

$$\frac{\partial D_2}{\partial u} = \frac{T_N}{V_J}(-1.25 + .0416\lambda) \tag{21}$$

$$\frac{\partial L_2}{\partial w} = \frac{\partial M_2}{\partial u} = \frac{\partial M_2}{\partial w} = 0$$

The derivatives due to the tail configuration when $i_t = 0$ are given by

$$\frac{\partial L_3}{\partial u} = \frac{\partial D_3}{\partial u} = \frac{\partial M_3}{\partial u} = 0$$

$$\frac{\partial L_3}{\partial w} = \frac{\partial D_3}{\partial w} = \frac{\partial M_3}{\partial w} = 0 \tag{22}$$

The expressions which give the derivative contribution due to a c.g. shift from the 28% $\bar{c}$ center of gravity location are

$$\frac{\partial M_4}{\partial u} = - \Delta X_{cg} \frac{\partial L_1}{\partial u}$$

$$\frac{\partial M_4}{\partial w} = - \Delta X_{cg} \frac{\partial L_1}{\partial w} \qquad (23)$$

where $\partial L_1/\partial u$ and $\partial L_1/\partial w$ are given in Equations 19 and 20.

This completes the determination of the derivatives given in Equation 18. Some of the above formulations contain the trim speed V in the denominator. Therefore, a singularity exists at V = 0 and trim computations should be performed at some finite value for trim velocity.

3. CONTROL DERIVATIVES

Equation 17 contains terms such as $X_\delta\delta$, $Z_\delta\delta$, and $M_\delta\delta$. These contributions to the linearized equations of motion reflect aerodynamic effects due to a control input to the dynamic system. For example, control changes to the vehicle can be made by varying i_p, λ, i_t, V_{J_p}, V_J, and T_N. If a step input is introduced to the horizontal tail angle, i_t say, then $\delta = i_t$ in Equation 17. The form of the equations of motion seems to indicate that only one control parameter can be varied at any one time. Nevertheless, the flight path resulting from multiple control can be deduced by means of linear superposition since the equations of motion used are linear. There are 18 possible control derivatives for longitudinal flight, and these are presented here.

Control changes to the engines at the aft end of the fuselage are made by varying i_p or V_{J_p}. The angle i_p is the inclination of these engines relative to the body fixed X axis, while V_{J_p} reflects the velocity of efflux at the engine exit plane. These 6 derivatives are as follows for $\theta = \alpha = 0$:

$$
\begin{aligned}
X_{V_{J_p}} &= \frac{1}{m}\left[2\rho A_{e_p} V_{J_p}\cos i_p - \rho A_{e_p} V\right] \\
Z_{V_{J_p}} &= \frac{-2}{m}\rho A_{e_p} V_{J_p}\sin i_p \\
X_{i_p} &= -\frac{\rho}{m} A_{e_p} V_{J_p}^2 \sin i_p \\
Z_{i_p} &= -\frac{\rho}{m} A_{e_p} V_{J_p}^2 \cos i_p \\
M_{V_{J_p}} &= \frac{mZ_p}{I_{yy}} X_{V_{J_p}} - \frac{mX_p}{I_{yy}} Z_{V_{J_p}} \\
M_{i_p} &= \frac{mZ_p}{I_{yy}} X_{i_p} - \frac{mX_p}{I_{yy}} Z_{i_p}
\end{aligned}
\qquad (24)
$$

Changes in climb rate and forward speed can be made by pilot input to the variables λ and V_J. The quantity λ is the wing ejector door angle and V_J is the mean velocity of efflux from the wing ejector. These 6 control derivatives about trim where $\theta = \alpha = 0$ are:

$$
\begin{aligned}
X_{V_J} &= -\frac{1}{m}\left[\frac{\partial D_1}{\partial V_J} + \frac{\partial D_2}{\partial V_J}\right] \\
Z_{V_J} &= -\frac{1}{m}\left[\frac{\partial L_1}{\partial V_J} + \frac{\partial L_2}{\partial V_J}\right] \\
M_{V_J} &= \frac{1}{I_{yy}}\left[\frac{\partial M_1}{\partial V_J} + \frac{\partial M_2}{\partial V_J} + \frac{\partial M_4}{\partial V_J}\right] \\
X_\lambda &= -\frac{1}{m}\left[\frac{\partial D_1}{\partial \lambda} + \frac{\partial D_2}{\partial \lambda}\right]
\end{aligned}
\qquad (25)
$$

$$Z_\lambda = -\frac{1}{m}\left[\frac{\partial L1}{\partial \lambda} + \frac{\partial L2}{\partial \lambda}\right]$$

$$M_\lambda = \frac{1}{I_{yy}}\left[\frac{\partial M1}{\partial \lambda} + \frac{\partial M2}{\partial \lambda} + \frac{\partial M4}{\partial \lambda}\right]$$

where

$$\frac{\partial L1}{\partial V_J} = 2\rho A e_\lambda V_J \hat{C}_L - \rho A e_\lambda \frac{V \partial \hat{C}_L}{\partial V/V_J} \quad ; \quad \frac{\partial L_1}{\partial \lambda} = 57.3\, \rho A e_\lambda V_J^2\, \partial \hat{C}_L/\partial\lambda$$

$$\frac{\partial D1}{\partial V_J} = 2\rho A e_\lambda V_J \hat{C}_D - \rho A e_\lambda V \partial \hat{C}_D/\partial V/V_J \quad ; \quad \frac{\partial D_1}{\partial \lambda} = 57.3 \rho A e_\lambda V_J^2 \partial\, C_D/\partial\lambda$$

$$\frac{\partial M1}{\partial V_J} = 2\rho A e_\lambda V_J \bar{c} \hat{C}_m - \rho A e_\lambda \overline{Vc} \partial C_m/\partial V/V_J \; ; \; \frac{\partial M_1}{\partial \lambda} = 57.3 \rho A e_\lambda\, V_J^2 \bar{c} \partial\, C_m/\partial\lambda$$

$$\frac{\partial L_2}{\partial V_J} = T_N(3-1.59\lambda)V/V_J^2 \Big|_{T_N = \text{Trim Value}} \; ; \; \frac{\partial L_2}{\partial \lambda} = 1.59 T_N V/V_J \Big|_{T_N = \text{Trim Value}}$$

$$\frac{\partial D_2}{\partial V_J} = T_N(1.25-2.39\lambda)V/V_J^2 \Big|_{T_N = \text{Trim Value}}; \; \frac{\partial D_2}{\partial \lambda} = T_N(.95+2.38V/V_J)\Big|_{T_N = \text{Trim Value}}$$

$$\frac{\partial M_2}{\partial V_J} = 0 \qquad ; \; \frac{\partial M_2}{\partial \lambda} = 0$$

$$\frac{\partial M_4}{\partial V_J} = -\Delta X_{cg} \frac{\partial L_1}{\partial V_J} \qquad ; \; \frac{\partial M_4}{\partial \lambda} = -\Delta X_{cg} \frac{\partial L_1}{\partial \lambda}$$

The derivatives $\partial L_1/\partial\lambda$, $\partial D_1/\partial\lambda$, $\partial L_2/\partial\lambda$, and $\partial D_2/\partial\lambda$ are in units of lbs/rad, $\partial M_1/\partial\lambda$ and $\partial M_2/\partial\lambda$ are in units of ft-lbs/rad, and $\partial \hat{C}_L/\partial\lambda$, $\partial \hat{C}_D/\partial\lambda$, and $\partial \hat{C}_m/\partial\lambda$ are in units of deg^{-1}. These derivatives are evaluated by forming cross-plots of the data given in Figures 49, 51, and 53 with V/V_J held constant at the trim value.

Pitch control is provided by the nose ejector system at low forward flight speeds and by the horizontal tail surface during conventional flight. The complete horizontal tail surface

can be deflected, coupled with the elevator deflection angle or the horizontal stabilizer angle setting. This schedule is given in Equation 8.

These control derivatives are as follows:

$$
\begin{aligned}
X_{T_N} &= -\frac{1}{m}\,\frac{\partial D_2}{\partial T_N} \\
Z_{T_N} &= -\frac{1}{m}\,\frac{\partial L_2}{\partial T_N} \\
M_{T_N} &= \frac{1}{I_{yy}}\,\frac{\partial M_2}{\partial T_N} \\
X_{i_t} &= -\frac{1}{m}\,\frac{\partial D_2}{\partial i_t} \\
Z_{i_t} &= -\frac{1}{m}\,\frac{\partial L_2}{\partial i_t} \\
M_{i_t} &= \frac{1}{I_{yy}}\,\frac{\partial M_3}{\partial i_t}
\end{aligned}
\qquad (27)
$$

where

$$
\frac{\partial L_2}{\partial T_N} = 1 - (3-1.59\lambda)V/V_J \quad ; \quad \frac{\partial L_3}{\partial i_t} = .43\rho V^2\, S_W \cdot S_{H\ \text{modified}} / S_H
$$

$$
\frac{\partial D_2}{\partial T_N} = (-1.05+.95\lambda)+(-1.25+2.39\lambda)V/V_J \quad ; \quad \frac{\partial D_3}{\partial i_t} = .984\rho V^2 S_W S_{H_{\text{Modified}}} i_t / S_H
$$

$$
\frac{\partial M_2}{\partial T_N} = \bar{c}/\left(1 - \frac{\Delta Xcg}{\ell_N}\right) \quad ; \quad \frac{\partial M_3}{\partial i_t} = \frac{1}{2}\rho V^2 \bar{c}\, \frac{S_w \cdot S_{H_{\text{Modified}}}}{S_H\left(\frac{1 - \Delta Xcg}{\ell_t}\right)} \cdot \frac{\partial C_m(i_t)}{\partial i_t} \qquad (28)
$$

$$
\frac{\partial C_m(i_t)}{\partial i_t} = -1.29 + 1.9 i_t \quad i_t \geq 0
$$

$$
\frac{\partial C_m(it)}{\partial i_t} = -1.09 + 1.51 i_t \quad i_t < 0
$$

The quantities λ and i_t are in radians in these expressions, T_N is the nose ejector thrust in pounds, and ΔX_{cg} reflects the shift of the center of gravity from the 28% $\bar{c}$ position in feet. This dimension is positive if the shift is in the positive X-direction of the body-fixed-axis system.

This completes the determination of the 18 control derivatives for the longitudinal mode of flight of the wing ejector system. Obviously, there must be control phasing and mix during transition as the pilot could not handle all of these controls simultaneously. The analysis for establishing this phasing and mix was beyond the scope of this study.

APPENDIX II

ANALYSIS OF FLIGHT TRANSIENTS

The longitudinal equations of motion as given in derivative form in Appendix I are:

$$\begin{aligned} \dot{u} + g\theta &= X_u u + X_\delta \delta \\ \dot{w} - V\dot{\theta} &= Z_u u + Z_w w + Z_\delta \delta \\ \ddot{\theta} &= M_u u + M_w w + M_q \dot{\theta} + M_\delta \delta \end{aligned} \tag{29}$$

for perturbed flight about a trimmed point in transition.

The transfer functions needed to determine the vehicle's responses and its control and handling characteristics can be readily determined in regard to these equations. This includes deriving the characteristic equations (Reference 3) which provide an estimate for the mode damping, frequency, and other parameters. The transfer functions of interest for the above equations are: $\frac{w(s)}{\delta(s)}$, $\frac{\theta(s)}{\delta(s)}$, and $\frac{u(s)}{\delta(s)}$, where δ could represent any of the control contributions discussed. These transfer functions provide an estimate for the design of any Stability Augmentation Systems (SAS) and can be used to generate time histories for the vehicle in perturbed flight about a prescribed trim point during transition. Existing digital computer programs at WPAFB were used to find these transfer functions and time responses at specified trim points during transition, and an existing CALCOMP plotting routine was used to provide a graphical representation of the responses.

1. TRANSFER FUNCTION REPRESENTATION

A digital computer program developed by Griffin (see Reference 12) was used to obtain the transfer functions. This digital computer program also computes the damping and the frequency of the phugoid and short period modes. In addition, it computes period, time to half and one-tenth amplitude, and cycles to half and one-tenth amplitude. Inputs to the program consist of stability derivatives calculated for the configuration under consideration. The stability derivatives can be in dimensional form and the forces and moments can be taken about the stability axis. This form for representing the derivatives is adapted here. For completeness, a summary of the analysis used by Griffin (Reference 12) is given now.

To solve for the characteristic equations and transfer functions, the Laplace transform of each equation of motion is taken, and using matrix notation gives:

$$\begin{bmatrix} s - Z_u & 0 & g \\ -Z_u & s - Z_w & -sV \\ -M_u & -M_w & s^2 - M_q \end{bmatrix} \begin{bmatrix} u(s) \\ w(s) \\ \theta(s) \end{bmatrix} = \begin{bmatrix} X_\delta \delta(s) \\ Z_\delta \delta(s) \\ M_\delta \delta(s) \end{bmatrix} \quad (30)$$

The characteristic equation of motion is obtained by setting the determinant of the squared matrix equal to zero or:

$$\Delta = \begin{vmatrix} s - X_u & 0 & g \\ -Z_u & s - Z_w & -sV \\ -M_u & -M_w & s^2 - sM_q \end{vmatrix} = 0 \quad (31)$$

This simplifies to:

$$= As^4 + Bs^3, + Cs^2 + Ds + E = 0 \tag{32}$$

where

$$\begin{aligned} A &= 1 \\ B &= -X_u - Z_w - M_q \\ C &= -X_u Z_w + X_u M_q + Z_w M_q - VM_w \\ D &= X_u Z_w M_q + VM_w X_u + M_u g \\ E &= Z_u M_u g - M_u Z_w g \end{aligned} \tag{33}$$

From the matrix equation, the three basic transfer functions can be derived by Cramer's rule and $u(s)/\delta(s)$ becomes:

$$\frac{u(s)}{\delta(s)} = \frac{\begin{bmatrix} X_\delta & 0 & g \\ Z_\delta & S-Z_w & -sV \\ M_\delta & -M_w & s^2 - sM_q \end{bmatrix}}{\Delta} \tag{34}$$

The numerator of this equation simplifies to:

$$NUM = A_u s^3 + B_u s^2 + C_u s + D_u \tag{35}$$

where

$$\begin{aligned} A_u &= X_\delta \\ B_u &= X_\delta Z_w - X_\delta M_\delta \\ C_u &= X_\delta Z_w M_q - VX_\delta M_w - M_\delta g \\ D_u &= Z_\delta M_w g + M_\delta Z_w g \end{aligned} \tag{36}$$

The transfer function for $\frac{w(s)}{\delta(s)}$ is derived in a similar manner:

$$\frac{w(s)}{\delta(s)} = \frac{\begin{bmatrix} s - X_u & X_\delta & g \\ -Z_u & Z_\delta & -sV \\ -M_u & M_\delta & s^2 - sM_q \end{bmatrix}}{\Delta} \tag{37}$$

The numerator simplifies to:

$$NUM = A_w s^3 + B_w s^2 + C_w s + D_w \tag{38}$$

where

$$\begin{aligned} A_w &= Z_\delta \\ B_w &= -Z_\delta X_u - Z_\delta M_q + VM_\delta + Z_u X_\delta \\ C_w &= Z_\delta X_u M_q - VX_u M_\delta - Z_u X_\delta M_q + M_u X_\delta V \\ D_w &= -Z_u M_\delta g + M_u Z_\delta g \end{aligned} \tag{39}$$

Note that the angle of attack transfer function differs from the vertical velocity transfer function only by V; that is, $\alpha = \frac{w}{V}$. Therefore

$$\frac{\alpha(s)}{\delta(s)} = \frac{1}{V}\,\frac{w(s)}{\delta(s)} \tag{40}$$

For the pitch angle transfer function,

$$\frac{\theta(s)}{\delta(s)} = \frac{\begin{bmatrix} -X_u & 0 & X_\delta \\ -Z_u & -Z_w & Z_\delta \\ -M_u & -M_w & M_\delta \end{bmatrix}}{\Delta} \tag{41}$$

The numerator simplifies to:

$$NUM = A_\theta s^2 + B_\theta s + C_\theta \tag{42}$$

where

$$\begin{aligned} A_\theta &= M_\delta \\ B_\theta &= -X_u M_\delta - Z_w M_\delta + Z_\delta M_w + M_u X_\delta \\ C_\theta &= X_u Z_w M_\delta - X_u Z_\delta M_w + Z_u X_\delta M_w - M_u X_\delta Z_w \end{aligned} \tag{43}$$

2. TIME RESPONSES

After determining the transfer functions as a ratio of two polynomials in s, these expand in partial fractions so that inverse Laplace transforms can be readily formed. The Heaviside Expansion (Reference 3) has been programmed on the CDC 6600 digital computer, and this program is used for calculating these partial fractions and generating the time histories from the transfer functions. The program was developed for the IBM 7094 in the Guidance and Control Division (ASBEG) of the Aeronautical Systems Division, WPAFB. This program was converted to the CDC 6600 during the course of this study.

The digital computer program can provide an analysis for any linear system, that is, any system which can be linearly expressed as a transfer function. There are five forcing functions which can be used to perturb the linear system from equilibrium, a step impulse, ramp, parabolic, and sinusoidal type input. The transfer function can be expressed in either of three formats: polynomial (unfactored),

bode (with factors, Ks+1), and root locus (with factors, s+K). In this study, the polynomial form was used. A CALCOMP or plotting subroutine is available at the user's option to display the output graphically. The input to the digital computer time response program along with its various options is listed below. A listing of the digital computer program for the CDC 6600 is also included for completeness.

3. HEAVISIDE DIGITAL COMPUTER PROGRAM

This section is provided as an aid to the user of the digital computer program reflecting the perturbed flight time history analysis presented above. The program was prepared for use on the CDC 6600 computer at WPAFB. A discussion of the input to the program and the listings for the program itself are provided here. The format of presentation is concise. It is recommended that the appropriate CDC 6600 manuals be consulted for an understanding of the FORMAT statements. The input preparation is as follows:

CARDS (1) and (2) FORMAT (5A6)

1. CMT - Up to 30 spaces per card may be utilized for comment.

CARD (3) FORMAT (412)

1. NUMBER - The number of cases to be considered (must be $\leq$ 10)
2. IOPT1 - 01 Data is in polynomial form
   - 02 Root locus form
   - 03 Bode form
3. IOPT2 - 01 Step input
   - 02 Impulse input
   - 03 Ramp input

- 04 Parabolic input

- 05 Sinusoidal input

4. IOPT3 - 01 Put all plots on the same graph

- 00 Put each plot on a separate graph

CARD (4) FORMAT (5A6, 3F10.0)

1. CMT - Lable of ordinate (Example: PITCH ANGLE-RADIANS). The lable of the abscissa is taken automatically as time in seconds.
2. SIZEX - Length of abscissa
3. SIZEY - Length of ordinate (must be $\leq$ 10 inches)
4. TIME - Maximum time (seconds) to be considered for the system response

CARD (5) FORMAT (3F10.0)

Omit this card unless IOPT2 - 05

1. A - Amplitude of sinusoidal input A sin ($\omega t + \phi$)
2. ω - Frequency (radians/second)
3. ϕ - Phase (radians)

CARD (6) FORMAT (4A6)

1. CMT - Comment to distinguish cases considered if IOPT3 = 00. If IOPT3 = 01 make this comment general.

CARD (7)

1. If IOPT1 - 01 Go to Polynomial Input

- 02 Go to Root Locus Input

- 03 Go to Bode Input

POLYNOMIAL INPUT

General Form of Polynomial:

$$TF = K \cdot \frac{s^n + a_n s^{n-1} + \ldots + a_2 s + a_1}{s^m + b_m s^{m-1} + \ldots + b_2 s + b_1}$$

CARD (7) FORMAT (1F10.0,2I2)

1. K - Gain of the system
2. n - Order of numerator
3. m - Order of denominator

CARD (8) FORMAT (8E10.0)

1. a_i - Coefficients of numerator in sequential order of a_i where i = n, n-1, . . . 2, 1. Delete this card if n is equal to zero.

CARD (9) FORMAT (8E10.0)

1. b_j - Coefficients of denominator in sequential order of b_j where j = m, m-1, . . . 2, 1.

Repeat cards (6) through (9) until all cases are read in.

BODE INPUT

General form of Bode Transfer Function:

$$TF = K \cdot \frac{s^P (a_1 s+1) \quad \ldots \quad (a_i s+1)(a_{i+1} s^2 + a_{i+2} s+1) \quad \ldots \quad (a_{n-1} s^2 + a_n s+1)}{(b_1 s+1) \quad \ldots \quad (b_j s+1) \quad \ldots \qquad\qquad (b_{m-1} s^2 + b_m s+1)}$$

CARD (7) FORMAT (1F10.0,5I2)

1. K - Gain of transfer function
2. n - Order of numerator
3. i - Number of linear terms of numerator

4. m - Order of denominator

5. j - Number of linear terms of denominator

6. P - Order of the free s and its associated sign. (NOTE: At present the program will not handle data in bode form if P is greater than zero.)

CARD (8) FORMAT (8F10.0)

1. a_i - Coefficients of numerator in sequential order of a_i where i = 1, 2, . . ., n. Delete this card if n is equal to zero.

CARD (9) FORMAT (8F10.0)

1. b_j - Coefficients of denominator in sequential order of b_j where j = 1, 2, . . ., m.

Repeat cards (6) through (9) until all cases are read in.

For input to a general form of a root locus transfer function such as

$$TF = K \cdot \frac{(s+a_1) \cdot \ldots \cdot (s+a_1) \cdot (s^2+a_{i+1}s+a_{i+2}) \cdot \ldots \cdot (s^2+a_{n-1}s+a_n)}{(s+b_1) \cdot \ldots \cdot (s+b_j) \cdot (s^2+b_{j+1}s+b_{j+2}) \cdot \ldots \cdot (s^2+b_{m-1}s+b_m)}$$

the following cards are prepared.

CARD (7) FORMAT (1F10.0,4I2)

1. K - Gain of transfer function

2. n - Order of numerator

3. i - Number of linear terms of numerator

4. m - Order of denominator

5. j - Number of linear terms of denominator

CARD (8) FORMAT (8F10.0)

1. a_i - Coefficients of numerator in sequential order of a_i where i = 1, 2, . . ., n. Delete this card if n is equal to zero.

CARD (9) FORMAT (8F10.0)

1. b_j - Coefficients of denominator in sequential order of b_j where j = 1, 2, . . ., m.

Repeat cards (6) through (9) until all cases are read in.

The listings are now given.

```
      PROGRAM MAIN(INPUT,OUTPUT,PLOT,TAPE5=INPUT,TAPE6=OUTPUT)
      DOUBLE PRECISION COE(21),ROOTR(20),ROOTI(20)
      DIMENSION X(3),Y(20),STORE(603),Z(20)
      COMPLEX A(40,2),S,ZPROD,OPROD,DUM
      COMPLEX GP,GF,FP,DIPROD
      COMPLEX TR,ITEMP,IHOLD
      COMPLEX B(20,2)
      COMMON/HEA/ A,IOPT1,ZERO(22),DENO(22),N1,N1L,M1,M1L,TFK,COEF(22),
     1ANG(22),JOG,R(22),ROTR(2),ROTI(2)
      COMMON/AD/ JIJ,IIP,IPI,IPIP,IPPI,IPPIA,KA,KB,KC,KD,KE,KF,KG,KH,KI
      COMMON/OUTT2/K1,NUMBER,SIZEX,SIZEY,TIME,CMT1(5),CMT2(5),CMT3(5),
     1CMT4(5),IOPT2,IOPT3,OMEGA,PHI,AMPL
      READ(5,100)(CMT1(I),I=1,5)
      READ(5,100)(CMT2(I),I=1,5)
  100 FORMAT(5A6,3F10.0)
      READ(5,101)NUMBER,IOPT1,IOPT2,IOPT3
  101 FORMAT(4I2)
      READ(5,100)(CMT3(I),I=1,5),SIZEX,SIZEY,TIME
      IF(IOPT2.NE.05) GO TO 10
      READ(5,102) AMPL,OMEGA,PHI
  102 FORMAT(8E10.0)
   10 DO 90 K=1,NUMBER
      READ(5,100)(CMT4(I),I=1,5)
      K1=K
      IF(IOPT1.NE.01) GO TO 15
C
C READING DATA WHEN IT IS IN POLYNOMIAL FORM
C
      READ(5,103)TFK,N1,M1
  103 FORMAT(1F10.0,5I2)
      N1L=0
      M1L=0
      P=0
      IF(IOPT2.NE.05) GO TO 18
      IF(PHI.EQ.0.) TFK=TFK*AMPL*OMEGA
      IF(PHI.NE.0.) TFK=TFK*AMPL*SIN(PHI)
      IF(N1.EQ.0) GO TO 80
      READ(5,102)(ZERO(I),I=1,N1)
   80 READ(5,102)(DENO(I),I=1,M1)
      IF(PHI.EQ.0.) GO TO 61
      IF(PHI.NE.0.) GO TO 50
C
C READING DATA WHEN IT IS IN ROOT LOCUS FORM
C
   15 IF(IOPT1.NE.02) GO TO 25
      READ(5,103) TFK,N1,N1L,M1,M1L
      P=0
      IF(IOPT2.NE.05) GO TO 18
      IF(PHI.EQ.0.) TFK=TFK*AMPL*OMEGA
      IF(PHI.NE.0.) TFK=TFK*AMPL*SIN(PHI)
      IF(PHI.NE.0.) GO TO 83
      IF(PHI.EQ.0.) GO TO 84
   83 ZERO(1)=OMEGA*COS(PHI)/SIN(PHI)
      N1L=N1L+1
      N1=N1+1
```

```
      IF(N1.EQ.1) GO TO 81
      READ(5,102)(ZERO(I),I=2,N1)
      GO TO 81
   84 IF(N1.EQ.0) GO TO 81
      READ(5,102)(ZERO(I),I=1,N1)
   81 READ(5,102)(DENO(I),I=1,M1)
      M1=M1+2
      DENO(M1+1)=0.0
      DENO(M1+2)=OMEGA**2
      GO TO 75
C
C READING DATA WHEN IT IS IN BODE FORM
C
   25 READ(5,103) TFK,N1,N1L,M1,M1L,P
      IF(IOPT2.NE.05) GO TO 18
      IF(PHI.EQ.0.) TFK=TFK*AMPL/OMEGA
      IF(PHI.NE.0.) TFK=TFK*AMPL*COS(PHI)/OMEGA
      IF(PHI.NE.0.) GO TO 88
      IF(PHI.EQ.0.) GO TO 87
   88 ZERO(1)=SIN(PHI)/(OMGEA*COS(PHI))
      N1L=N1L+1
      N1=N1+1
      IF(N1.EQ.1) GO TO 82
      READ(5,102)(ZERO(I),I=2,N1)
      GO TO 82
   87 IF(N1.EQ.0) GO TO 82
      READ(5,102)(ZERO(I),I=1,N1)
   82 READ(5,102)(DENO(I),I=1,M1)
      M1=M1+2
      DENO(M1+1)=1.0/OMEGA**2
      DENO(M1+2)=0.0
      GO TO 75
   18 IF(N1.EQ.0) GO TO 30
   20 READ(5,102)(ZERO(I),I=1,N1)
   30 READ(5,102)(DENO(I),I=1,M1)
   34 IF(IOPT2.EQ.01) GO TO 35
      IF(IOPT2.EQ.02) GO TO 75
      IF(IOPT2.EQ.03) GO TO 40
      IF(IOPT2.EQ.04) GO TO 45
      IF(IOPT2.EQ.05.AND.IOPT1.EQ.01) GO TO 50
   35 M1=M1+1
      GO TO 75
   40 M1=M1+2
      GO TO 75
   45 M1=M1+3
      GO TO 75
   50 X(1)=OMEGA*COS(PHI)/SIN(PHI)
      X(2)=1.0
      N2=N1
      DO 55 I=1,N2
      Y(I)=ZERO(N1)
      N1=N1-1
   55 CONTINUE
      N2=N2+1
      Y(N2)=1.0
```

```
      CALL PMPY(Z,IDIMZ,X,2,Y,N2)
      N2=IDIMZ-1
      DO 60 I=1,N2
      IDIMZ=IDIMZ-1
      ZERO(I)=Z(IDIMZ)
   60 CONTINUE
      N1=N2
   61 CONTINUE
      X(1)=OMEGA**2
      X(2)=0.0
      X(3)=1.0
      M2=M1
      DO 65 I=1,M2
      Y(I)=DENO(M1)
      M1=M1-1
   65 CONTINUE
      M2=M2+1
      Y(M2)=1.0
      CALL PMPY(Z,IDIMZ,X,3,Y,M2)
      M2=IDIMZ-1
      DO 70 I=1,M2
      IDIMZ=IDIMZ-1
      DENO(I)=Z(IDIMZ)
   70 CONTINUE
      M1=M2
   75 CALL HEAVY
      CALL OUTPUT
      CALL OUTPT2
   90 CONTINUE
      STOP
      END
```

```
      SUBROUTINE HEAVY
      DOUBLE PRECISION COE(21),ROOTR(20),ROOTI(20)
      DIMENSION NG(10),D(10),DI(10),IO(10),JG(10)
      DIMENSION NF(10),F(20,10),IOU(10)
      COMPLEX A(40,2),S,ZPROD,DPROD,DUM
      COMPLEX GP,GF,FP,DIPROD
      COMPLEX TR,ITEMP,IHOLD
      COMPLEX B(20,2)
      COMMON/HEA/ A,IOPT1,ZERO(22),DENO(22),N1,N1L,M1,M1L,TFK,COEF(22),
     1ANG(22),JOG,R(22),ROTR(2),ROTI(2)
      COMMON/AD/ JIJ,IIP,IPI,IPIP,IPPI,IPPIA,KA,KB,KC,KD,KE,KF,KG,KH,KI
 3001 FORMAT(6F10.5)
  815 FORMAT(1H0,5(3H***,3X),11HNO MULT RTS)
  401 FORMAT(1H3,70H*****WARNING*****TERMS MAY BE OMITTED IN THE EXPANSI
     1ON BELOW**********)
C WHEN IOPT = 1,POLY/=2,ROOT LOCUS/=3,BODE
      NZ=N1
      NZL=N1L
      NP=M1
      NPL=M1L
      AKK=TFK
      IOPT=IOPT1
      DO 1010 MN=1,10
      A(MN,2)=(0.0,0.0)
 1010 CONTINUE
      DO 17 MS=1,10
      NF(MS)=0
      NG(MS)=0
      JG(MS)=0
      IO(MS)=0
   17 IOU(MS)=0
      IIP=0
      IPI=0
      IPIP=0
      IPPI=0
      IPPIA=0
      JAY=0
      MPS=0
      MPI=0
      NPB=0
      NZB=0
      MUD=0
      JOG=0
      GO TO (1,2,3),IOPT
C POLYNOMIAL FORM
C   SOLVING AND LOADING ZEROS
    1 IF(NZ)55,54,55
   55 COE(1)=DBLE(1.0)
      DO 50 I=1,NZ
      COE(I+1)=DBLE(ZERO(I))
   50 CONTINUE
      CALL DMULR(COE,NZ,ROOTR,ROOTI)
      DO 51 I=1,NZ
      A(I,1)=CMPLX(-SNGL(ROOTR(I)),-SNGL(ROOTI(I)))
   51 CONTINUE
```

```
C    SOLVING AND LOADING POLES
  54 COE(1)=DBLE(1.0)
     DO 52 I=1,NP
     COE(I+1)=DBLE(DENO(I))
  52 CONTINUE
     CALL DMULR(COE,NP,ROOTR,ROOTI)
     DO 53 I=1,NP
     A(I,2)=CMPLX(-SNGL(ROOTR(I)),-SNGL(ROOTI(I)))
     PRINT 3001, COE(I),ROOTR(I),ROOTI(I)
  53 CONTINUE
C    THE POLES AND ZEROS ARE NOW LOADED
     GO TO 28
C ROOT LOCUS FORM-LOADING COEFS INTO ARRAY
C    LOADING LINEAR ZEROS
   2 NZQ=(NZ-NZL)/2
     NPQ=(NP-NPL)/2
     IF(NZL) 20,20,21
  21 DO 4 I=1,NZL
     A(I,1)=CMPLX(ZERO(I),0.0)
   4 CONTINUE
C    FACTORING AND LOADING QUADRADIC ZEROS
  20 IF(NZQ) 22,22,23
  23 II=NZL + 1
     NN=NZ-1
     DO 6 I=II,NN,2
     COE(1)=1.0
     COE(2)=ZERO(I)
     COE(3)=ZERO(I+1)
     CALL DMULR(COE,2,ROOTR,ROOTI)
     DO 6 J=1,2
     K=I+J
     A(K-1,1)=CMPLX(-SNGL(ROOTR(J)),-SNGL(ROOTI(J)))
   6 CONTINUE
C    LOADING LINEAR POLES
  22 IF(NPL) 24,24,25
  25 DO 5 I=1,NPL
     A(I,2)=CMPLX(DENO(I),0.0)
   5 CONTINUE
C    FACTORING AND LOADING QUADRADIC POLES
  24 IF(NPQ) 26,26,27
  26 IF(NPL) 29,29,28
  27 II=NPL+1
     NN=NP-1
     DO 8 I=II,NN,2
     COE(1)=1.0
     COE(2)=DENO(I)
     COE(3)=DENO(I+1)
     CALL DMULR(COE,2,ROOTR,ROOTI)
     DO 8 J=1,2
     K=I+J
     A(K-1,2)=CMPLX(-SNGL(ROOTR(J)),-SNGL(ROOTI(J)))
   8 CONTINUE
     GO TO 28
C BODE FORM
C    FORMING AND LOADING LINEAR ZEROS
```

```
    3 NZQ=(NZ-NZL)/2
      NPQ=(NP-NPL)/2
      IF(NZL)70,70,71
   71 DO 72 I=1,NZL
      IF(ZERO(I).EQ.0.0) GO TO 1018
      ZERO(I)=1.0/ZERO(I)
      A(I,1)=CMPLX(ZERO(I),0.0)
      GO TO 1019
 1018 A(I,1)=CMPLX(0.0,0.0)
 1019 IF(ZERO(I).EQ.0.0) GO TO 1020
      AKK=AKK/ZERO(I)
      GO TO 72
 1020 AKK=AKK
   72 CONTINUE
C    FORMING AND LOADING QUADRADIC ZEROS
   70 IF(NZQ)73,73,74
   74 II=NZL+1
      NN=NZ-1
      DO 75 I=II,NN,2
      COE(1)=1.0
      COE(2)=ZERO(I+1)/ZERO(I)
      COE(3)=1.0/ZERO(I)
      AKK=AKK*ZERO(I)
      CALL DMULR(COE,2,ROOTR,ROOTI)
      DO 75 J=1,2
      K=I+J
      A(K-1,1)=CMPLX(-SNGL(ROOTR(J)),-SNGL(ROOTI(J)))
   75 CONTINUE
C    FORMING AND LOADING LINEAR POLES
   73 IF(NPL)76,76,77
   77 DO 78 I=1,NPL
      IF(DENO(I).EQ.0.0) GO TO 1012
      DENO(I)=1.0/DENO(I)
      A(I,2)=CMPLX(DENO(I),0.0)
      GO TO 1013
 1012 A(I,2)=CMPLX(0.0,0.0)
 1013 IF(DENO(I).EQ.0.0) GO TO 1011
      AKK=AKK*DENO(I)
      GO TO 78
 1011 AKK=AKK
   78 CONTINUE
C    FORMING AND LOADING QUADRADIC POLES
   76 IF(NPQ)79,79,80
   79 IF(NPL)29,29,28
   80 II=NPL+1
      NN=NP-1
      DO 81 I=II,NN,2
      COE(1)=1.0
      COE(2)=DENO(I+1)/DENO(I)
      COE(3)=1.0/DENO(I)
      AKK=AKK/DENO(I)
      CALL DMULR(COE,2,ROOTR,ROOTI)
      DO 81 J=1,2
      K=I+J
      A(K-1,2)=CMPLX(-SNGL(ROOTR(J)),-SNGL(ROOTI(J)))
```

```
     81 CONTINUE
C CHECK FOR MULTIPLE ROOTS
     28 IF (NZ.EQ.NP) GO TO 400
        IF (NZ.GT.NP) GO TO 400
     30 KK=NP-1
        DO 100 I=1,KK
        K=I+1
        DO 100 J=K,NP
        IF(REAL(A(I,2)).NE.0.0.AND.REAL(A(J,2)).NE.0.0) GO TO 200
        IF(REAL(A(I,2)).EQ.0.0.AND.REAL(A(J,2)).EQ.0.0) GO TO 103
        GO TO 110
    200 X1=REAL(A(I,2))
        X2=REAL(A(J,2))
        IF(ABS(X1-X2).GT..0001) GO TO 110
    103 IF(AIMAG(A(I,2)).NE.0.0.AND.AIMAG(A(J,2)).NE.0.0) GO TO 765
        IF(AIMAG(A(I,2)).EQ.0.0.AND.AIMAG(A(J,2)).EQ.0.0) GO TO 101
        GO TO 110
    765 Y1=AIMAG(A(I,2))
        Y2=AIMAG(A(J,2))
        IF(ABS(Y1-Y2).GT..0001) GO TO 110
    101 JOG=1
    110 CONTINUE
    100 CONTINUE
        IF(JOG.EQ.1) GO TO 500
C DOUBLING THE ARRAY OF POLES
        DO 10 I=1,NP
        WRITE(6,815)
        K=I+NP
        A(K,2)=A(I,2)
     10 CONTINUE
C COMPUTING THE COEFICIENTS
        DO 11 I=1,NP
        S=-A(I,2)
C    COMPUTING NUMERATOR
        ZPROD=(1.0,0.0)
        IF(NZ)90,91,90
     90 DO 12 I2=1,NZ
        ZPROD=ZPROD*(S+A(I2,1))
     12 CONTINUE
C    COMPUTING DENOMINATOR
     91 DPROD = (1.0,0.0)
        NPI=I+NP-1
        NPS=I+1
        DO 13 IP=NPS,NPI
        DPROD=DPROD*(S+A(IP,2))
     13 CONTINUE
C    TAKING QUOTIENT
        DUM=ZPROD/DPROD
        COEF(I)=AKK*SQRT(REAL(DUM)*REAL(DUM)+AIMAG(DUM)*AIMAG(DUM))
C    COMPUTING ANGLE
        ANG(I)=(ATAN2(AIMAG(DUM),REAL(DUM)))*57.3
     11 CONTINUE
     29 RETURN
C MULTIPLE ROOT CALCULATION
    500 JR=0
```

```
      LI=NP-1
C     ARRANGE SIMILAR MULTIPLE ROOTS TOGETHER
      DO 850 IR=1,LI
      IS=IR+1
  854 IT=IS
  852 IF(ABS(REAL(A(IR,2))-REAL(A(IT,2))).LT.0.001.AND.ABS(AIMAG(A(IR,2)
     1)-AIMAG(A(IT,2))).LT.0.001) GO TO 851
      IF(IT.EQ.NP) GO TO 850
      IT=IT+1
      GO TO 852
  851 IF(IT.EQ.IS) GO TO 875
      GO TO 855
  875 A(IS,2)=A(IT,2)
      IF(IT.EQ.NP) GO TO 850
      GO TO 853
  855 ITEMP=A(IS,2)
      A(IS,2)=A(IT,2)
      A(IT,2)=ITEMP
  853 IS=IS+1
      GO TO 854
  850 CONTINUE
C     PLACE MULTIPLE ROOTS BEFORE ALL SINGULAR ROOTS
      DO 869 MR=1,4
      IB=1
  879 IF(ABS(REAL(A(IB,2))-REAL(A(IB+1,2))).LT.0.001.AND.ABS(AIMAG(A(IB,
     22))-AIMAG(A(IB+1,2))).LT.0.001) GO TO 890
      IF(IBOLD.EQ.10) GO TO 891
      IHOLD=A(IB,2)
      A(IB,2)=A(IB+1,2)
      A(IB+1,2)=IHOLD
      GO TO 891
  890 IF(IB.EQ.NP) GO TO 869
      IB=IB+1
      IBOLD=10
      GO TO 879
  891 IF(IB.EQ.LI) GO TO 869
      IB=IB+1
      IBOLD=0
      GO TO 879
  869 CONTINUE
C     COUNT SINGULAR ROOTS(JR)
      ICOLD=0
      IJ=1
  305 IF(ABS(REAL(A(IJ,2))-REAL(A(IJ+1,2))).LT.0.001.AND.ABS(AIMAG(A(IJ,
     32))-AIMAG(A(IJ+1,2))).LT.0.001) GO TO 310
      IF(ICOLD.EQ.10) GO TO 307
      JR=JR+1
      GO TO 307
  310 IF(IJ.EQ.NP-1) GO TO 317
      IJ=IJ+1
      ICOLD=10
      GO TO 305
  307 IF(IJ.EQ.NP-1) GO TO 318
      IJ=IJ+1
      ICOLD=0
```

```
      GO TO 305
  318 JR=JR+1
  317 CONTINUE
C     COUNT MULTIPLE ROOTS(JIJ)
      IIP=1
      JIJ=NP-JR
      LJ=JIJ-1
C     COUNT FIRST GROUP OF MULTIPLE ROOTS(IIP)
      DO 900 IJJ=1,LJ
      IF(ABS(REAL(A(IJJ,2))-REAL(A(IJJ+1,2))).LT.0.001.AND.ABS(AIMAG(A(I
     4JJ,2))-AIMAG(A(IJJ+1,2))).LT.0.001) GO TO 905
      GO TO 907
  305 IIP=IIP+1
  900 CONTINUE
  907 JIJP=JIJ-IIP
      IF(JIJP) 925,925,911
  911 IPI=1
      LL=IJJ+1
C     COUNT SECOND GROUP OF MULTIPLE ROOTS(IPI)
      DO 910 JT=LL,LJ
      IF(ABS(REAL(A(JT,2))-REAL(A(JT+1,2))).LT.0.001.AND.ABS(AIMAG(A(JT,
     52))-AIMAG(A(JT+1,2))).LT.0.001) GO TO 909
      GO TO 917
  909 IPI=IPI+1
  910 CONTINUE
  917 JS=JIJP-IPI
      IF(JS) 925,925,921
  921 IPIP=1
      LK=JT+1
C     COUNT THIRD GROUP OF MULTIPLE ROOTS(IPIP)
      DO 920 JI=LK,LJ
      IF(ABS(REAL(A(JI,2))-REAL(A(JI+1,2))).LT.0.001.AND.ABS(AIMAG(A(JI,
     62))-AIMAG(A(JI+1,2))).LT.0.001) GO TO 919
      GO TO 927
  919 IPIP=IPIP+1
  920 CONTINUE
  927 JSI=JS-IPIP
      IF(JSI) 925,925,931
  931 IPPI=1
      LM=JI+1
C     COUNT FOURTH GROUP OF MULTIPLE ROOTS(IPPI)
      DO 930 JA=LM,LJ
      IF(ABS(REAL(A(JA,2))-REAL(A(JA+1,2))).LT.0.001.AND.ABS(AIMAG(A(JA,
     72))-AIMAG(A(JA+1,2))).LT.0.001) GO TO 929
      GO TO 937
  929 IPPI=IPPI+1
  930 CONTINUE
  937 JSIA=JSI-IPPI
      IF(JSIA) 925,925,941
  941 IPPIA=1
      LN=JA+1
C     COUNT FIFTH GROUP OF MULTIPLE ROOTS(IPPIA)
      DO 940 JB=LN,LJ
      IF(ABS(REAL(A(JB,2))-REAL(A(JB+1,2))).LT.0.001.AND.ABS(AIMAG(A(JB,
     82))-AIMAG(A(JB+1,2))).LT.0.001) GO TO 939
```

```
      GO TO 925
  939 IPPIA=IPPIA+1
  940 CONTINUE
  925 I=1
      IF(IOPT.EQ.1) GO TO 420
      CALL MULTI(A,ZERO,DENO,NZ,NP)
  420 CONTINUE
C     DOUBLE POLE ARRAY
      DO 45 K1=1,NP
      K=K1+NP
      A(K,2)=A(K1,2)
   45 CONTINUE
  190 S=-A(I,2)
      ZPROD=(1.0,0.0)
C     NON-REPEATED ROOT NUMERATOR SOLUTION
      IF(NZ)60,61,60
   60 DO 35 I2=1,NZ
      ZPROD=ZPROD*(S+A(I2,1))
   35 CONTINUE
C     SET MULTIPLE ROOT VALUES
   61 KA=IIP
      KB=IIP+IPI
      KC=IIP+IPI+IPIP
      KD=JIJ-IPPIA
      KE=JIJ
      KF=2+IIP
      KG=2+IIP+IPI
      KH=2+IIP+IPI+IPIP
      KI=2+IIP+IPI+IPIP+IPPI
      IF(I.GE.2.AND.KA.GE.I) GO TO 170
      IF(I.GE.KF.AND.KB.GE.I) GO TO 171
      IF(I.GE.KG.AND.KC.GE.I) GO TO 172
      IF(I.GE.KH.AND.KD.GE.I) GO TO 173
      IF(I.GE.KI.AND.KE.GE.I) GO TO 174
      JAY=IIP
      IF(I.GT.IIP) JAY=IPI
      IF(I.GT.KB) JAY=IPIP
      IF(I.GT.KC) JAY=IPPI
      IF(I.GT.KD) JAY=IPPIA
      IF(I.LT.JIJ) GO TO 915
      MPS=MPS+1
      MPI=NP+I-1
      GO TO 150
  915 MPS=I+JAY
      MPI=NP+I-1
  150 DPROD=(1.0,0.0)
      F(1,1)=1.0
      F(1,2)=1.0
      F(1,8)=1.0
C     SETTING INITIAL DENOMINATOR COEFFICIENT AND POWER
      DO 601 IG=1,NP
      F(IG+1,2)=DENO(IG)
      NG(IG)=NP+1-IG
      F(IG+1,8)=F(IG+1,2)
  601 JG(IG)=NG(IG)
```

```
C     SETTING INITIAL NUMERATOR COEFFICIENT AND POWER
      DO 600 IV=1,NZ
      F(IV+1,1)=ZERO(IV)
  600 NF(IV)=NZ+1-IV
      MUD=0
C     NON-REPEATED ROOT DENOMINATOR SOLUTION
      DO 130 IP=MPS,MPI
      DPROD=DPROD*(S+A(IP,2))
  130 CONTINUE
      DUM=ZPROD/DPROD
      GO TO 138
  170 MUD=MUD+1
      JIG=1
      GO TO 550
  171 MUD=MUD+1
      JIG=2
      GO TO 550
  172 MUD=MUD+1
      JIG=3
      GO TO 550
  173 MUD=MUD+1
      JIG=4
      GO TO 550
  174 MUD=MUD+1
      JIG=5
  550 IF(NZ.LT.2) GO TO 654
      FP=(0.0,0.0)
      IF(MUD.GT.1) GO TO 657
      NT=NZ-1
      DO 650 NI=1,NT
      Z=FLOAT(NF(NI))
      FP=(F(NI,1)*Z)*(S**(NF(NI)-1))+FP
      D(NI)=F(NI,1)*Z
  650 IO(NI)=NF(NI)-1
      Z=FLOAT(NF(NZ))
      FP=(F(NZ,1)*Z)+FP
      D(NZ)=F(NZ,1)
      IO(NZ)=0
      GO TO 656
  657 IJJJ=IO(1)+1
      DO 1117 IVV=1,10
 1117 F(IVV,5)=0.
      IRT=0
      IRS=0
      IIII=JG(1)+1
      ING=NF(1)+1
      IGN=ICU(1)+1
  649 IRS=IRS+1
      IT=0
      IF(IRS.GT.IIII) GO TO 653
  647 IT=IT+1
      IF(IT.GT.IJJJ) GO TO 649
      LR=IRS+IT-1
      DOT=(D(IT)*F(IRS,8))+F(LR,5)
      F(LR,5)=DOT
```

```
      GO TO 647
  653 IRT=IRT+1
      ITT=0
      IF(IRT.GT.IGN) GO TO 651
  652 ITT=ITT+1
      IF(ITT.GT.ING) GO TO 653
      LPT=IRT+ITT-1
      DOT=F(LPT,5)-(F(ITT,1)*DI(IRT))
      F(LPT,5)=DOT
      GO TO 652
  651 NUR=JG(1)+IO(1)
      I2=NUR
      I3=I2+1
      DO 1114 IOP=1,I3
 1114 D(IOP)=F(IOP,5)
      ZPROD=(0.0,0.0)
      DO 1115 IOGG=1,I2
      IO(IOGG)=NUR-IOGG+1
 1115 ZPROD=D(IOGG)*(S**IO(IOGG))+ZPROD
      ZPROD=ZPROD+D(I3)
      LAMP=I2-1
      FP=(0.0,0.0)
      DO 1116 IIGG=1,LAMP
      Z=FLOAT(IO(IIGG))
      FP=(D(IIGG)*Z)*(S**(IO(IIGG)-1))+FP
      D(IIGG)=D(IIGG)*Z
 1116 IO(IIGG)=IO(IIGG)-1
      FP=FP+D(I2)
      IO(I2)=0
      DIPROD=DPROD
      GP=2.0*GP
      GO TO 1237
  654 FP=(1.0,0.0)
  656 FP=FP
 2000 GO TO (350,351,352,353,354),JIG
  350 L=IIP
      GO TO 1500
  351 L=IPI
      GO TO 1500
  352 L=IPIP
      GO TO 1500
  353 L=IPPI
      GO TO 1500
  354 L=IPPIA
 1500 DO 1501 IGG=1,L
      F(1,4)=1.0
      V=REAL(S)
      IBA=NP-IGG
      DO 2787 INN=1,IBA
      F(INN,6)=F(INN+1,8)+(F(INN,4)*V)
      F(INN+1,4)=F(INN,6)
 2787 JG(INN)=JG(INN)-1
      IGV=IBA+1
      DO 2797 IX=1,IGV
 2797 F(IX,8)=F(IX,4)
```

```
      JG(IGV)=0
 1501 CONTINUE
      GP=(0.0,0.0)
      NIX=IBA+1
      DIPROD=(0.0,0.0)
      DO 1234 IBAT=1,IBA
 1234 DIPROD=(F(IBAT,8)*(S**(JG(IBAT))))+DIPROD
      DIPROD=F(NIX,8)+DIPROD
      IGUE=IBA-1
      IF(IGUE.LT.1) GO TO 1236
      DO 1235 IBAD=1,IGUE
      RS=FLOAT(JG(IBAD))
      GP=(F(IBAD,8)*RS)*(S**(JG(IBAD)-1))+GP
      DI(IBAD)=F(IBAD,8)*RS
 1235 IOU(IBAD)=JG(IBAD)-1
 1236 RS=FLOAT(JG(IBA))
      GP=(F(IBA,8)*RS)+GP
      DI(IBA)=F(IBA,8)*RS
      IOU(IBA)=0
 1237 DPROD=DIPROD*DIPROD
      IF(MUD.EQ.1) DPROD=1. *DPROD
      IF(MUD.EQ.2) DPROD=2. *DPROD
      IF(MUD.EQ.3) DPROD=6. *DPROD
      IF(MUD.EQ.4) DPROD=24.*DPROD
      DUM=(FP*DIPROD-ZPROD*GP)/DPROD
  138 COEF(I)=AKK*SQRT(REAL(DUM)*REAL(DUM)+AIMAG(DUM)*AIMAG(DUM))
      ANG(I)=(ATAN2(AIMAG(DUM),REAL(DUM)))*57.3
      IF(I.EQ.NP) GO TO 40
      I=I+1
      GO TO 190
   40 CONTINUE
  290 RETURN
  400 WRITE(6,401)
      GO TO 30
C THE SUBROUTINE IS FINISHED
C  FOR NO. OF POLES = I,
C       A(I,2) CONTAINS THE ROOT LOCATIONS IN THE FORM (S + A(I,2))
C       COEF(I) CONTAINS THE MAGNITUDE OF THE (I)TH ROOT COEFICIENT
C       ANG(I) CONTAINS THE ANGLE(DEG) OF THE (I)TH ROOT COEFICIENT
C       A(J,1) CONTAINS THE ZERO LOCATIONS IN THE FORM (S + A(J,1))
      END
```

```
      SUBROUTINE DMULR (COE,N1,ROOTR,ROOTI)
C
C
C*************************************************************************
C
C     POLYNOMIAL ROOT FINDER SUBROUTINE ....
C
C     ITERATIVE METHOD FOR POLYNOMIAL EQUATIONS ....
C
C     THIS METHOD APPROXIMATES THE FUNCTION F(Z) BY A QUADRATIC
C   WHICH MAY ,IN GENERAL, HAVE COMPLEX COEFFICIENTS AND DOES NOT
C   REQUIRE A KNOWLEDGE OF THE DERIVATIVE OF F(Z) THOUGH
C   THE FUNCTION F(Z) MUST BE EVALUATED ONCE PER ITERATION ....
C
C     THIS SUBROUTINE FINDS REAL AND COMPLEX ROOTS OF A POLYNOMIAL
C   WITH REAL COEFFICIENTS ....
C
C
C     USE OF MULLER SUBROUTINE ....
C   1.  CALL DMULR  (COE,N1,ROOTR,ROOTI) ....
C   2.  COE IS THE TAG OF THE ARRAY OF COEFFICIENTS.
C       THE COEFFICIENTS MUST BE ORDERED FROM HIGHEST DEGREE
C       TO LOWEST DEGREE .
C   3.  N1 IS DEGREE OF THE POLYNOMIAL .
C   4.  ROOTR IS THE TAG OF THE ARRAY WHERE THE REAL PARTS
C       OF THE COMPLEX ROOTS ARE STORED .
C   5.  ROOTI IS THE TAG OF THE ARRAY WHERE THE IMAGINARY
C       PARTS OF THE COMPLEX ROOTS ARE STORED ....
C
C     ALL ARITHMETIC IS IN THE COMPLEX MODE ....
C     THEREFORE UNDER-FLOW IS NORMAL FOR REAL ROOTS ....
C
C     MULTIPLE ROOTS DECREASES ACCURACY OF THIS SUBROUTINE .
C     WHEN MULTIPLICITY IS FOUR THE ACCURACY DECREASES TO
C     ABOUT TWO PLACES ....
C
C     DEGREE SQUARED DIVIDED BY TWENTY ....
C     FOR DEGREE ELEVEN IT TAKES SIX SECONDS ....
C
C
C
C*************************************************************************
C
C
C
      DOUBLE PRECISION ROOTR,ROOTI,AXR,AXI,ALP1R,ALP1I,TEM
      DOUBLE PRECISION BET1R,BET1I,ALP2R,ALP2I,BET2R,BET2I
      DOUBLE PRECISION TEMR,TEMI,ALP3R,ALP3I,BET3R,BET3I
      DOUBLE PRECISION ALP4R,ALP4I,TEM1,TEM2,HELL,BELL
      DOUBLE PRECISION TE1,TE2,TE3,TE4,TE5,TE6,TE7,TE8,TE9,TE10
      DOUBLE PRECISION TE11,TE12,TE13,TE14,TE15,TE16,DE15,DE16,COE
C
      DIMENSION COE(1),ROOTR(1),ROOTI(1)
C
      N2=N1+1
```

```
            N4=0
            I=N1+1
      19    IF(COE(I))9,7,9
      7     N4=N4+1
            ROOTR(N4)=0.0D0
            ROOTI(N4)=0.0D0
            I=I-1
            IF(N4-N1)19,37,19
      9     CONTINUE
      C
      10    AXR=0.8D0
            AXI=0.0D0
            L=1
            N3=1
            ALP1R=AXR
            ALP1I=AXI
            M=1
            GO TO 99
      C
      11    BET1R=TEMR
            BET1I=TEMI
            AXR=0.85D0
            ALP2R=AXR
            ALP2I=AXI
            M=2
            GO TO 99
      C
      12    BET2R=TEMR
            BET2I=TEMI
            AXR=0.9D0
            ALP3R=AXR
            ALP3I=AXI
            M=3
            GO TO 99
      C
      13    BET3R=TEMR
            BET3I=TEMI
      14    TE1=ALP1R-ALP3R
            TE2=ALP1I-ALP3I
            TE5=ALP3R-ALP2R
            TE6=ALP3I-ALP2I
            TEM=TE5*TE5+TE6*TE6
            TE3=(TE1*TE5+TE2*TE6)/TEM
            TE4=(TE2*TE5-TE1*TE6)/TEM
            TE7=TE3+1.0D0
            TE9=TE3*TE3-TE4*TE4
            TE10=2.0D0*TE3*TE4
            DE15=TE7*BET3R-TE4*BET3I
            DE16=TE7*BET3I+TE4*BET3R
            TE11=TE3*BET2R-TE4*BET2I+BET1R-DE15
            TE12=TE3*BET2I+TE4*BET2R+BET1I-DE16
            TE7=TE9-1.0D0
            TE1=TE9*BET2R-TE10*BET2I
            TE2=TE9*BET2I+TE10*BET2R
            TE13=TE1-BET1R-TE7*BET3R+TE10*BET3I
```

```
      TE14=TE2-BET1I-TE7*BET3I-TE10*BET3R
      TE15=DE15*TE3-DE16*TE4
      TE16=DE15*TE4+DE16*TE3
      TE1=TE13*TE13-TE14*TE14-4.0D0*(TE11*TE15-TE12*TE16)
      TE2=2.0D0*TE13*TE14-4.0D0*(TE12*TE15+TE11*TE16)
      TEM=DSQRT(TE1*TE1+TE2*TE2)
      IF(TE1)113,113,112
  113 TE4=DSQRT(0.5D0*(TEM-TE1))
      TE3=0.5D0*TE2/TE4
      GO TO 111
C
  112 TE3=DSQRT(0.5D0*(TEM+TE1))
      IF(TE2)110,200,200
  110 TE3=-TE3
  200 TE4=0.5D0*TE2/TE3
  111 TE7=TE13+TE3
      TE8=TE14+TE4
      TE9=TE13-TE3
      TE10=TE14-TE4
      TE1=2.0D0*TE15
      TE2=2.0D0*TE16
      IF(TE7*TE7+TE8*TE8-TE9*TE9-TE10*TE10)204,204,205
  204 TE7=TE9
      TE8=TE10
  205 TEM=TE7*TE7+TE8*TE8
      TE3=(TE1*TE7+TE2*TE8)/TEM
      TE4=(TE2*TE7-TE1*TE8)/TEM
      AXR=ALP3R+TE3*TE5-TE4*TE6
      AXI=ALP3I+TE3*TE6+TE4*TE5
      ALP4R=AXR
      ALP4I=AXI
      M=4
      GO TO 99
C
   15 N6=1
C*************************************************************************
   38 IF(DABS(HELL)+DABS(BELL)-1.0D-20)18,18,16
   16 TE7=DABS(ALP3R-AXR)+DABS(ALP3I-AXI)
      IF(TE7/(DABS(AXR)+DABS(AXI))-1.0D-7)18,18,17
C*************************************************************************
   17 N3=N3+1
      ALP1R=ALP2R
      ALP1I=ALP2I
      ALP2R=ALP3R
      ALP2I=ALP3I
      ALP3R=ALP4R
      ALP3I=ALP4I
      BET1R=BET2R
      BET1I=BET2I
      BET2R=BET3R
      BET2I=BET3I
      BET3R=TEMR
      BET3I=TEMI
      IF(N3-100)14,18,18
   18 N4=N4+1
```

```
      ROOTR(N4)=ALP4R
      ROOTI(N4)=ALP4I
      N3=0
   41 IF(N4-N1)30,37,37
   37 RETURN
C*****************************************************************************
   30 IF(DABS(ROOTI(N4))-1.0D-5)10,10,31
   31 GO TO (32,10),L
   32 AXR=ALP1R
      AXI=-ALP1I
      ALP1I=-ALP1I
      M=5
      GO TO 99
   33 BET1R=TEMR
      BET1I=TEMI
      AXR=ALP2R
      AXI=-ALP2I
      ALP2I=-ALP2I
      M=6
      GO TO 99
C
   34 BET2R=TEMR
      BET2I=TEMI
      AXR=ALP3R
      AXI=-ALP3I
      ALP3I=-ALP3I
      L=2
      M=3
   99 TEMR=COE(1)
      TEMI=0.000
      DO 100 I=1,N1
      TE1=TEMR*AXR-TEMI*AXI
      TEMI=TEMI*AXR+TEMR*AXI
  100 TEMR=TE1+COE(I+1)
      HELL=TEMR
      BELL=TEMI
   42 IF(N4)102,103,102
  102 DO 101 I=1,N4
      TEM1=AXR-ROOTR(I)
      TEM2=AXI-ROOTI(I)
      TE1=TEM1*TEM1+TEM2*TEM2
      TE2=(TEMR*TEM1+TEMI*TEM2)/TE1
      TEMI=(TEMI*TEM1-TEMR*TEM2)/TE1
  101 TEMR=TE2
  103 GO TO (11,12,13,15,33,34),M
      END
```

```
      SUBROUTINE MULTI(A,ZERO,DENO,NZ,NP)
      DIMENSION ZERO(NZ),DENO(NP)
      COMPLEX A(40,2),B(20,2)
C     MULTIPLY OUT ROOT LOCUS OR BODE INTO POLYNOMIAL FORM
      B(1,1)=A(1,1)+A(2,1)
      B(1,2)=A(1,2)+A(2,2)
      B(2,1)=B(1,1)+A(3,1)
      B(2,2)=B(1,2)+A(3,2)
      B(3,1)=B(2,1)+A(4,1)
      B(3,2)=B(2,2)+A(4,2)
      B(4,1)=B(3,1)+A(5,1)
      B(4,2)=B(3,2)+A(5,2)
      B(5,1)=B(4,1)+A(6,1)
      B(5,2)=B(4,2)+A(6,2)
      B(6,2)=B(5,2)+A(7,2)
      B(10,1)=A(1,1)*A(2,1)
      B(10,2)=A(1,2)*A(2,2)
      B(11,1)=B(10,1)*A(3,1)
      B(11,2)=B(10,2)*A(3,2)
      B(12,1)=B(11,1)*A(4,1)
      B(12,2)=B(11,2)*A(4,2)
      B(13,1)=B(12,1)*A(5,1)
      B(13,2)=B(12,2)*A(5,2)
      B(14,1)=B(13,1)*A(6,1)
      B(14,2)=B(13,2)*A(6,2)
      B(15,2)=B(14,2)*A(7,2)
      IF(NZ.EQ.1) GO TO 410
      IF(NZ.EQ.2) GO TO 402
      IF(NZ.EQ.3) GO TO 403
      IF(NZ.EQ.4) GO TO 404
  402 ZERO(1)=REAL(B(1,1))
      ZERO(2)=REAL(B(10,1))
      GO TO 410
  403 ZERO(1)=REAL(B(2,1))
      ZERO(2)=REAL(B(10,1)+A(3,1)*B(1,1))
      ZERO(3)=REAL(B(11,1))
      GO TO 410
  404 ZERO(1)=REAL(B(3,1))
      ZERO(2)=REAL(B(10,1)+A(3,1)*B(1,1)+A(4,1)*B(2,1))
      ZERO(3)=REAL(B(11,1)+A(4,1)*(B(10,1)+A(3,1)*B(1,1)))
      ZERO(4)=REAL(B(12,1))
      GO TO 410
  410 IF(NP.EQ.1) GO TO 420
      IF(NP.EQ.2) GO TO 412
      IF(NP.EQ.3) GO TO 413
      IF(NP.EQ.4) GO TO 414
      IF(NP.EQ.5) GO TO 415
  412 DENO(1)=REAL(B(1,2))
      DENO(2)=REAL(B(10,2))
      GO TO 420
  413 DENO(1)=REAL(B(2,2))
      DENO(2)=REAL(B(10,2)+A(3,2)*B(1,2))
      DENO(3)=REAL(B(11,2))
      GO TO 420
  414 DENO(1)=REAL(B(3,2))
```

```
      DENO(2)=REAL(B(10,2)+A(3,2)*B(1,2)+A(4,2)*B(2,2))
      DENO(3)=REAL(B(11,2)+A(4,2)*(B(10,2)+A(3,2)*B(1,2)))
      DENO(4)=REAL(B(12,2))
      GO TO 420
  415 DENO(1)=REAL(B(4,2))
      DENO(2)=REAL(B(10,2)+A(3,2)*B(1,2)+A(4,2)*B(2,2)+A(5,2)*B(3,2))
      DENO(3)=REAL(B(11,2)+A(4,2)*(B(10,2)+A(3,2)*B(10,2))+A(5,2)*
     1(B(10,2)+A(3,2)*B(10,2)+A(4,2)*B(2,2)))
      DENO(4)=REAL(B(12,2)+A(5,2)*(B(11,2)+A(4,2)*(B(10,2)+A(3,2)*
     1B(1,2))))
      DENO(5)=REAL(B(13,2))
      GO TO 420
  420 RETURN
      END
```

```
      SUBROUTINE OUTPT2
      DIMENSION RESPNY(11,902),TIMEX(902),A1(902),A2(902),VECT3(4)
      COMPLEX A(40,2)
      COMMON/HEA/ A,IOPT1,ZERO(22),DENO(22),N1,N1L,M1,M1L,TFK,COEF(22),
     1ANG(22),JOG,R(22),ROTR(2),ROTI(2)
      COMMON/OUTT2/K1,NUMBER,SIZEX,SIZEY,TIME,CMT1(5),CMT2(5),CMT3(5),
     1CMT4(5),IOPT2,IOPT3,OMEGA,PHI,AMPL
      K5=K1+1
      K4=NUMBER+1
      DELT=TIME/900.
      DO 19 I=1,10
   19 RESPNY(I,1)=0.
      DO 10 I=1,900
      IF(I.EQ.1) TIMEX(I)=0.0
      IF(I.GT.1) TIMEX(I)=TIMEX(I-1)+DELT
      IF(IOPT2.EQ.01) RESPNY(1,I)=1.
      IF(IOPT2.EQ.02) RESPNY(1,I)=0.0
      IF(IOPT2.EQ.03) RESPNY(1,I)=TIMEX(I)
      IF(IOPT2.EQ.04) RESPNY(1,I)=TIMEX(I)**2/2.
      IF(IOPT2.EQ.05) RESPNY(1,I)=AMPL*SIN(OMEGA*TIMEX(I)+PHI)
      RESPNY(K5,I)=0.0
      DO 12 J=1,M1
      N=R(J)-1.
      NFACT=1
      IF(N.LT.2) GO TO 8
      DO 9 L=1,N
      NFACT=NFACT*L
    9 CONTINUE
    8 CONTINUE
      IF(I.EQ.1) TRJ=1.0
      IF(I.EQ.1.AND.R(J).GT.1.) TRJ=0.0
      IF(I.GT.1) TRJ=TIMEX(I)**(R(J)-1.)
      B=COEF(J)*TRJ
      C=EXP(-REAL(A(J,2))*TIMEX(I))
      D=COS(AIMAG(A(J,2))*TIMEX(I)-ANG(J)/57.2957)
      E=FLOAT(NFACT)
      RESPNY(K5,I)=RESPNY(K5,I)+B*C*D/E
   12 CONTINUE
   10 CONTINUE
      IF(K1.NE.NUMBER)GO TO 18
      WRITE(6,100)(CMT1(I),I=1,5)
      WRITE(6,101)(CMT2(I),I=1,5)
  100 FORMAT(1H1,5A6)
  101 FORMAT(1H ,5A6)
      WRITE(6,102)(I,I=1,10)
  102 FORMAT(1H ,4X,4HTIME,4X,5HINPUT,4X,10(5HCASE ,I2,4X),//)
      DO 20 I=1,900,12
      WRITE(6,103)TIMEX(I),(RESPNY(J,I),J=1,K4)
  103 FORMAT(12(F9.3,2X))
   20 CONTINUE
      CALL PLOT(0.0,0.0,-3)
      CALL SCALE(TIMEX,SIZEX,900,1)
      IF(IOPT3.NE.01) GO TO 15
      CALL POLYS(RESPNY,K4    ,902,SIZEY)
      CALL AXIS(0.,0.,12HTIME-SECONDS,-12,SIZEX,0.,TIMEX(901),TIMEX(90
```

```
     12))
      CALL AXIS(0.,0.,CMT3,30,SIZEY,90.,RESPNY(1,901),RESPNY(1,902))
      DO 14 K2=1,K4
      DO 13 K3=1,900
      A1(K3)=RESPNY(K2,K3)
   13 CONTINUE
      A1(901)=RESPNY(1,901)
      A1(902)=RESPNY(1,902)
      J1=0
      J2=4
      IF(K2.GT.1) J1=45
      CALL LINE(TIMEX,A1,900,1,J1,J2)
   14 CONTINUE
      GO TO 18
   15 DO 16 K2=1,NUMBER
      ADJMAX=0.0
      ADJMIN=0.0
      DO 17 K3=1,900
      A2(K3)=RESPNY(K2+1,K3)
      A1(K3)=RESPNY(1,K3)
      IF(A1(K3).GT.ADJMAX) ADJMAX=A1(K3)
      IF(A1(K3).LT.ADJMIN) ADJMIN=A1(K3)
      IF(A2(K3).GT.ADJMAX) ADJMAX=A2(K3)
      IF(A2(K3).LT.ADJMIN) ADJMIN=A2(K3)
   17 CONTINUE
      VECT3(1)=ADJMAX
      VECT3(2)=ADJMIN
      CALL SCALE(VECT3,SIZEY,2,1)
      A1(901)=VECT3(3)
      A1(902)=VECT3(4)
      A2(901)=VECT3(3)
      A2(902)=VECT3(4)
      CALL AXIS(0.,0.,12HTIME-SECONDS,-12,SIZEX,0.,TIMEX(901),TIMEX(90
     12))
      CALL AXIS(0.,0.,CMT3,30,SIZEY,90.,A1(901),A1(902))
      CALL LINE(TIMEX,A1,900,1,0,4)
      CALL LINE(TIMEX,A2,900,1,45,4)
   16 CONTINUE
   18 X1=SIZEX+4.0
      CALL PLOT(X1,-1.,-3)
      RETURN
      END
```

```
      SUBROUTINE POLYS(RESPNY,NROW,NCOLMN,SIZEY)
      DIMENSION VECT2(4),RESPNY(11,902)
      ADJMAX=0.0
      ADJMIN=0.0
      NCOL = NCOLMN-2
      DO 10 I=1,NROW
      DO 10 J=1,NCOL
      IF(RESPNY(I,J).GT.ADJMAX) ADJMAX=RESPNY(I,J)
      IF(RESPNY(I,J).LT.ADJMIN) ADJMIN=RESPNY(I,J)
   10 CONTINUE
      VECT2(1)=ADJMAX
      VECT2(2)=ADJMIN
      CALL SCALE(VECT2,SIZEY,2,1,10.)
      NN=NCOL  +1
      RESPNY(1,NN)=VECT2(3)
      MM=NCOL  +2
      RESPNY(1,MM)=VECT2(4)
      RETURN
      END
```

```
C
C     ******************************************************************
C
C        SUBROUTINE PMPY
C
C        PURPOSE
C           MULTIPLY TWO POLYNOMIALS
C
C        USAGE
C           CALL PMPY(Z,IDIMZ,X,IDIMX,Y,IDIMY)
C
C        DESCRIPTION OF PARAMETERS
C           Z      - VECTOR OF RESULTANT COEFFICIENTS, ORDERED FROM
C                    SMALLEST TO LARGEST POWER
C           IDIMZ - DIMENSION OF Z (CALCULATED)
C           X      - VECTOR OF COEFFICIENTS FOR FIRST POLYNOMIAL, ORDERED
C                    FROM SMALLEST TO LARGEST POWER
C           IDIMX - DIMENSION OF X (DEGREE IS IDIMX-1)
C           Y      - VECTOR OF COEFFICIENTS FOR SECOND POLYNOMIAL,
C                    ORDERED FROM SMALLEST TO LARGEST POWER
C           IDIMY - DIMENSION OF Y (DEGREE IS IDIMY-1)
C
C        REMARKS
C           Z CANNOT BE IN THE SAME LOCATION AS X
C           Z CANNOT BE IN THE SAME LOCATION AS Y
C
C        SUBROUTINES AND FUNCTION SUBPROGRAMS REQUIRED
C           NONE
C
C        METHOD
C           DIMENSION OF Z IS CALCULATED AS IDIMX+IDIMY-1
C           THE COEFFICIENTS OF Z ARE CALCULATED AS SUM OF PRODUCTS
C           OF COEFFICIENTS OF X AND Y , WHOSE EXPONENTS ADD UP TO THE
C           CORRESPONDING EXPONENT OF Z.
C
C     ******************************************************************
C
      SUBROUTINE PMPY(Z,IDIMZ,X,IDIMX,Y,IDIMY)
      DIMENSION Z(1),X(1),Y(1)
C
      IF(IDIMX*IDIMY)10,10,20
   10 IDIMZ=0
      GO TO 50
   20 IDIMZ=IDIMX+IDIMY-1
      DO 30 I=1,IDIMZ
   30 Z(I)=0.
      DO 40 I=1,IDIMX
      DO 40 J=1,IDIMY
      K=I+J-1
   40 Z(K)=X(I)*Y(J)+Z(K)
   50 RETURN
      END
```

```
      SUBROUTINE OUTPUT
      COMPLEX A(40,2)
      COMMON/HEA/ A,IOPT1,ZERO(22),DENO(22),N1,N1L,M1,M1L,TFK,COEF(22),
     1ANG(22),JOG,R(22),ROTR(2),ROTI(2)
      COMMON/AD/ JIJ,IIP,IPI,IPIP,IPPI,IPPIA,KA,KB,KC,KD,KE,KF,KG,KH,KI
      NZ=N1
      NZL=N1L
      NP=M1
      NPL=M1L
      AKK=TFK
      IOPT=IOPT1
      WRITE(6,6)
      DO 10 I=1,NP
      R(I)=1.0
      WRITE(6,1)I
      WRITE(6,2) ANG(I)
      WRITE(6,5) COEF(I)
      WRITE(6,3)
      IF(JOG.EQ.1) GO TO 25
      GO TO 17
   25 IF(I.GE.2.AND.KA.GE.I) GO TO 190
      IF(I.GE.KF.AND.KB.GE.I) GO TO 190
      IF(I.GE.KG.AND.KC.GE.I) GO TO 190
      IF(I.GE.KH.AND.KD.GE.I) GO TO 190
      IF(I.GE.KI.AND.KE.GE.I) GO TO 190
      NUMB=IIP
      IF(I.GT.IIP) NUMB=IPI
      IF(I.GT.KB) NUMB=IPIP
      IF(I.GT.KC) NUMB=IPPI
      IF(I.GT.KD) NUMB=IPPIA
      IF(I.GT.JIJ) NUMB=1
      GO TO 30
  190 NUMB=NUMB-1
   30 R(I)=NUMB
      WRITE(6,15) NUMB
   17 WRITE(6,4)A(I,2)
   10 CONTINUE
      WRITE(6,11)
      DO 100 I=1,NP
      X1=AIMAG(A(I,2))
      IF(ABS(X1).LT.0.00001) X1=0.0
      IF(X1)100,102,103
  102 IF(ABS(ANG(I))-1.0)104,104,105
  105 IF(ABS(ANG(I))-181.)106,106,107
  107 IF(ABS(ANG(I))-361.)104,104,109
  109 WRITE(6,7)
      RETURN
  106 X2=-COEF(I)
  110 X3=-REAL(A(I,2))
      IF(I.GE.2.AND.KA.GE.I) GO TO 45
      IF(I.GE.KF.AND.KB.GE.I) GO TO 45
      IF(I.GE.KG.AND.KC.GE.I) GO TO 45
      IF(I.GE.KH.AND.KD.GE.I) GO TO 45
      IF(I.GE.KI.AND.KE.GE.I) GO TO 45
      NUMBE=IIP-1
```

```
      IF(I.GT.IIP) NUMBE=IPI-1
      IF(I.GT.K3) NUMBE=IPIP-1
      IF(I.GT.KC) NUMBE=IPPI-1
      IF(I.GT.KD) NUMBE=IPPIA-1
      IF(I.GT.JIJ) GO TO 20
      GO TO 39
   45 NUMBE=NUMBE-1
      IF(NUMBE.LT.1) GO TO 20
   39 NUMBER=NUMBE-1
      IF(NUMBE.LT.2) NUMBER=1
      IJKL=NUMBER*NUMBE
      ABCDE=FLOAT(IJKL)
      X2=X2/ABCDE
      WRITE(6,18) NUMBE,X3,X2
      GO TO 100
   20 WRITE(6,8) X3,X2
      GO TO 100
  104 X2=COEF(I)
      GO TO 110
  103 X2=2.*COEF(I)
      X3=-REAL(A(I,2))
      WRITE(6,9)X3,X2,X1,ANG(I)
  100 CONTINUE
      RETURN
    1 FORMAT(1H ,9HTERM NO. ,I2/2X)
    2 FORMAT(1H ,25X,1H(,F12.6,2H)J)
    3 FORMAT(1H ,10X,8(6H******))
    4 FORMAT(1H ,10X,5H(S + ,F12.6,3H + ,F12.6,2HJ)//2X)
    5 FORMAT(1H ,10X,1H(,F12.6,2H)E)
    6 FORMAT(1H1,25X,32HPARTIAL FRACTION EXPANSION TERMS)
    7 FORMAT(1H0,37HCANNOT INTERPRET ANGLES ON REAL ROOTS)
    8 FORMAT(1H0,2X///23X,1H(,F12.6,3H*T)/10X,F12.6,1HE)
    9 FORMAT(1H0,2X///23X,1H(,F12.6,3H*T)/10X,F12.6,1HE,16X,4HCOS(,F12.6
     1,5H*T - ,F12.6,1H))
   11 FORMAT(1H1,25X,17HTIME DOMAIN TERMS)
   15 FORMAT(1H ,44X,1H(,I1,1H))
   18 FORMAT(1H0,2X///23X,1H(,I1,1H),1X,1H(,F12.6,3H*T)/10X,F12.6,1HT,3X
     1,1HE)
      END
```

APPENDIX III

THRUST ESTIMATE FOR A PROPROTOR AT ANGLE OF ATTACK

The thrust produced by the proprotors of the Sikorsky stowable rotor configuration during transition was needed to determine the thrust-to-weight ratio for the stowable rotor configuration so that comparisons could be made with the T/W required by the ejector wing configuration. The collective pitch angle and the rotor shaft tilt angle schedules are shown in Figures 14 and 15. The thrust was determined by the analysis given below.

Momentum considerations and blade element theory are used to derive the thrust produced by a propeller, rotor, or proprotor operating under steady flow conditions and at large angles of attack relative to the forward flight speed. The following assumptions were made:

1. The flow through the propeller disk plane is nonviscous and incompressible. Similarly, the effects of compressibility upon blade C_L and C_D aerodynamic characteristics are not significant.

2. No coning, flapping, and lead-lag modes of blade motion occur, nor do torsional deflections along the blade alter the blade twist schedule significantly.

3. Two-dimensional isolated or cascade airfoil data are applicable provided the C_L coefficient at a blade spanwise

station can be represented by $C_L = C_{L_o} + C_{L_\alpha} \alpha_b$. The retention of only the first-order term in angle of attack means that stall effects are not accounted for by this lift representation.

4. Linearization of flow angles at a blade section or ϕ_b and α_b shown in Figure 59 is permissible.

5. The effect of swirl in the slipstream can be ignored in estimating the thrust of the propeller, rotor, or proprotor. This means that the analysis should not be applicable to heavily loaded propellers where disk loading exceeds approximately 20 psf.

6. The thrust of the propeller is positive and the analysis does not apply to the vortex-ring state which is characterized by large recirculation effects and the absence of a clearly defined slipstream.

7. The regions of reverse flow on the blade retreating side during edgewise forward flight are not large relative to the area of the propeller disk.

8. The propeller is operated outside of the influence of a ground plane.

This analysis is an extension of the one given in Reference 14 for rotors at angle of attack to the forward flight speed vector. The extension consists of including nonuniform in-flow into the rotor disk plane where the rotor blade's spanwise distribution for chord, twist, camber, and airfoil section are arbitrary; the rotor blade

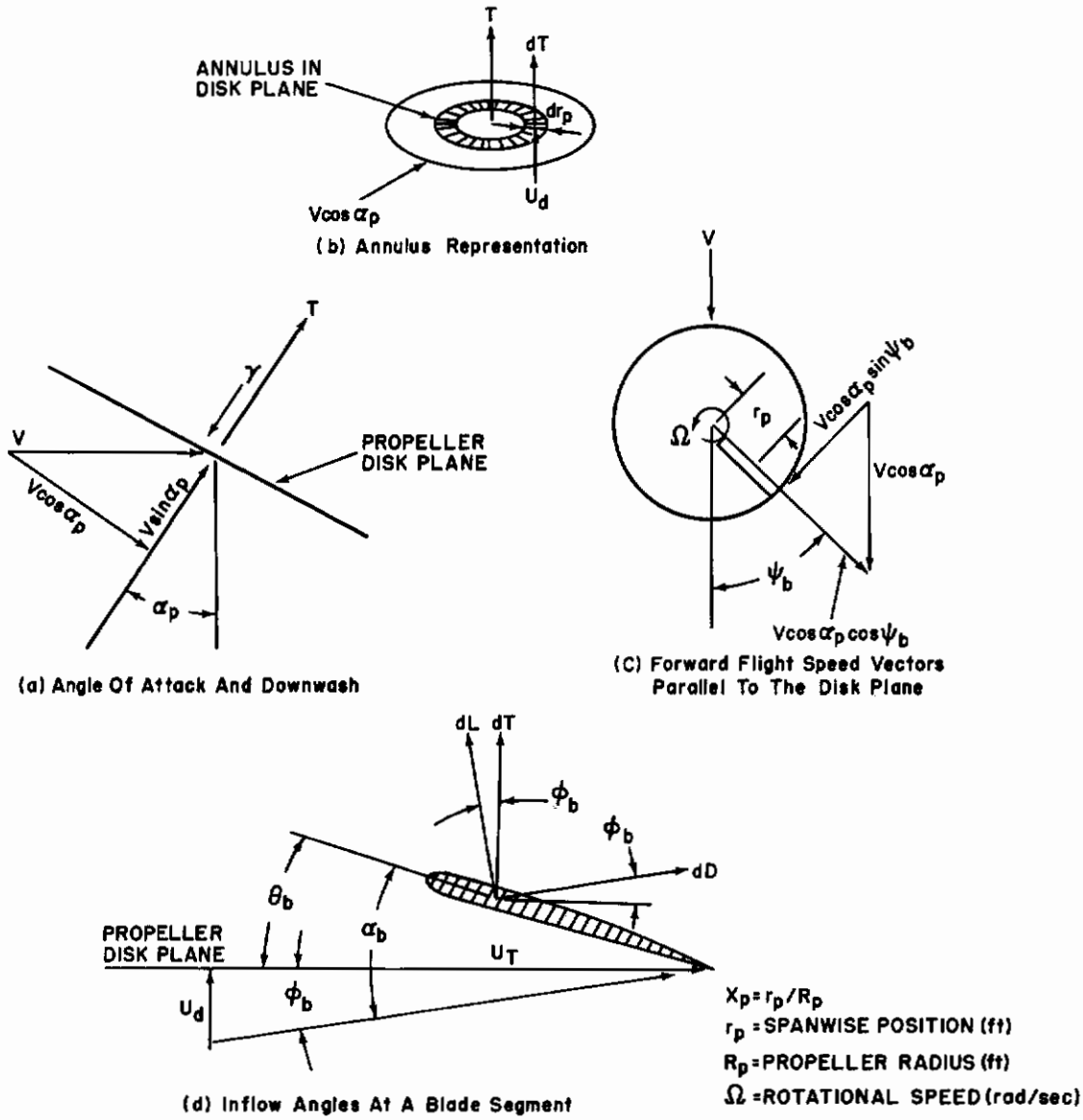

Figure 59. Schematic for Proprotor Analysis

characteristics must be specified a priori for input to the analysis. In addition, small angle approximations are not used in considering the angle of attack α_p of the disk plane relative to V. As a result, the analysis is applicable through transition to the proprotor mode of flight (Figure 59 and Reference 14).

The net velocity perpendicular through the propeller disk plane at a point r_p, Ψ_b is taken to be

$$U_d(r_p, \Psi_b) = V \sin\alpha_p - \nu(r_b)(1 + KX_p \cos \Psi_b \cos\alpha_p) \qquad (44)$$

where $\nu(r_b)(1 + KX_p\cos\Psi_b\cos\alpha_p)$ is the induced velocity through the disk plane, X_p is the nondimensional spanwise position along the blade ($X_p = r_p/R_p$), and Ψ_b is the azimuth position of the blade as shown in Figure 59.

Experimental and analytical studies suggest that the induced velocity increases between the leading and trailing edge of the disk plane during edgewise flight. This increase is reflected in the $KX_p \cos \Psi_b\cos\alpha_p$ term in Equation 44. Coleman (Reference 15) obtained fair agreement with experimental blade-motion data for an articulated rotor when $K \approx 0.5$ and α_p was small.

Assuming the slipstream swirl velocity component is negligible in comparison to the rotational speed of the rotor blade,

$$U_T(r_p,\Psi_b) = V\cos\alpha_p\sin\Psi_b + \Omega\, r_p \qquad (45)$$

The quantity U_T is the velocity of fluid flow relative to a segment of the rotor blade at r_p and at the azimuthal position ψ_b. This velocity vector is perpendicular to the blade segment and lies in the propeller disk plane as shown in Figure 59. Now, the angle of attack of the propeller blade at spanwise section r_p and at azimuth position ψ_b is given as

$$\alpha_b(r_p) = \theta_o(r_p) + \theta_{.75R_p} + \frac{U_d(r_p,\psi_b)}{U_T(r_p,\psi_b)} \tag{46}$$

when small angle approximations are used in defining blade angle of attack. This approximation is valid according to assumptions 3 and 4. The twist schedule $\theta_o(r_p)$ is the spanwise distribution along the blade where $\theta_o(.75R_p) = 0$ or where the twist schedule passes through zero at the 75% R spanwise station. The quantity $\theta_{.75R_p}$ is the collective angle at $r_p = .75R_p$ as shown for a nominal transition for the Sikorsky stowable rotor configuration in Figure 15.

$$\theta_b(r_p) = \theta_o(r_p) + \theta_{.75R_p} \tag{46a}$$

and is the total angle between the blade segment chord line and the propeller disk plane as shown in Figure 59.

Applying blade theory at any blade spanwise station gives

$$dL \simeq \frac{1}{2}\rho U_T^2(r_p,\psi_b)c(r_p)[C_{L_o}(r_p)+C_{L_\alpha}(r_p)(\theta_o(r_p)+\theta_{.75R_p} + \frac{U_d(r_p,\psi_b)}{U_T(r_p,\psi_b)})]dr_p \tag{47}$$

Now

$$dT = b(dL + \phi_b dD) \tag{48}$$

from Figure 59, where

$\cos\phi_b \simeq 1$,

$\sin\phi_b \simeq \phi_b$

b = the number of propeller blades.

Assuming that $\phi_b\, dD/dL << 1$, the incremental thrust produced in an

annulus of the propeller disk plane becomes

$$dT = \frac{\rho b c(r_p)}{2}\{[C_{L_o}(r_p)+C_{L_\alpha}(r_p)(\theta_o(r_p)+\theta_{.75R_p})]U_T^2(r_p,\psi_b)+C_{L_\alpha}(r_p)U_T(r_p,\psi_b)$$
$$U_d(r_p,\psi_b)\}dr_p \qquad (49)$$

Let the mean incremental thrust produced within the annulus of the rotor disk be given by

$$\overline{dT} = \frac{1}{2\Pi}\int_o^{2\Pi} dT d\psi_b \qquad (50)$$

Then

$$\overline{dT} = \frac{b\rho c(r_p)}{2}\{[C_{L_o}(r_p)+C_{L_\alpha}(r_p)(\theta_o(r_p)+\theta_{.75R_p})](V^2\frac{\cos^2\alpha_p}{2}+\Omega^2 r_p^2)$$
$$+ C_{L_\alpha}(r_p)\Omega r_p(V\sin\alpha_p-\nu)\}dr_p \qquad (51)$$

where Equation 49 is substituted in Equation 50 and the integration with respect to ψ_b is performed.

By taking $X_p = r_p/R_p$ and $d\overline{C}_T = d\overline{T}/\rho\Pi R_p^2 V_T^2$ where $V_T = \Omega R_p$, we obtain a nondimensional expression for Equation 51 which is

$$\frac{d\overline{C_T}}{dX_p} = A - B(\frac{\nu}{\nu_T}) \qquad (52)$$

where

$$A = \frac{bc(r_p)}{2\Pi R_p}\{(C_{L_o}(r_p)+C_{L_\alpha}(r_p)(\theta_o(r_p)+\theta_{.75R_p}))((\frac{V}{V_T})^2\frac{\cos^2\alpha_p}{2}+X_p^2)+C_{L_\alpha}(r_p)$$
$$X_p(\frac{V}{V_T})\sin\alpha_p\}$$
$$B = \frac{bc(r_p)}{2\Pi R_p}C_{L_\alpha}(r_p)X_p \qquad (53)$$

and where the induced flow velocity ν is unknown at this point in the analysis.

Using momentum theory, the mean momentum flux through an annulus in the disk plane is

$$\overline{dT} = 2\rho\Pi r_p \bar{V}'(2\nu) \tag{54}$$

where

$$V' = \sqrt{V^2\cos^2\alpha_p + U_d^2} \tag{55}$$

or

$$V' = \sqrt{A' + B'\cos\Psi_b + C'\cos^2\Psi_b} \tag{56}$$

with

$$A' = V^2 + 2\nu \sin\alpha_p + \nu^2 \tag{57}$$

$$B' = 2KX_p\nu^2\cos\alpha_p - 2\nu KX_p \sin\alpha_p \cos\alpha_p$$

$$C' = X_p^2 K^2 \nu^2 \cos^2\alpha_p$$

when Equation 44 is substituted into Equation 55.

The arithmetic mean for V' about the azimuth within an annulus is given by $\bar{V}' = \frac{1}{2\Pi}\int_0^{2\Pi} V' d\Psi_b$ and this form of averaging was used above in forming $\overline{dT}$ from blade element theory. The evaluation of $\bar{V}'$, however, leads to an elliptic integral solution whose form depends upon the type of roots produced by the solution of $C'\cos^2\Psi_b + B'\cos\Psi_b + A' = 0$. This means that the downwash velocity must be known before A', B', and C' can be evaluated and the quadratic equation solved. Other parameters in A', B', and C' such as V, α_p X_p and K are prescribed inputs. Yet ν is unknown at this point in the analysis; all that is known is that the solution for ν must be such that $\bar{V}'$ is real and positive when $\overline{dT}$ is positive or that $\bar{V}'$ is real and negative when $\overline{dT}$ is negative. To avoid complications in the programming of this analysis for the digital

computer, an engineering simplification was made by taking

$$\bar{V}' = \sqrt{\frac{1}{2\pi}\int_0^{2\pi} V'^2 d\Psi_b} \tag{58}$$

to form

$$\bar{V}' = \sqrt{V^2 - 2V\nu\sin\alpha_p + \nu^2\left(\frac{1+K^2X_p^2\cos^2\alpha_p}{2}\right)} \tag{59}$$

when Equation 56 is substituted into Equation 58 and the integration with respect to Ψ_b is performed. The assumption permitting this engineering simplification is that V' is primarily greater than zero for $0° \leq \Psi_b > 360°$. This means that this analysis is not applicable for estimating the thrust for a propeller when significant reverse flow occurs on the blade retreating side of the disk plane (i.e., $\Psi_b > 180°$) during edgewise or near edgewise forward flight (reference assumptions 6 and 7).

Substitution of Equation 59 into Equation 54 forms

$$\bar{dT} = 4\rho\pi r_p dr_p \nu \sqrt{V^2 - 2V\nu\sin\alpha_p + \nu^2\left(\frac{1+K^2X_p^2\cos^2\alpha_p}{2}\right)} \tag{60}$$

Nondimensionalizing this expression for the incremental thrust from an annulus on the rotor disk plane produces

$$\frac{\bar{dC}_T}{dX_p} = 4X_p\left(\frac{\nu}{V_T}\right)\sqrt{\left(\frac{V}{V_T}\right)^2 - 2\left(\frac{V}{V_T}\right)\left(\frac{\nu}{V_T}\right)\sin\alpha_p + \left(\frac{\nu}{V_T}\right)^2\left(\frac{1+K^2X_p^2\cos^2\alpha_p}{2}\right)} \tag{61}$$

where $X_p = r_p/R_p$ and $\bar{C}_T = \bar{dT}/\rho\pi R_p^2 V_T^2$ are substituted into Equation 60.

Now, two expressions have been formulated for the nondimensional spanwise variation in mean thrust or $d\bar{C}_T/dX_p$. The first of these is given by Equation 52, which was developed by considering blade element theory, and the second in Equation 61, where momentum considerations were used in deriving this expression. Both of these equations for $d\bar{C}_T/dX_p$ are equivalent and a solution for $\frac{\nu}{V_T}$ can be obtained by making the right-hand sides of these two equations equal to each other. The result of doing this is

$$\bar{A}\left(\frac{\nu}{V_T}\right)^4+\bar{B}\left(\frac{\nu}{V_T}\right)^3+\bar{C}\left(\frac{\nu}{V_T}\right)^2+\bar{D}\left(\frac{\nu}{V_T}\right)+\bar{E} = 0 \tag{62}$$

where

$$\begin{aligned}
\bar{A} &= 16X_p^2\left(1+\frac{X_p^2K^2\cos^2\alpha_p}{2}\right)\\
\bar{B} &= -32X_p^2\left(\frac{\nu}{V_T}\right)\sin\alpha_p\\
\bar{C} &= 16X_p^2\left(\frac{\nu}{V_T}\right)^2-B^2\\
\bar{D} &= 2AB\\
\bar{E} &= -A^2
\end{aligned} \tag{63}$$

and A and B are defined by Equation 53.

Solving Equation 62 for $\frac{\nu}{V_T}$ yields 4 solutions. Two of these are complex and therefore not applicable, since it is known that a solution for $\frac{\nu}{V_T}$ must be real. Of the remaining two real roots, one is positive while the other is negative. From momentum considerations, the positive root is the one of interest if the C_L at the blade segment is positive, and vice versa. And so, the correct

value for ν/V_T can be obtained by testing each of the four roots.

Application of Equation 62 to several spanwise stations along the blade yields the variation of $\frac{\nu}{V_T}$ with r_p. These data can be used in Equation 54 to obtain thrust. That is,

$$T=4\Pi\rho R_p^2 V_T^2 \int_{X_h}^{Xe} X_p \left(\frac{\nu}{V_T}\right) \sqrt{\left(\frac{V}{V_T}\right)^2 - 2\left(\frac{V}{V_T}\right)\left(\frac{\nu}{V_T}\right)\sin\alpha_p + \left(\frac{\nu}{V_T}\right)^2 \left(1+\frac{K^2\cos^2\alpha_p}{2}\right)}\, dX_p \qquad (64)$$

where some numerical scheme is used to perform the integration, where X_h is the nondimensional spanwise position for the radius of the hub or spinner, and X_e is as discussed below.

There are tip losses associated with the formation of the vortex at the blade tip. Here, air flows around the tip from the high pressure region below a lifting blade to the low pressure region above the blade. The following expression is suggested in Reference 14 to approximate this tip loss

$$X_e = 1 - \frac{\text{CHORD AT BLADE TIP}}{2R_p} \qquad (65)$$

The integration in Equation 64 is performed up to the X_e nondimensional spanwise position. The profile-drag torque expression, on the other hand, is integrated out to the blade tip inasmuch as drag exists even when there is a loss in thrust. The expression for torque has not been included in this analysis or in the digital computer program below since it was not necessary to the evaluation of thrust to weight ratio for the stowed rotor V/STOL.

The above analysis was used to calculate the thrust produced by the Sikorsky proprotor in hover. The blade geometry, twist, chord, and airfoil sections used can be found in Reference 8. The results correlated to within 3% of data generated by an analysis used to provide Sikorsky stowable rotor mission profiles for Reference 17. More correlations, especially with test data, will be required before any confidence can be placed in the analysis, and these correlations are expected to be performed in the near future. In addition, future analyses will include computation of torque and horsepower required by the proprotor. Correlation with test data will then be performed for Figure of Merit in hover and efficiency in the propeller mode of flight when the wind vector is coaligned with the shaft axis. Also, correlations with test data will be performed for propeller or rotor performance at large angles of attack.

2. PROPROTOR DIGITAL COMPUTER PROGRAM

This section is provided to aid the user of the digital computer program for the proprotor analysis. The program was written for use on the CDC 6600 computer at WPAFB. The inputs to the program and the listings for the program itself are discussed here. The format of presentation is concise.

The general format in preparing the input cards for the computer program is summarized as follows. Data card input is achieved by using the NAMELIST capabilities of the CDC 6600. The input set for a thrust computation at a test point must be in special form. Each

data card must be blank in the first column with the first data card of each data input set containing the characters $ INPUT starting in column 2 and followed by at least one blank. This is followed by the propeller input codes given below. The character $ signifies the end of a data input set for one case. The major advantages of the NAMELIST input procedure are that the ordering of the input variables may be as desired to the program user and that singular modifications can be made to inputs in back to back cases without input card preparation for all of the other initiating variables to the analysis. An illustration of the above is now given

CASE #1

CARD 1

$ INPUT GEN=--,--,--,--,X=--,--,--,--,C=--,--,--,--,

CARD 2

CLØ=--,--,--,--,CLA=--,--,--,--,CDØ=--,--,--,--,

CARD 3

CDA=--,--,--,--,TWIST=--,--,--,--$

This completes the first input case to be run through the analysis via the digital computer. If the follow-up case requires only a modification to GEN(1), say, where these input codes are discussed in full below, another run through the analysis is performed by adding

SUBSEQUENT CARD

$ INPUT GEN(1)=--$

behind the above cards. This procedure can be continued for as many back to back cases as required. One is referred to the appropriate manuals for programming on the CDC 6600 digital computer.

The input codes are now given. The various parameters in the dimensioning of these input codes are given in floating point format and in the nomenclature of the above proprotor analysis. These are

GEN(1) = α_p (DEG)

GEN(2) = V (FPS)

GEN (3) = V_T (FPS)

GEN(4) = $\theta_{.75R_p}$ (DEG)

GEN(5) = b (N.D.)

GEN(6) = ρ (SLUGS/FT^3)

GEN(7) = R_p (FT)

GEN(8) = K (N.D.)

GEN(9) = 0. (This location is prepared for rotor horsepower. This analysis has not been included in the program)

Also

X(I) = X_p, where spanwise station is ordered from hub to blade tip (N.D.)-- I=1,10

C(I) = C, where chord distribution corresponds to X_p locations (FT)--I=1,10

CLØ(I) = C_{L_o}, where zero α_b blade lift distribution corresponds to X(I) locations (N.D.)--I=1,10

CLA(I) = C_{L_α}, where blade lift slope corresponds to X(I) locations (/RAD)--I=1,10

CDA(J) = 10*0.; blade drag characteristics have not been included in the proprotor analysis above.

TWIST(I) = $\theta_o(r_p)$, where blade twist distribution corresponds to X(I) locations--I=1,10

The input preparation is complete for one test run through the analysis given above via the digital computer. If the next case required a change in forward flight speed to 90 psf, for example, the following input card would be added to the above input cards.

```
SUBSEQUENT CARD
$ INPUT GEN(2)=90.$
```

The user may add as many cases as he wishes behind Case 1. The listings for the FORTRAN language used to reflect the proprotor analysis are now given.

```
      PROGRAM MAIN(INPUT,OUTPUT,TAPE 5=INPUT,TAPE 6=OUTPUT)
C     PROP-ROTOR PROGRAM
C     G.KURYLOWICH
C
C     INTERNAL DIMENSIONS
      DIMENSION TH(10),VNVT(4,10),SUM(4),CTX(4,10),CT(4),T(4)
      DOUBLE PRECISION COE(5),ROOTR(4),ROOTI(4),DVNVT(4,10)
C     NAMELIST DIMENSIONS
      DIMENSION X(10),C(10),CLO(10),CLA(10),CDO(10),CDA(10),GEN(9),
     1TWIST(10)
      NAMELIST/INPUT/GEN,X,C,CLO,CLA,CDO,CDA,TWIST
C
C
      PI  =3.14159265
      TPI =2.*PI
      DETRA=.017453295
    1 READ(5,INPUT)
      DO 10 I=1,10
      DO 11 J=1,4
      ROOTR(J)=0.0000
      ROOTI(J)=0.0000
      DVNVT(J,I)=0.0000
      VNVT(J,I)=0.0
      CTX(J,I)=0.0
      CT(J)=0.0
      T(J)=0.0
   11 CONTINUE
   10 CONTINUE
C     IDENTIFY PARAMETERS
C
C
      ALPHA=GEN(1)*DETRA
          V=GEN(2)
         VT=GEN(3)
       TH75=GEN(4)
          B=GEN(5)
        RHO=GEN(6)
          R=GEN(7)
         AK=GEN(8)
        WII=GEN(9)
C     GET TWIST OF BLADES IN RADIANS
      DO 2 I=1,10
    2 TH(I)=DETRA*(TWIST(I)+TH75)
C     COMPUTE RELEVANT DATA OR PARAMETERS
      B2PR=B/(TPI*R)
      VOVT=V/VT
      VOVTS=VOVT**2
        CSA=COS(ALPHA)
        SNA=SIN(ALPHA)
       CSAS=CSA**2
       SNAS=SNA**2
        AKS=AK**2
         A1=.5*CSAS*VOVTS
         A2=VOVT*SNA
         A4=-32.*VOVT*SNA
```

```
            A5=16.*VOVTS
      C     SOL'N FOR INDUCED INFLOW NOW PERFORMED
            DO 3 I=1,10
               XS=X(I)**2
               AA=B2PR*C(I)*((CLO(I)+CLA(I)*TH(I))*(A1+XS)+CLA(I)*A2*X(I))
               BB=C(I)*B2PR*CLA(I)*X(I)
      C
      C     DMULR COEF. NOW OBTAINED
            ACOE=XS*16.*(1.+.5*XS*AKS*CSAS)
             COE(1)=DBLE(1.0)
            COE(2)=DBLE(XS*A4/ACOE)
            COE(3)=DBLE((XS*A5-BB**2)/ACOE)
            COE(4)=DBLE(2.*AA*BB/ACOE)
            COE(5)=DBLE(-AA**2/ACOE)
            WRITE(6,101)A1,A2,A4,A5,XS,AA,BB,ACOE
        101 FORMAT(8F12.6)
            WRITE(6,102)(COE(K),K=1,5)
        102 FORMAT(5D15.7)
      C     SOLVE FOR ROOTS,REAL ROOTS IN ROOTR(J),J=1,4
      C     IMAGINARY ROOTS IN ROOTI(J),J=1,4
      C
            CALL DMULR(COE,4,ROOTR,ROOTI)
            WRITE(6,100)(ROOTR(J),ROOTI(J),J=1,4)
        100 FORMAT(8D15.7)
            DO 500 J=1,4
            IF(ABS(ROOTI(J)).GT.1.D-10)ROOTR(J)=0.000
            IF(ROOTR(J).LT.0.000) ROOTR(J)=0.0000
            IF(RCOTR(J).GT.0.000) VNVT(1,I)=RCOTR(J)
        500 CONTINUE
            J=1
        570 CTX(J,I)=AA-BB*VNVT(J,I)
          3 CONTINUE
      C     SET SUMERS TO ZERO
          5 SUM(J)=0.
      C     COMPUTE INTEGRATED CT AND THRUST
      C
      C     TIP LOSS FACTOR FROM FG.201 OF GESSOW & MYERS(B=1-CT/2R)
            TIP =.5*C(10)/R
            DO 7 I=1,9
          7 SUM(J)=SUM(J)+.5*(CTX(J,I+1)+CTX(J,I))*(X(I+1)-X(I))
             CT(J)=SUM(J)-.5*(CTX(J,9)+CTX(J,10))*TIP
      C     CT CORRECT FOR TIP LOSSES
          6   T(J)=RHO*PI*(R**2)*(VT**2)*CT(J)
      C     OUTPUT OF DATA
            WRITE(6,800)GEN,X,C,CLO,CLA,CDO,CDA,TWIST
        800 FORMAT(//T6,*INPUT DATA*//T6,*ALPHA(DEG)*,5X,*V(FPS)*,5X,
           1*VT(FPS)*,5X,*TH75(D)*,5X,*B*,5X,*RHO*,5X,*R(FT)*,5X,
           2*K(INFLOW FACT)*/T6,9F10.6//T6,*X=R/R STATION*/T6,10F10.6//T6,
           3*CHORD DIST.(FT)*/T6,10F10.6//T6,*CLO DIST*/T6,10F10.6//T6,
           4*CLA DIST(1/RAD)*/T6,10F10.6//T6,*CDO DIST*/T6,10F10.6//T6,
           5*CDA DIST(1/RAD2)*/T6,10F10.6//T6,*TWIST DIST.(DEG)*/T6,10F10.6)
      C     ALPHA AT X=.75 ESTIMATED WITH VN=0.1F + T=+,1F - T=-.
            ALP75=TH75+V*SNA/(.75*VT*DETRA)
            WRITE(6,801)ALP75
        801 FORMAT(//T6,*COMPUTATIONAL OUTPUT*//T6,
```

```
     1*ALPH75(DEG) NOW ESTIMATE FOR VN=0.THRUST IS POS WHEN THIS NUMBER
     2IS POS.*/T6,*ALPHA75=*,2X,1F10.6)
C      FORMAT STATEMENTS FOR ROOT SOL'NS
       WRITE(6,802)J
  802  FORMAT(//T6,*ROOT SOLUTION=*,2X,I2)
       WRITE(6,803)(VNVT(J,I),I=1,10),(CTX(J,I),I=1,10),T(J)
  803  FORMAT(//T6,*SPANWISE VN/VT DISTRIBUTION FOR ABOVE X STATIONS*/T6,
     110F10.6//T6,*DCT/DX ALONG SPAN FOR ABOVE X STATIONS*/T6,10F10.6//T
     26,*THRUST IN LBS =*1F20.6)
C
C      GO BACK FOR NEXT CASE
       GO TO 1
C
C
C
       END
```

```
      SUBROUTINE DMULR (COE,N1,ROOTR,ROOTI)
C
C
C*****************************************************************
C
C     POLYNOMIAL ROOT FINDER SUBROUTINE ....
C
C     ITERATIVE METHOD FOR POLYNOMIAL EQUATIONS ....
C
C     THIS METHOD APPROXIMATES THE FUNCTION F(Z) BY A QUADRATIC
C   WHICH MAY ,IN GENERAL, HAVE COMPLEX COEFFICIENTS AND DOES NOT
C   REQUIRE A KNOWLEDGE OF THE DERIVATIVE OF F(Z) THOUGH
C   THE FUNCTION F(Z) MUST BE EVALUATED ONCE PER ITERATION ....
C
C     THIS SUBROUTINE FINDS REAL AND COMPLEX ROOTS OF A POLYNOMIAL
C   WITH REAL COEFFICIENTS ....
C
C
C     USE OF MULLER SUBROUTINE ....
C   1.  CALL DMULR  (COE,N1,ROOTR,ROOTI) ....
C   2.  COE IS THE TAG OF THE ARRAY OF COEFFICIENTS.
C       THE COEFFICIENTS MUST BE ORDERED FROM HIGHEST DEGREE
C       TO LOWEST DEGREE .
C   3.  N1 IS DEGREE OF THE POLYNOMIAL .
C   4.  ROOTR IS THE TAG OF THE ARRAY WHERE THE REAL PARTS
C       OF THE COMPLEX ROOTS ARE STORED .
C   5.  ROOTI IS THE TAG OF THE ARRAY WHERE THE IMAGINARY
C       PARTS OF THE COMPLEX ROOTS ARE STORED ....
C
C     ALL ARITHMETIC IS IN THE COMPLEX MODE ....
C     THEREFORE UNDER-FLOW IS NORMAL FOR REAL ROOTS ....
C
C     MULTIPLE ROOTS DECREASES ACCURACY OF THIS SUBROUTINE .
C     WHEN MULTIPLICITY IS FOUR THE ACCURACY DECREASES TO
C     ABOUT TWO PLACES ....
C
C     DEGREE SQUARED DIVIDED BY TWENTY ....
C     FOR DEGREE ELEVEN IT TAKES SIX SECONDS ....
C
C
C
C*****************************************************************
C
C
C
      DOUBLE PRECISION ROOTR,ROOTI,AXR,AXI,ALP1R,ALP1I,TEM
      DOUBLE PRECISION BET1R,BET1I,ALP2R,ALP2I,BET2R,BET2I
      DOUBLE PRECISION TEMR,TEMI,ALP3R,ALP3I,BET3R,BET3I
      DOUBLE PRECISION ALP4R,ALP4I,TEM1,TEM2,HELL,BELL
      DOUBLE PRECISION TE1,TE2,TE3,TE4,TE5,TE6,TE7,TE8,TE9,TE10
      DOUBLE PRECISION TE11,TE12,TE13,TE14,TE15,TE16,DE15,DE16,COE
C
      DIMENSION COE(1),ROOTR(1),ROOTI(1)
C
      N2=N1+1
```

```
      N4=0
      I=N1+1
19    IF(COE(I))9,7,9
7     N4=N4+1
      ROOTR(N4)=0.0D0
      ROOTI(N4)=0.0D0
      I=I-1
      IF(N4-N1)19,37,19
9     CONTINUE
C
10    AXR=0.8D0
      AXI=0.0D0
      L=1
      N3=1
      ALP1R=AXR
      ALP1I=AXI
      M=1
      GO TO 99
C
11    BET1R=TEMR
      BET1I=TEMI
      AXR=0.85D0
      ALP2R=AXR
      ALP2I=AXI
      M=2
      GO TO 99
C
12    BET2R=TEMR
      BET2I=TEMI
      AXR=0.9D0
      ALP3R=AXR
      ALP3I=AXI
      M=3
      GO TO 99
C
13    BET3R=TEMR
      BET3I=TEMI
14    TE1=ALP1R-ALP3R
      TE2=ALP1I-ALP3I
      TE5=ALP3R-ALP2R
      TE6=ALP3I-ALP2I
      TEM=TE5*TE5+TE6*TE6
      TE3=(TE1*TE5+TE2*TE6)/TEM
      TE4=(TE2*TE5-TE1*TE6)/TEM
      TE7=TE3+1.0D0
      TE9=TE3*TE3-TE4*TE4
      TE10=2.0D0*TE3*TE4
      DE15=TE7*BET3R-TE4*BET3I
      DE16=TE7*BET3I+TE4*BET3R
      TE11=TE3*BET2R-TE4*BET2I+BET1R-DE15
      TE12=TE3*BET2I+TE4*BET2R+BET1I-DE16
      TE7=TE9-1.0D0
      TE1=TE9*BET2R-TE10*BET2I
      TE2=TE9*BET2I+TE10*BET2R
      TE13=TE1-BET1R-TE7*BET3R+TE10*BET3I
```

```
      TE14=TE2-BET1I-TE7*BET3I-TE10*BET3R
      TE15=DE15*TE3-DE16*TE4
      TE16=DE15*TE4+DE16*TE3
      TE1=TE13*TE13-TE14*TE14-4.0D0*(TE11*TE15-TE12*TE16)
      TE2=2.0D0*TE13*TE14-4.0D0*(TE12*TE15+TE11*TE16)
      TEM=DSQRT(TE1*TE1+TE2*TE2)
      IF(TE1)113,113,112
  113 TE4=DSQRT(0.5D0*(TEM-TE1))
      TE3=0.5D0*TE2/TE4
      GO TO 111
C
  112 TE3=DSQRT(0.5D0*(TEM+TE1))
      IF(TE2)110,200,200
  110 TE3=-TE3
  200 TE4=0.5D0*TE2/TE3
  111 TE7=TE13+TE3
      TE8=TE14+TE4
      TE9=TE13-TE3
      TE10=TE14-TE4
      TE1=2.0D0*TE15
      TE2=2.0D0*TE16
      IF(TE7*TE7+TE8*TE8-TE9*TE9-TE10*TE10)204,204,205
  204 TE7=TE9
      TE8=TE10
  205 TEM=TE7*TE7+TE8*TE8
      TE3=(TE1*TE7+TE2*TE8)/TEM
      TE4=(TE2*TE7-TE1*TE8)/TEM
      AXR=ALP3R+TE3*TE5-TE4*TE6
      AXI=ALP3I+TE3*TE6+TE4*TE5
      ALP4R=AXR
      ALP4I=AXI
      M=4
      GO TO 99
C
   15 N6=1
C*****************************************************************************
   38 IF(DABS(HELL)+DABS(BELL)-1.0D-20)18,18,16
   16 TE7=DABS(ALP3R-AXR)+DABS(ALP3I-AXI)
      IF(TE7/(DABS(AXR)+DABS(AXI))-1.0D-7)18,18,17
C*****************************************************************************
   17 N3=N3+1
      ALP1R=ALP2R
      ALP1I=ALP2I
      ALP2R=ALP3R
      ALP2I=ALP3I
      ALP3R=ALP4R
      ALP3I=ALP4I
      BET1R=BET2R
      BET1I=BET2I
      BET2R=BET3R
      BET2I=BET3I
      BET3R=TEMR
      BET3I=TEMI
      IF(N3-100)14,18,18
   18 N4=N4+1
```

```
      ROOTR(N4)=ALP4R
      ROOTI(N4)=ALP4I
      N3=0
41    IF(N4-N1)30,37,37
37    RETURN
C*****************************************************************************
30    IF(DABS(ROOTI(N4))-1.0D-5)10,10,31
31    GO TO (32,10),L
32    AXR=ALP1R
      AXI=-ALP1I
      ALP1I=-ALP1I
      M=5
      GO TO 99
33    BET1R=TEMR
      BET1I=TEMI
      AXR=ALP2R
      AXI=-ALP2I
      ALP2I=-ALP2I
      M=6
      GO TO 99
C
34    BET2R=TEMR
      BET2I=TEMI
      AXR=ALP3R
      AXI=-ALP3I
      ALP3I=-ALP3I
      L=2
      M=3
99    TEMR=COE(1)
      TEMI=0.0D0
      DO 100 I=1,N1
      TE1=TEMR*AXR-TEMI*AXI
      TEMI=TEMI*AXR+TEMR*AXI
100   TEMR=TE1+COE(I+1)
      HELL=TEMR
      BELL=TEMI
42    IF(N4)102,103,102
102   DO 101 I=1,N4
      TEM1=AXR-ROOTR(I)
      TEM2=AXI-ROOTI(I)
      TE1=TEM1*TEM1+TEM2*TEM2
      TE2=(TEMR*TEM1+TEMI*TEM2)/TE1
      TEMI=(TEMI*TEM1-TEMR*TEM2)/TE1
101   TEMR=TE2
103   GO TO (11,12,13,15,33,34),M
      END
```

REFERENCES

1. Anon., Military Specification--Flying Qualities of Piloted V/STOL Aircraft, MIL-F-83300, May 1971.

2. Klingloff, R. F., Ruttledge, D. C. G., Stability and Control Study Stoppable Rotor, Volume I, Sikorsky Aircraft Division, 1971.

3. Etkin, B., Dynamics of Flight, John Wiley & Sons, Ltd., 1959.

4. Statler, I. C., Kurylowich, G., et al, Predictive Methods for the Dynamic Response of a Quad Tilt-Duct V/STOL Aircraft in Transition, AFFDL-TR-70-140, December 1970.

5. Ryan, P. E., Breidenstein, R. M., Wind Tunnel Test Data Report of a Powered 1/5 Scale ARL/Bell V/STOL Aircraft Model, Bell Aerosystems Co., Report No. 2353-921002, June 1969.

6. Ryan, P. E., et al, Wind Tunnel Test Data Report of a Powered 1/5 Scale ARL/Bell V/STOL Aircraft Model--Phase II, Bell Aerosystems Co., Report No. 2353-921003, December 1969.

7. Anon., Haven Max (Cold Thrust Augmentation, V/STOL), Air Rescue Aircraft Design Study, Bell Aerosystems Co., Report No. 2352-933012, May 1971.

8. Anon., Stoppable Rotor Study--Phase 1--Final Report, Sikorsky Aircraft Company, Report No. SER-50621(Vol. I), October 1969.

9. Curtiss, H. C., Jr., Dynamic Stability of V/STOL Aircraft at Low Speeds, AIAA Paper No. 69-194, February 1969.

10. Livingston, C., Maneuverability Prediction, Bell Helicopter Co., Presented to the Southwest Region of the American Helicopter Society, December 1966.

11. Anon., Military Specification--Flying Qualities of Piloted Airplanes, MIL-F-8785B(ASG), August 1969.

12. Griffin, J. M., Digital Computer Solution of Aircraft Longitudinal and Lateral-Directional Dynamic Characteristics, WPAFB Tech. Report No. SEG-TR-60-52, December 1966.

13. Kurylowich, G., Ritter, A., Experiments on Pilot Visibility from a V/STOL in Overwater Hover, presented at the Joint Symposium on Environmental Effects on VTOL Designs sponsored by the AHS, AIAA and the University of Texas at Arlington, Texas, November 1970.

14. Gessow, A., Myers, G. C., Jr., Aerodynamics of the Helicopter, The MacMillan Company, 1952.

15. Coleman, R. P., et al, Evaluation of the Induced-Velocity Field of an Idealized Helicopter Rotor, NACA ARR L5E10, 1945.

16. Corning, G., Supersonic and Subsonic Airplane Design, 3rd Edition, Brown-Brumfield, Inc., Ann Arbor, Michigan, 1960.

17. Anon., A Comparative Evaluation of the Ejector Wing V/STOL Concept (Applications of Cold Thrust Augmentation Technology (V/STOL)), Deputy for Development Planning of ASD, Report No. ASD/XR 72-6, April 1972.

UNCLASSIFIED

Security Classification

DOCUMENT CONTROL DATA - R & D

(Security classification of title, body of abstract and indexing annotation must be entered when the overall report is classified)

1. ORIGINATING ACTIVITY *(Corporate author)* Air Force Flight Dynamics Laboratory Wright-Patterson Air Force Base, Ohio	2a. REPORT SECURITY CLASSIFICATION UNCLASSIFIED 2b. GROUP

3. REPORT TITLE

AN ANALYSIS OF THE STABILITY AND CONTROL CHARACTERISTICS OF AN EJECTOR WING V/STOL DURING TRANSITION

4. DESCRIPTIVE NOTES *(Type of report and inclusive dates)*

5. AUTHOR(S) *(First name, middle initial, last name)*

George Kurylowich, James M. Martin

6. REPORT DATE	7a. TOTAL NO. OF PAGES	7b. NO. OF REFS
February 1973	194	17

8a. CONTRACT OR GRANT NO. b. PROJECT NO. D095 c. d.	9a. ORIGINATOR'S REPORT NUMBER(S) AFFDL-TR-72-37 9b. OTHER REPORT NO(S) *(Any other numbers that may be assigned this report)*

10. DISTRIBUTION STATEMENT

Distribution limited to U. S. Government agencies only; test and evaluation; statement applied Feb 1973. Other requests for this document must be referred to AF Flight Dynamics Laboratory (FGC) Wright-Patterson AFB, Ohio 45433

11. SUPPLEMENTARY NOTES	12. SPONSORING MILITARY ACTIVITY
	Air Force Flight Dynamics Laboratory Air Force Systems Commend Wright-Patterson Air Force Base, Ohio

13. ABSTRACT

An analysis was performed to investigate the longitudinal stability and control characteristics of an ejector wing configuration V/STOL in transition. A derivative approach was used to obtain dynamic responses about specified trim speeds, and analysis of these responses provided an insight into the significant characteristics that might affect the pilot's control over the aircraft. The thrust levels necessary to meet the control requirements specified in MIL-F-83300 for a Level 1 category vehicle were determined as well. A similar study was made for a stowable rotor configuration, and results for the stowable rotor V/STOL and the ejector wing configuration were compared. Finally, the downwash characteristics of the ejector wing configuration were evaluated in terms of their effect on ground equipment and personnel. Spray generation during hover over water is also discussed.

DD FORM 1 NOV 65 1473

UNCLASSIFIED

Security Classification

14. KEY WORDS	LINK A		LINK B		LINK C	
	ROLE	WT	ROLE	WT	ROLE	WT
Ejector Wing V/STOL						
Stability Analysis						
Downwash Characteristics						
Handling Qualities						
Stability and Control						
Transitional Flight						

*U.S.Government Printing Office: 1973 — 759-495/602